Dynamical Properties of Neuronal Systems with Complex Network Structure

D I S S E R T A T I O N

zur Erlangung des akademischen Grades

doctor rerum naturalium
(Dr. rer. nat.)

im Fach Physik

Spezialisierung: Theoretische Physik

eingereicht an der

Mathematisch-Naturwissenschaftlichen Fakultät
der Humboldt-Universität zu Berlin

von

Dipl.-Phys. Christian Claus Schmeltzer

Präsident der Humboldt-Universität zu Berlin:
Prof. Dr. Jan-Hendrik Olbertz

Dekan der Mathematisch-Naturwissenschaftlichen Fakultät:
Prof. Dr. Elmar Kulke

Gutachter:
1. PD Dr. Sten Rüdiger
2. Prof. Dr. Alexandre Kihara
3. Prof. Dr. Enrique Alvarez Lacalle

Tag der mündlichen Prüfung: 10.02.2016

Dynamical Properties of Neuronal Systems with Complex Network Structure

Christian Schmeltzer

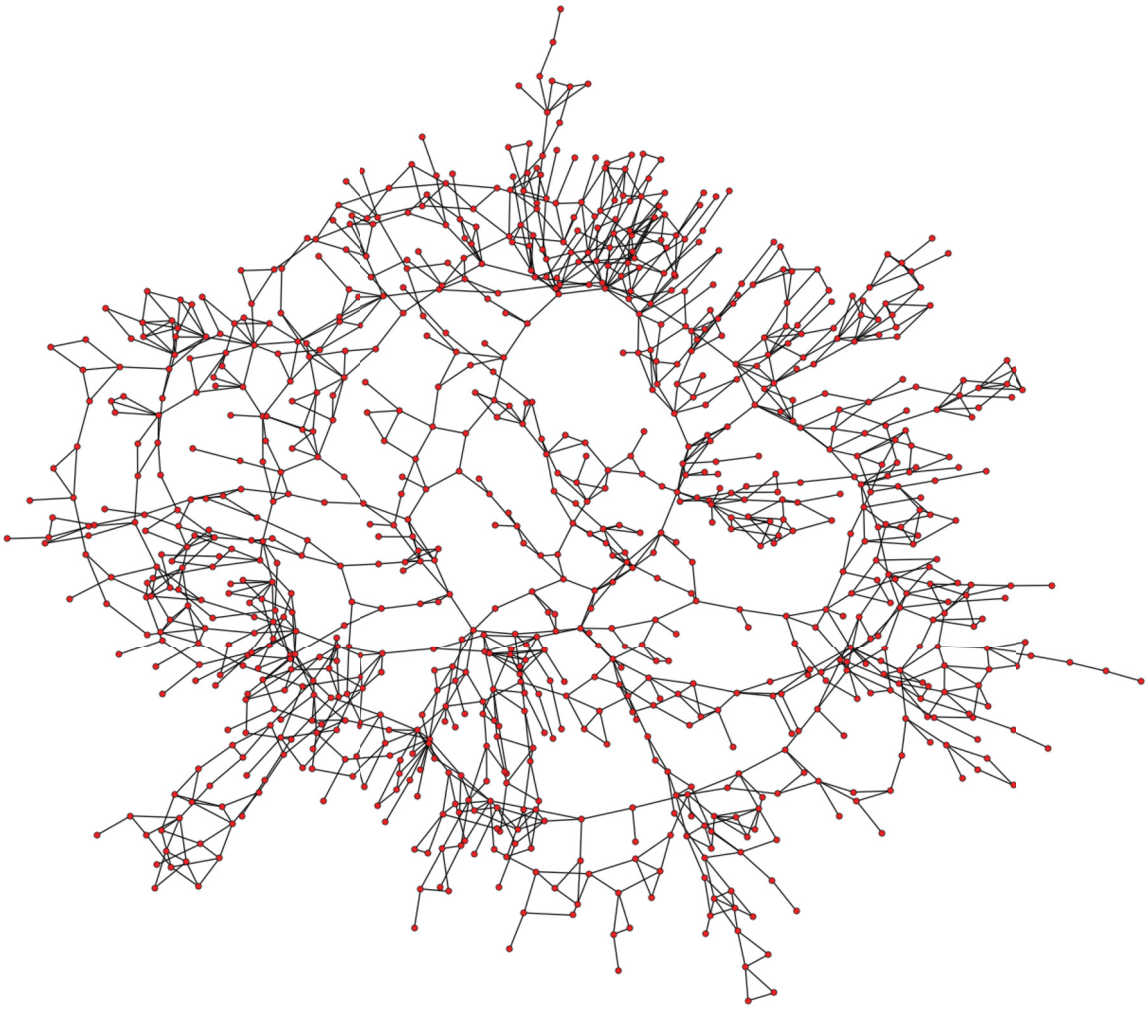

DISSERTATION

Dipl.-Phys. C. Schmeltzer
Institut für Physik
Humboldt-Universität zu Berlin
IRTG 1740

Abstract

An important question in neuroscience is how the structure and dynamics of a neuronal network relate to each other. We approach this problem by modeling the spiking activity of large-scale neuronal networks that exhibit several complex network properties. Our main focus lies on the relevance of two particular attributes for the dynamics, namely structural heterogeneity and degree correlations. Although these are fundamental properties of many brain networks, their influence on the system's activity is not yet well understood.

As a central result, we introduce a novel mean-field method that makes it possible to calculate the average activity of heterogeneous, degree-correlated neuronal networks without having to simulate each neuron explicitly. The method is based on grouping neurons with equal number of inputs (their in-degree) into populations and describing the dynamics of these populations in terms of reduced firing rate equations. We find that the connectivity structure is sufficiently captured by a reduced matrix that contains only the coupling between the populations. This matrix can be calculated analytically for some generic random networks, which allows for an efficient analysis of the system's dynamics. With the mean-field method and numerical simulations we demonstrate that assortative degree correlations enhance the network's ability to sustain activity for low external excitation, thus making it more sensitive to small input signals. This effect is reminiscent of an increased structural robustness of assortative networks that is well-known in network sciences.

Therefore, we additionally examine the structural robustness of correlated networks with a simplified percolation model, additionally taking into account the fact that neuronal networks - among other real-world systems - are subject to metric constraints: Spatially close neurons are usually more likely to connect to each other than distant neurons. The main result of this examination is that for weak metric constraints assortativity generally makes the network more robust, whereas for strong metric constraints assortativity can strengthen or weaken the network, depending on its local structure. Therefore, we conclude that degree correlations and metric constraints strongly interplay and that they should not be regarded as independent features of real-world networks.

Keywords: Complex Network, Neuronal Dynamics, Statistical Physics, Degree Correlations, Percolation

Zusammenfassung

In welcher Weise hängt die Dynamik eines neuronalen Systems von den Eigenschaften seiner Netzwerkstruktur ab? Diese wichtige Fragestellung der Neurowissenschaft untersuchen wir in dieser Dissertation anhand einer analytischen und numerischen Modellierung der Aktivität großer neuronaler Netzwerke mit komplexer Struktur. Im Fokus steht die Relevanz zweier bestimmter Merkmale für die Dynamik: strukturelle Heterogenität und Gradkorrelationen. Beide Eigenschaften sind charakteristisch für neuronale Netzwerke, dennoch ist bislang unklar, wie sie sich auf ihre Aktivität auswirken.

Ein zentraler Bestandteil der Dissertation ist die Entwicklung einer Molekularfeldnäherung, mit der die mittlere Aktivität heterogener, gradkorrelierter neuronaler Netzwerke berechnet werden kann, ohne dass einzelne Neuronen explizit simuliert werden müssen. Innerhalb des Modells werden Neuronen mit gleicher Anzahl von Inputs jeweils einer Gruppe zugeordnet und im Folgenden die mittlere Feuerrate dieser Neuronengruppen analysiert. Die Netzwerkstruktur wird von einer reduzierten Matrix erfasst, welche die Verbindungsstärke zwischen den Neuronengruppen beschreibt. Für einige generische Zufallsnetzwerke kann diese Matrix analytisch berechnet werden, was eine effiziente Analyse der Dynamik dieser Systeme erlaubt. Mit der Molekularfeldnäherung und numerischen Simulationen zeigen wir, dass assortative Gradkorrelationen einem neuronalen System ermöglichen, seine Aktivität bei geringer externer Anregung aufrecht zu erhalten und somit besonders sensitiv auf schwache Stimuli zu reagieren. Dieser Effekt ist vergleichbar mit einer erhöhten strukturellen Robustheit assortativer Netzwerke, welche in der Netzwerkforschung wohlbekannt ist.

Aus diesem Grund untersuchen wir außerdem die Robustheit gradkorrelierter Netzwerke mit einem vereinfachten Perkolationsmodell unter Berücksichtigung einer weiteren wichtigen Eigenschaft neuronaler Systeme: die räumliche Einschränkung der Verbindungslängen. Dicht beieinander liegende Neuronen sind in der Regel mit größerer Wahrscheinlichkeit verbunden als weit voneinander entfernte. Das wichtigste Ergebnis dieser Untersuchung ist, dass Assortativität die Robustheit schwach räumlich eingeschränkter Netzwerke erhöht, jedoch in stark eingeschränkten Netzwerken auch das Gegenteil bewirken kann, abhängig von der lokalen Struktur. Hieraus schließen wir, dass die räumliche Struktur und Gradkorrelationen eng miteinander verknüpft sind und somit nicht als unabhängige Eigenschaften realer Netzwerke angesehen werden sollten.

Schlagwörter: Komplexes Netzwerk, Neuronale Dynamik, Statistische Physik, Gradkorrelationen, Perkolation

Contents

List of abbreviations

Network theory

$\mathcal{G}$	Network, or graph. Mathematically, it is defined as a tuple $\mathcal{G}(\mathbf{N}, \mathbf{E})$ of a set $\mathbf{N}$ of nodes and a set $\mathbf{E}$ of links.
N	Number of nodes in a network. Also called the size of a network.
E	Number of links in a network.
$\mathbf{A}$	Adjacency matrix.
k	Degree of a node in an undirected network. In-degree of a node in a directed network.
j	Out-degree of a node in a directed network.
$P(k)$	Degree distribution in an undirected network. $P^{\text{in}}(k)$ and $P^{\text{out}}(j)$ are the in-degree distribution and out-degree distribution in a directed network, respectively.
p	Pearson degree correlation coefficient in an undirected network. p_{in} is the Pearson correlation coefficient for in-degrees in a directed network.
$\mathcal{C}$	Global clustering coefficient.

Modeling neuronal dynamics

V	Membrane potential of a neuron. Also sometimes called depolarization, if the resting potential of the neuron is set to zero.
r	Firing rate. It can be estimated by counting the number of spikes in a small time-window, and deviding that number by the size of the window.
f_R	Response function that describes a series of spikes.
J	Synaptic strength. Voltage jump that is induced in a neuron's soma by an arriving action potential.
I_{ion}, R_{ion}	Ion current and total membrane resistance, respectively, for ions of type ion.
I_s	Synaptic input current.
I_L, R_L	Leakage current and leakage resistance, respectively.

C	Capacitance of a neuron's cell membrane.
τ	Time-constant of a neuron, analogous to the time-constant of the corresponding RC-circuit.
Θ	Voltage threshold. Whenever a neuron's membrane potential exceeds this threshold, the neuron generates an action potential.

Population activity and information theory

V_i	Membrane potential of the i-th neuron in the network.
I_i	Total input current to the i-th neuron in the network.
$V_i^{(k)}$	Membrane potential of the i-th neuron that has k inputs (a k-neuron).
$\hat{r}_k$	Population firing rate. Ensemble-averaged firing rate of a population of k-neurons (a k-population).
s	Stimulus strength. Rate of spikes that are injected independently into each neuron. For convenience we express it in multiples of the minimum rate that generates neuronal spiking in the absence of recurrent input.
$N_{kk'}$	Joint-in-degree distribution. Average number of inputs a k-neuron receives from k'-neurons.
$f(k, k')$	Probability for a random input of a k-neuron to originate at a k'-neuron. It is related to the joint-in-degree distribution as follows: $kf(k, k') = N_{kk'}$.
μ_k	Mean of the noisy input current to a k-neuron.
σ_k^2	Variance of the noisy input current to a k-neuron.
$p_k(v_k, t)$	Probability density for a k-population. Probability of a k-neuron to have a membrane potential in the interval $[v_k, v_k + dv_k]$ at time t.
$J_k(v_k, t)$	Probability current for a k-population, sometimes called probability flux.
ϕ_k	Transfer function for a k-population.
$\mathbf{\Theta}$	Vector of all population transfer functions.
τ_x	Time-constant for the approximate dynamics of a neuronal system. It is used to model the low-pass behavior of a network's response to transient changes of the stimulus.
H	Shannon entropy of the network's responses to a set of stimuli.

H_{noise}	Noise entropy of the network's responses to a set of stimuli.
I	Mutual Information of the stimulus/response relation, $I = H - H_{\text{noise}}$. It quantifies in bits how much information a set of network responses contains about the set of stimuli that evoked the responses.

Percolation

q	Density of links, $q = E/N$.
q_c	Percolation threshold. Critical density of links, where the infinite network transitions into the percolating phase.
D	Fractal dimension.
G	Largest cluster density.
S	Mean cluster size.
L	Side length of a lattice, or domain.
d	Spatial dimension of a system.
α	Distance exponent. Large negative α impose strong metric constraints on the graph.
ρ	Parameter in the connection probability for spatial model 1 networks, which controls the type and strength of degree correlations imposed on the graph.
ν, β, γ	Percolation exponents.

1 Introduction

Our brain is a truly remarkable product of evolution. It endows us with the ability to invent increasingly sophisticated technologies, reflect on ourselves and solve intricate problems, which sets us apart from all the other animals we share the planet with. It is no surprise that an organ capable of performing such complex tasks is itself complex. It comprises about eighty billion nerve cells that make one hundred trillion connections to each other, forming an elaborate structure that is organized on multiple spatial scales [151, 247]. How does this system carry out higher cognitive processes such as memory, thoughts and perception? No single nerve cell can accomplish any of these tasks, it is rather the concerted activity of a great many neurons communicating with each other through electrical and chemical signals that gives rise to these abilities.

Therefore, it is important to quantify and understand how these interactions are structurally and functionally organized, which can be approached by describing the system as a *complex network*. In principle, a network is a collection of entities that are connected to each other. In a neuronal system these entities are, at the microscopic scale, the neurons forming chemical and electrical conjunctions with each other. On larger scales we can describe the network of anatomical or functional brain regions that integrate the activity of small and large groups of neurons. Complex network theory provides powerful tools and statistical measures to examine the non-trivial structural patterns of this multiscale architecture and thus, it has been increasingly applied in neuroscientific research [196, 247].

Advancing neuroimaging techniques make it possible to map the brain's wiring structure with increasing detail. Ultimately, this information could be organized into a database containing the full connection matrix of the human brain, the so-called *connectome* [248]. However, knowing the exact wiring diagram of the nervous system does not necessarily give us insight into its principles of function. An illustrative example is the nervous system of the roundworm C. Elegans, whose anatomical network structure has been comprehensively mapped. Although this system is relatively simple, comprising only 302 neurons, its function is not yet understood, despite considerable effort [282, 274, 157]. Thus, it is crucial to comprehend how the structural properties of a neuronal system are related to its dynamical and functional behavior. In this thesis we approach this problem with analytical and numerical modeling.

A wide spectrum of models has been used to study the function and dynamics of neuronal networks at various levels of detail and complexity [118, 216, 49]. At the

one end of the spectrum, biological and neuroscientific models attempt to capture the realistic behavior of a brain region by taking into account relatively detailed information about the connectivity structure and electrophysiological properties of the neurons [158, 186, 251, 135, 137, 147]. At the other end, physical and mathematical models examine the global behavior of the system parametrically by using simplified neurons that are interconnected in a random network with specific topological properties [155, 10, 119, 2, 12, 156, 205, 118, 223]. The latter models allow for a reduced mathematical description of the global network dynamics in terms of a stochastic process, relying on the assumption that irregularities in neuronal spiking can be treated as noise that does not carry any meaningful information. First, the stochastic description of neuronal spiking goes hand in hand with a statistical description of the random network topology and second, it allows for a simplified mathematical analysis of the neuronal activity, since it is not necessary to keep track of individual spikes. Hence, these models are particularly suited for an efficient examination of how specific network properties influence the system's behavior.

The stochastic description of the global dynamics is based on a 'coarse-graining' of the neuronal activity: Neurons with similar properties are grouped into *populations* and the mean activity of these populations is described rather than the spiking of individual neurons. This coarse-graining procedure requires to average over the connectivity structure of the system. Therefore, studies using this approach have mainly focused on networks with a relatively simple connectivity structure that is either based on random assignment of neuronal connections or all-to-all coupling [155, 10, 119, 2, 12, 156, 205, 118, 223]. A systematic investigation of more complex structural properties in this context has been addressed only recently [224, 66, 295, 275, 209].

Indeed, real neuronal systems are rather heterogeneous, having regions that are highly connected and others that are sparse [42, 247]. This variability is reflected in heterogeneous neuronal activity patterns. For instance, a large proportion of neurons in the mammalian neocortex fires at very low rates, wheras a small subset of strongly connected neurons is highly active [181, 43, 143, 290]. Another important property of neuronal networks is the systematic tendency of neurons to connect to others that are similar (or dissimilar), which is a form of connectivity correlations[1] [42, 247, 196]. In neuroscience, considerable effort has been spent to understand correlations in the activity patterns of spiking neurons [14, 118, 242], but much less attention has been paid to correlations in the connectivity structure. It is known that connectivity correlations strongly influence the structural robustness of a network [197, 289, 287, 276, 123, 196], but how do they affect the dynamics of a neuronal system? Can they be relevant for neuronal processing? These are two central problems we approach in this thesis. In

[1] Specifically, in this thesis we consider so-called *degree correlations*, where neurons preferably connect to neurons with similar (or dissimilar) number of inputs (their *in-degree*). A more detailed description is given in Section 1.1.1.

short, we focus on three research questions:

- Can we devise a stochastic model of the global network dynamics that integrates structural heterogeneity and connectivity correlations?
- How do these two features influence the dynamical and structural behavior of the system?
- Can we interpret the network's dynamics in terms of neuronal processing?

Along the way we will integrate a statistical description of the network structure into a reduced model of the neuronal activity, which we complement with numerical simulations.

The thesis is structured as follows. We begin by introducing the concept of network theory in **this chapter**, where we present several important measures and approaches that are commonly used to characterize the structure of a network. Moreover, we discuss how network theory is used in the field of neuroscience to describe the wiring architecture of the mammalian nervous system and we present several important observations in this regard. To be able to purposefully model the dynamical behavior of a neuronal system it is important to have a mathematical concept of the code embedded in the neuron's spiking patterns. Therefore, we briefly introduce the basic mathematical description of neuronal spike trains and discuss how they may encode information. In the final part of this chapter, we describe models of spiking neurons and, in particular, the leaky integrate-and-fire neuron model that is used in the next chapter.

In **chapter 2** we examine how connectivity correlations influence the global spiking dynamics of a heterogeneous neuronal network. At first, we develop a theoretical framework to calculate the mean activity in such a network in response to an external stimulus and we compare numerical simulations of large-scale networks with theoretical predictions. After that, we analyze how connectivity correlations affect the stimulus/response relationship and discuss the implications for the signal transmission capabilities of the network. We demonstrate that positive correlations significantly enhance the network's sensitivity to weak stimuli.

In **chapter 3** we characterize the structural properties of a correlated neuronal network in terms of a percolation process, complementing recent experimental studies on percolation of a developing neuronal culture [45, 246]. In addition to connectivity correlations we take into account metric constraints on the neuronal connections that emerge from the spatial embedding of a neuronal system. With numerical simulations we demonstrate that the percolation behavior of the network is strongly affected by an interplay of these properties so that one misses important features of the network by considering them individually.

1.1 Network theory

> *A Network is, in its simplest form, a collection of points joined together in pairs by lines.* (M. E. J. Newman, [196, page 1])

Put in simple terms as elegantly done by Mark Newman, the concept of a network seems unpretentious, yet its principle of abstraction allows us to describe immensely complicated systems. In general, networks represent systems that are comprised of individual elements which form connections with each other, and network theory enables us to analyze the patterns of these connections [196]. Even though we may not always recognize it, networks are an integral part of our daily lives. For example, we use transportation networks to be mobile, we communicate with each other via the internet and telephone networks, and even our social environment can be represented as a network of affiliations, which is the basis of social media such as Facebook and Twitter.

Indeed, social network models dealing with the patterns of human interactions laid the foundation of modern network sciences: Many measures and tools that are commonly used to characterize networks have been originally defined in social sciences [189, 188, 294, 108] (see [281, 231] for reviews). During the last decades there has been an explosion of interest in network theory across many different fields of science, including biology [183], transportation [31], communication [222] and neuroscience [247]. The increasing availability of large data-sets in these fields makes it possible to analyze and model systems of higher complexity, which increases the demand for analytic and descriptive mathematical methods that may rest on a network-theoretical approach. This development is supported by the increasing computational power that allows for crunching massive data-sets and improving software for network visualization and analysis [196].

The reduced mathematical representation of a network in terms of points and lines is called a *graph*. Graph theory is believed to originate in 1735, where Leonhard Euler first used the concept of a graph to solve the problem of seven bridges of Königsberg (now Kaliningrad) [8]. The seven bridges spanned the various branches of the river Pregal flowing through the town, creating four different parts of the city that could only be reached by passing a bridge as illustrated in Figure 1.1A. Euler was concerned with the question whether it was possible to take a walk by crossing all bridges, but every bridge only once. He used a graph representation of this problem, with nodes as the reachable parts of the city and edges as bridges (Figure 1.1B). From this abstraction he concluded that a traveler has to use two edges for each visit of a node - one for coming into the node and one for leaving it. Therefore, the desired walk is only possible if every node has has even number of edges connected to it, except for the starting and ending node. One can see by looking at Figure 1.1B that the desired trail in Königsberg does not exist.

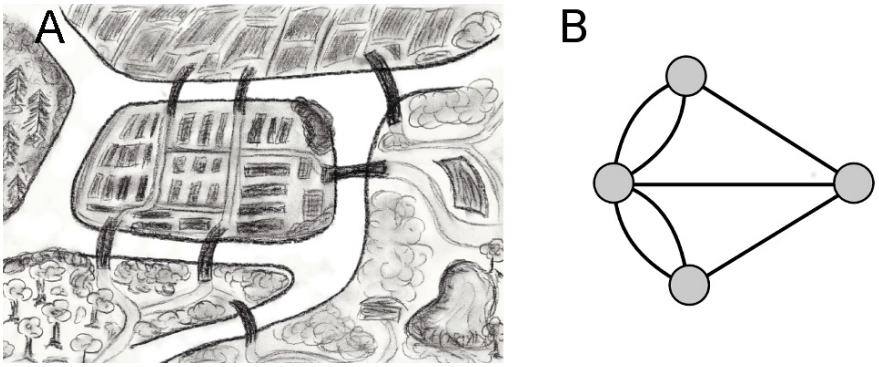

Figure 1.1. Schematic of the seven bridges of Königsberg (left) and the corresponding graph representation (right). Drawn from Katja Schäfer for this thesis.

Before we turn to a more quantitative description of network-theoretical concepts and measures, let us clarify some useful terminology. According to the previous definition by Newman, a network is a collection of points that are joined together by lines. Depending on the field of research, the points and lines are also called vertices and edges, nodes and links, or sites and bonds. A network may have more than one connection between any pair of nodes, or a connection of a node with itself. Such edges are known as *multiedges* and *self-edges*, respectively, and the corresponding network is called a *multigraph*. In our study we focus on networks without self-edges and multiedges, which are referred to as *simple graphs*.

Mathematically, a graph $\mathcal{G}(\mathbf{N}, \mathbf{E})$ is defined as a set of nodes $\mathbf{N}$ and a set of links $\mathbf{E}$, where each link connects a pair of nodes and thus can be represented by a tuple of these nodes, e.g. the link $e_{ij} = \{i, j\}$ connects node i and j. In an undirected network, the presence of a link connecting node i and j implies that there is also a connection between node j and i so that $e_{ij} = e_{ji}$. The two most fundamental properties of a graph are its number of nodes N and number of links E.

One of the most common mathematical representations of a graph is the *adjacency matrix* $\mathbf{A}$, with elements

$$A_{ij} = \begin{cases} 1 & \text{if node i is connected to node j,} \\ 0, & \text{otherwise.} \end{cases} \tag{1.1}$$

A simple example of a directed network and the corresponding adjacency matrix is shown in Figure 1.2. The adjacency matrix of an undirected network is symmetric, which implies $A_{ij} = A_{ji}$.

Self-edges in the graph are represented by the diagonal elements in the adjacency matrix. The i-th row represents the out-neighborhood of a node i, and consequently,

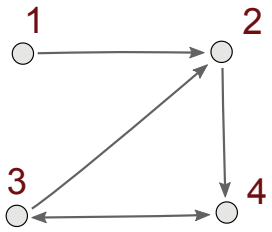

$$\mathbf{A} = \begin{pmatrix} 0 & 1 & 0 & 0 \\ 0 & 0 & 0 & 1 \\ 0 & 1 & 0 & 1 \\ 0 & 0 & 1 & 0 \end{pmatrix}$$

Figure 1.2. Example of a simple directed network and the corresponding adjacency matrix $\mathbf{A}$. The corresponding edgelist is given by $\{(1,2),(2,4),(3,2),(3,4),(4,3)\}$.

the i-th column represents its in-neighborhood. In the undirected case the in- and out-neighborhood of a node are equal to each other. Sometimes it is useful to provide additional information about the links in a network, e.g. some form of connection strength, by using graduate entries in the matrix instead of zeros and ones, which gives a *weighted graph*. Many structural properties of a network can be related to the spectral properties of the adjacency matrix, and the field of research dealing with these relationships is called *spectral graph theory*. [78].

For a network with N nodes the adjacency matrix is of size N^2, since it contains all pairs of nodes that possibly connect to each other. However, many real-world networks have much fewer edges so that they are labeled *sparse*. Since the adjacency matrix of sparse networks contains mostly zeros and only few ones it is more efficient to store only the nonzero entries that correspond to present edges. These edges can be represented efficiently by an edgelist that contains the tuples of nodes for each edge. For example, the network in Figure 1.2 has following edgelist: $\{(1,2),(2,4),(3,2),(3,4),(4,3)\}$. In addition to the above described adjacency matrix and edgelist there are other useful graph representations, e.g. in form of trees or incidence matrices, which are explained in [196].

1.1.1 Important measures

Networks can be characterized at multiple scales. At the finest scale, we can quantify the connectivity of single nodes and the topology of their immediate neighborhood with various local measures. At the macroscale it is meaningful to characterize the network architecture in terms of global measures and distributions of local quantities.

Degree. Certainly the most important local measure is the *degree* of a node, which is simply the number of its neighbors. In an undirected network the degree k_i of a node i is $k_i = \sum_j A_{ij}$. In a directed network we distinguish between the in-degree k_i and out-degree j_i of a node, where

$$k_i = \sum_j A_{ji}, \quad \text{and} \quad j_i = \sum_j A_{ij}. \tag{1.2}$$

In the example of Figure 1.2, node 2 has in-degree $k_2 = 2$ and out-degree $j_2 = 1$. The

mean degree of a network is an important global measure of its connectivity and it is defined in undirected networks as

$$\langle k \rangle = \frac{1}{N} \sum_i k_i = \frac{2E}{N}. \tag{1.3}$$

In directed networks, we can calculate the mean in-degree $\langle k \rangle$ and mean out-degree $\langle j \rangle$. The number of ingoing links in the network has to match the number of outgoing links, which implies $\langle j \rangle = \langle k \rangle = E/N$.

Degree distribution. An important global property of a network is the probability distribution $P(k)$ of node degrees, which is called *degree distribution*. A network, where all nodes have the same degree, is called *regular*. Common examples for regular networks are various lattices, e.g. the square lattice, where each node has degree 4. However, a large number of real-world networks has a non-trivial degree distribution, where the node degrees vary over several orders of magnitude [196]. It has been found that for large k these degree-distributions can often be approximated by a power-law,

$$P(k) \sim k^{\bar{\gamma}}, \quad \bar{\gamma} < 0. \tag{1.4}$$

For many real-world networks, the exponent has been identified as $-3 < \bar{\gamma} < -2$ [199, 20]. Unfortunately, most empirical data exhibits large fluctuations in the region of large k, since only few large-degree nodes are present. Therefore, care has to be taken in identifying power-laws in such data, and many studies reporting power-law distributions in real-world networks have been questioned after re-examination with meticulous statistical analysis [80].

Networks with power-law degree distribution are called *scale-free*, because they lack a characteristic measure: A rescaling of the argument in a power-law degree distribution $P(ak)$ with a constant a simply leads to the rescaled distribution $bP(k)$ with constant b so that its form is maintained. Examples for scale-free networks are the world wide web [19], the network of internet routers [101], scientific citations [21], and functional brain networks [97].

Degree correlations. Roughly speaking, degree correlations describe the preference of nodes to attach to others with similar (or dissimilar) degree, which is a form of a mixing pattern, or connectivity correlation. If nodes preferably join to others with similar degree, the network is said to be *assortative*. Conversely, in a *disassortative* network, nodes prefer to attach to those with a dissimilar degree. In directed networks the distinction between in- and out-degree allows for two types of degree correlations, (1) correlations between in- and out-degree per node and (2) degree correlations between pairs of nodes. The latter constitute correlations between the in-degrees (in-in) and out-degrees (out-out) of the connected nodes, and correlations between their in- and out- degrees (in-out and out-in). Mixing patterns in networks can also be associated

with other node attributes than the degree [198].

Pearson coefficient. Often it is useful to measure degree correlations with a single quantity. One of the most widely used measure in this regard is the Pearson degree correlation coefficient [198], which is defined as follows for undirected networks. Assume that we point to a random edge in the network. We are interested in the degrees of the nodes at either end of the edge. In fact, we consider their *excess degrees* (or remaining degrees) l and m, which is one less than their actual degree. The excess degree at either end of a random edge is distributed as

$$Q_m = \frac{(m+1)P(m+1)}{Z}, \tag{1.5}$$

where $P(m)$ is the degree distribution of the network and $Z = \sum_m mP(m) = \langle m \rangle$. Let us define e_{lm} as the probability that a randomly chosen link joins together two nodes with excess degrees l and m, respectively. The excess degree distribution is related to e_{lm} via

$$Q_m = \sum_l e_{lm}. \tag{1.6}$$

With these quantities the Pearson degree correlation coefficient can be defined as [198]

$$p = \frac{1}{\sigma^2} \sum_{lm} lm(e_{lm} - Q_l Q_m), \tag{1.7}$$

where the variance $\sigma^2 = \sum_m m^2 Q_m - (\sum_m mQ_m)^2$ normalizes the Pearson coefficient such that it ranges from -1 for a fully disassortative network to 1 for a fully assortative network. For an uncorrelated network e_{lm} takes the value $Q_l Q_m$ and the Pearson coefficient becomes zero. For directed networks, p can be defined slightly differently to measure correlations between in-degrees, out-degrees, or in- and out-degrees of pairs of nodes. We are interested in the in-degree correlations (in-in) of graphs where nodes have equal in- and out-degree. Following [198] these correlations can be measured by

$$p_{\text{in}} = \frac{1}{\sigma^2_{\text{in}}} \left[\sum_{mm'} mm' e_{mm'} - Q^{\text{in}}_m Q^{\text{in}}_{m'} \right], \tag{1.8}$$

where $e_{mm'}$ is now the probability that a randomly chosen directed link goes into a node of excess in-degree m and out of a node of excess in-degree m' (which is equal to its excess out-degree). Q^{in}_m is the excess in-degree distribution of a node

$$Q^{\text{in}}_m = \frac{(m+1)P^{\text{in}}(m+1)}{Z}, \tag{1.9}$$

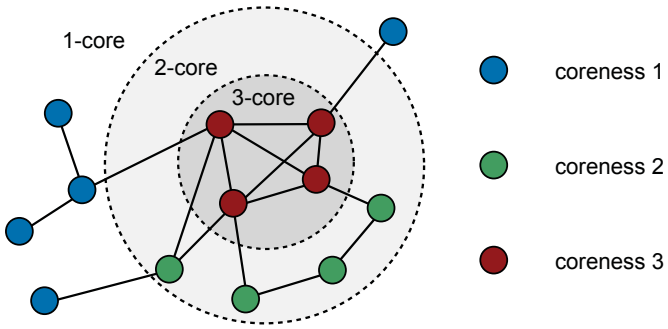

Figure 1.3. Schematic of the k-cores of a simple graph. A k-core subgraph is obtained by successively removing all nodes with degree less than k from the original graph. The coreness of a node denotes the highest k-core it belongs to.

where $Z = \sum_m m P^{\text{in}}(m) = \langle m \rangle$. The directed Pearson degree correlation coefficient is normalized by the variance of the excess in-degree distribution $\sigma^2_{\text{in}} = \sum_m m^2 Q^{\text{in}}_m - (\sum_m m Q^{\text{in}}_m)^2$ so that it ranges from -1 for a fully disassortative network to 1 for a fully assortative network as in the undirected case. Note that the measure of Equation (1.8) is sufficient to quantify in-degree correlations when in- and out-degree are equal for each node. Otherwise, it may be required to use alternative measures as proposed by [211].

k-Core decomposition. A useful tool for the visualization and analysis of large-scale networks is the k-core decomposition: The network is dissected into components of increasing connectivity, called *k-cores* [232]. A k-core subgraph is obtained by successively removing all nodes with degree less than k from the original network (Figure 1.3). Originally, k-core decomposition was mainly used to understand the structure of social networks [232] and soon it has been found valuable for many other systems, e.g. for epidemic spreading in complex networks [91, 234, 120], protein interaction networks [285], and for the visualization of large-scale networks [9].

Path. A path is defined as a sequence of links that connects two nodes, and the number of links making up the sequence is considered as the path length. In a densely connected network it is common that two nodes are connected by several different paths. Then, the shortest path is called the *chemical distance* between the nodes. If the network is embedded in Euclidian space, the chemical distance between two nodes can be related to their Euclidian distance. A useful global measure is the average path length of a network, which is defined as the average length of all shortest paths.

Clustering coefficient. Many real-world networks have the tendency to be transitive, which means that they contain a large number of triangles. This tendency is very prominent in social networks, where people knowing each other often have mutual friends. The transitivity of a network can be measured by the global clustering coeffient [196]

$$\mathcal{C} = \frac{3 \text{ x number of triangles}}{\text{number of connected triplets of nodes}}, \tag{1.10}$$

which is normalized such that it ranges from 0 to 1. There is also a local clustering coefficient that can be used to examine the transitivity of a node's neighborhood [196].
Small-world effect. The concept of the small-world phenomenon was originally developed about 50 years ago by Stanley Milgram, who found that in social networks people are linked by surprisingly short chains of acquaintances [189]. In laymans terms, the effect is also known as the 'six degrees of separation'. The problem was then studied more mathematically by Watts and Strogatz, who introduced a small-world network model that could mimic the behavior from Milgrams observation [282]. In essence, the model constitutes a regular lattice, where a proportion of links is randomly rewired, so that they act as short-cuts. Consequently, the model resembles an interpolation between a highly ordered lattice and a highly disordered random network, featuring a high clustering coefficient that is characteristic for lattices and a short average path length that is typical for random networks. Watts and Strogatz declared a network as small-world, if it exhibited a high clustering coefficient and at the same time a small average shortest path length, although they did not define a sharp quantitative criterion. Many real-world networks have been found to show small-world features, e.g. transportation networks [162, 163, 233], or neuronal networks [42, 26, 3, 132, 56, 207].

1.1.2 Random network models

Graph-theoretical measures, such as the above described, are very useful for characterizing the structure and behavior of real-world networks. In turn, they can be used to create random network models that mirror a system of interest. A random network, or random graph, generally refers to an ensemble of graphs which are generated by a probabilistic method. Consequently, a single graph is only one of all possible realizations. Random network models are particularly useful for studying how specific structural attributes emerge in the process of generating the network, and how such attributes influence other network properties, e.g. its structural robustness. Moreover, it is often possible to examine the structural behavior of the network (or the dynamics taking place on it) mathematically the limit of infinitely large size.

Erdős-Rényi (ER) model. Back in 1959, Paul Erdős and Alfréd Rényi were the first to study random networks systematically using a simple probabilistic generation mechanism. An Erdős-Rényi graph $\mathcal{G}(N, p)$ with N nodes is generated by connecting each of the possible $\frac{N(N-1)}{2}$ node pairs by an undirected link with probability p. Alternatively, one can fix the number of edges E in the graph and choose a realization uniformly at random from the ensemble $\mathcal{G}(N, E)$ of all possible conformations with N nodes and E edges. Since the ER network was the first random network model to appear in the technical literature, it is often referred to as the *random graph*. In the limit of infinite network size both construction methods produce graphs with equal behavior. We here

focus on the first and more popular construction method $\mathcal{G}(N, p)$, and we give a quick introduction into some important features of this model.

From the construction algorithm we immediately see that the expected mean degree of the network is $\langle k \rangle = p(N-1) \simeq pN$ for large N. The probability for a random node to be of degree k equals the probability that it is connected to k other nodes, but not to the $N-k-1$ remaining nodes in the network. Thus, the distribution of degrees is binomial

$$P(k) = \binom{N-1}{k} p^k (1-p)^{N-k-1}. \tag{1.11}$$

For large N this distribution can be approximated by a Poisson distribution

$$P(k) = \frac{(pN)^k}{k!} e^{-pN}. \tag{1.12}$$

Erdős and Rényi studied the behavior of the graph for increasing density of links in the limit of large N. They observed that for small p the graph consists mainly of isolated nodes and small connected components. As p increases, clusters of increasing size are formed until the graph undergoes a sudden structural change: For a certain 'critical' value of $p = p_c$ a so-called *giant connected component* emerges that contains the majority of nodes in the network. At this point, the graph is said to undergo a phase transition into a percolating phase. Phase transitions in lattices and random networks are the main topic of percolation theory, which we introduce in Chapter 3. The threshold $p_c = 1/N$ for which the giant component emerges in the ER graph was found by Erdős and Rényi one year after they developed the model [99]. Decades later, Newman proposed a method to calculate the complete distribution of component sizes for the graph [199].

Another quantity that can be immediately calculated for the ER graph is the global clustering coefficient. The clustering coefficient can be defined as the probability that two neighbors of a node in the network are also neighbors of each other. According to the construction algorithm, any pair of nodes is connected independently with probability p and thus, the clustering coefficient is

$$\mathcal{C} = p = \frac{\langle k \rangle}{N-1}. \tag{1.13}$$

We see that for $N \to \infty$ the clustering coefficient vanishes if the mean degree is held constant.

Configuration model. The configuration model can be used to construct graphs with arbitrary degree distribution [200]. The algorithm works as follows for directed networks: First, it assigns each node a target in-degree and out-degree, which are

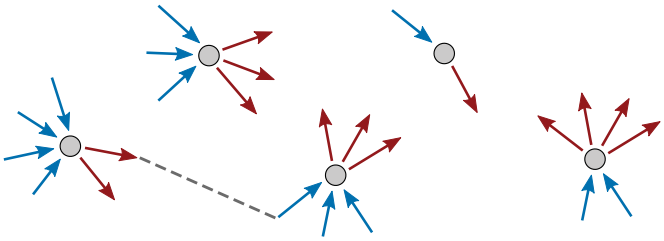

Figure 1.4. Schematic of constructing a directed graph according to the configuration model. Nodes are assigned ingoing and outgoing stubs according to the corresponding in- and out-degree distributions (blue and red arrows). Then, random pairs of these stubs are joined together to form directed links (dashed line).

drawn from the desired in- and out-degree distributions[2]. The target in-degree of a node can be regarded as a number of ingoing stubs and its target out-degree as a number of outgoing stubs, respectively (Figure 1.4). Pairs of outgoing and ingoing stubs are drawn at random to create directed links. In the undirected case, pairs of stubs can be drawn from the same list. The configuration model is based on the *matching*-method, where links are generated according to a desired property of the network. An alternative approach is the *switching*-method, which starts from a given network with the desired properties and performs edge swaps to randomize the graph. Advantages and disadvantages of both methods are discussed in [190]. Random graphs that are generated with the configuration model can be examined analytically to some extent for $N \to \infty$. For example, the minimum density of links required for the existence of a giant component could be derived in [192, 193] for undirected graphs. Further, Newman et al. developed a powerful method based on generating functions to calculate many other statistical properties of the network, e.g. the average path length, the clustering coefficient and the distribution of component sizes [200].

Besides the two network models introduced above, there are many other random graph models that are reviewed in [199, 7, 39, 41, 196]. Among the most important are diverse *lattice models*, where nodes are embedded in space with a regular pattern, the *Barabási-Albert* model [18] that generates a graph according to the principle of preferential attachment, and the *exponential random graphs* [259] that describe random networks in terms of their ensemble statistics.

1.2 Networks of the brain

First steps towards understanding the structural organization of the nervous system were made in the late 19th century with the finding that the nervous system is made up of discrete processing units, the nerve cells. This *neuron doctrine* opposed the common view of the nervous system as a continuous network of thin neuronal fibers. A

[2]The total number of ingoing and outgoing links has to match, which implies that the in- and out-degree distributions must have the same mean.

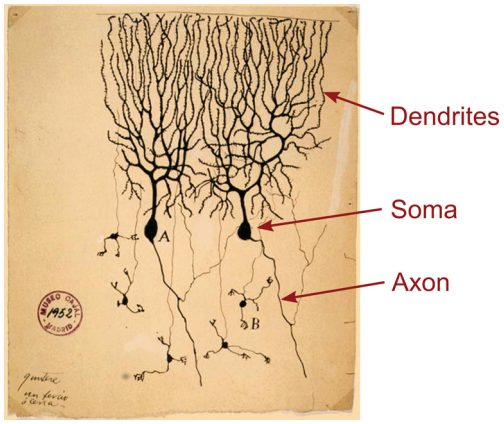

Figure 1.5. Original drawing of several pigeon neurons from Santiago Ramón Cajal in 1899 using Golgi's silver staining method [67]. Shown are two cell types, (A) purkinje cells and (B) granule cells from the cerebellum. The picture illustrates the high level of detail that could be inferred from the stained nervous tissue.

major reason for this controversy was the limited possibility to actually observe the detailed structure of nervous tissue. In 1873 Golgi invented the silver staining method that made it possible for the first time to see nerve cells with their soma (cell body), extended axon and highly branched dendrite structure. Figure 1.5 shows a drawing of several pigeon nerve cells from his close colleague Santiago Ramón Cajal, who extensively used Golgi's staining method. Paradoxically, Golgi himself rejected the idea that neurons function individually, arguing that the nervous system acted as a whole integrated system. Nowadays, it is known that the elaborate global behavior of a system may very well emerge from the activity of individual elements that communicate in a network.

During the 20th century, advances in experimental techniques led to a large amount of anatomical and electrophysiological research on brain activity in humans and animals. An important finding was that the brain is functionally and structurally segregated into different localized regions [210, 293, 103]. These regions are specialized on a neuronal level and on a structural level, since they are composed of different neuron types and they exhibit distinct connectivity structures. However, the idea of functional localization was not new. Even before the neuron doctrine was established, Franz Joseph Gall [115] proposed that personality traits could be identified on the basis of the scull shape. His idea created a new scientific field called *phrenology*. Soon phrenology was rejected because it lacked scientific proof, but it can be credited for establishing the idea to relate the brain's anatomy to specific functions. The relation between structure and function of neuronal tissue becomes particularly apparent if certain brain regions are damaged and malfunction. Observational studies and neuroanatomical experiments on damaged brain areas laid the foundation for the generation of the first cortical maps that associated several brain areas with certain cognitive tasks [52].

Soon the development of extremely powerful imaging technologies allowed for noninvasive detection of neuronal activity. For example, electro- and magnetoencephalogra-

phy (EEG and MEG) measure the electric and magnetic fields the brain generates on the skull surface. Magnet resonance imaging (MRI) reveals microscopic details about the nervous tissue that can also be related to the actual activity of the neurons in the scanned region. These and many more modern imaging methods provide information about the structure and dynamics of the human brain at various spatial and temporal scales. An ambitious goal is to create a complete map of the brain's wiring structure, which has been termed the *human connectome* [252, 248]. So far, the connectome has been successfully constructed only for one animal, the roundworm C. Elegans [283, 274]. White et al. [283] were the first to reconstruct the anatomical connectivity structure of its nervous system from serial sections of 50 nm thickness. Comprised of 302 neurons and 6393 chemical synapses, the system is rather simple and stereotypic for an animal [274]. Mapping the human connectome is far more challenging: It is made up of about 10^{11} neurons and thousand as many chemical (and electrical) synapses [151, 247].

1.2.1 Measuring the connectivity structure

The increasing availability of data describing our neural system comes with a number of challenges. First of all, the various imaging methods differ not only in spatial and temporal scale of the measured brain region, but also in the type of data they produce and the definition of connectivity they are based on [141, 167, 252]. Therefore, it is difficult to define an exact universal concept of how the connectivity structure of the nervous system should be quantified. Three different definitions of connectivity are commonly used. First, the *anatomical connectivity* describes the physiological connections between neurons or brain regions. Second, the *functional connectivity* is based on the functional interaction between brain areas that can be inferred from correlations of activity, e.g. from noninvasive measurements. Functional connectivity cannot be directly related to the anatomical connectivity, since correlations between the activity in distinct areas may arise without a direct anatomical connection between them. To overcome this problem, a third measure of connectivity was proposed, the *effective connectivity*, which requires taking into account causality in functional correlations [112, 270].

Neuroscientists examine the brain at various levels of organization, which can be roughly divided into [247]

- the microscopic level of individual neurons and their connections,
- the mesoscopic level of neuronal populations and local circuits,
- the macroscopic level of brain areas, large-scale networks and information pathways.

Unfortunately, it is difficult to cross the scales, since each level can only be examined with specific measurement tools that produce different types of data.

Another problem in quantifying the connectivity structure of the nervous system is that neuronal networks are not static. Anatomical networks are subject to plasticity and functional networks depend on the actual dynamical state of the system. Moreover, we cannot consider each of the network types independently if we want to understand how the nervous system operates. On the one hand, if we consider only the anatomical connectivity, it still remains unknown whether neurons that are coupled to each other also exhibit functional correlations. On the other hand, we cannot properly interpret the functional relation between neurons (or brain areas) without knowledge of their anatomical wiring, because we lack information about the causality of these relations. For instance, correlations between the spike trains of two neurons may arise without a direct anatomical coupling between them. Relating the structure and function of neuronal networks is therefore a central problem in neuroscience. However, even for the relatively simple neuronal network of the C. Elegans the relation between network structure and function is still not understood, partly because the electrophysiological properties of some cell types have not yet been characterized [124, 274].

A major challenge is the sheer complexity of a neural system: It usually comprises various different types of neurons, which themselves exhibit complex activity patterns. Moreover, the transmission of signals by chemical and electrical synapses is modulated by various neurophysiological processes. To make matters worse, the anatomical and functional brain structure is highly variable across distinct species, and individual animals are characterized by unique traits. However, the nervous systems of distinct species also share many similarities, because all of them serve the same purpose of survival. Hence, it is reasonable to assume that the architecture of the brain is driven towards functional homeostatis and at the same time allows for the realization of individual features. This requires for some amount of flexibility of the brain structure with respect to its functional properties, which is supported by the observation that certain processing task can be achieved by different neuronal circuits [215, 180].

1.2.2 Architecture of the brain

Although it is possible that every single connection between neurons serves a function which we are unable to reveal with our current methods, some redundancy must be present, since the failure of single neurons usually does not change the overall performance of a neuronal network [151, 85, 247]. Therefore, the emphasis has shifted to a probabilistic description of the nervous system's structure and modern network science and graph analysis tools have been increasingly used to reveal relevant aspects of the network architecture. Much effort has been spent to find common features across distinct species, because these features likely point to basic principles of organization that are worth to explore. Neuronal networks are sparse with a mix of repeating patterns and seemingly random features [42, 56, 247], which we briefly introduce in the following

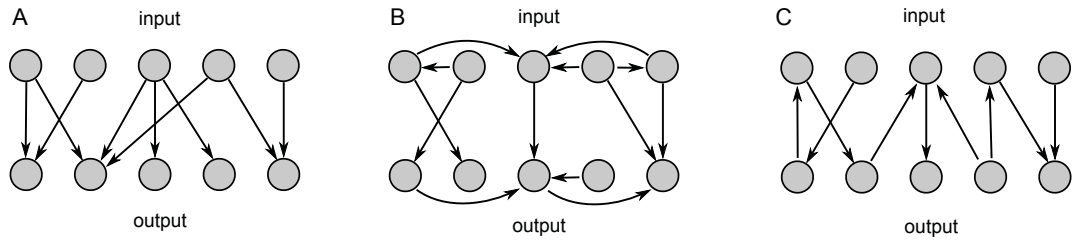

Figure 1.6. Different types of the local circuitry. (**A**) Feedforward network, where one layer of neurons transmits activity to another layer at a later stage of processing. (**B**) Recurrent network, where activity of the neurons at within a layer is fed back through recurrent connections. (**C**) Top-down network, where signals are sent back to earlier stages.

.

At the microscopic scale, it has been empirically observed that chemical synapses can be divided into two types, excitatory and inhibitory synapses. Excitatory synapses, if activated, promote activity in the postsynaptic neuron and inhibitory synapses demote it. A neuron can make dendritic connections with both synaptic types so that it can receive a mix of excitatory and inhibitory input. On the other hand, its axon almost always connects to synapses of the same type. Therefore, neurons are commonly classified as excitatory or inhibitory, although this distinction is really a feature of their axonal connections. Most areas of the nervous system are made up of about 80% excitatory neurons and 20% inhibitory neurons [151]. Often the inhibitory neurons are more strongly connected to 'compensate' for their smaller number, so that the spread of activity of excitatory and inhibitory neurons is somewhat balanced. Most of the neurons form synaptic connections with a large number of other neurons in a complex pattern that is constantly modified by factors such as nutrition or learning mechanisms.

Most of the synaptic connections are rather local [42, 133, 126], which likely results from minimizing the wiring volume [191, 76, 57]. A small proportion of long-range connections allows for rapid information flow across distant areas. The locality of links results in a high clustering coefficient, and the long-range connections promote a short average path length. Consequently, a large number of neural systems has been identified as small-world [42, 26, 3, 132, 56, 207]. Interestingly, small-world features have also been observed in neuronal networks grown *in-vitro* [94, 87]. Although distance is an important factor in the development of neuronal connections, limited space is not the only constraint. The brain must maximize its capacity for processing information, which involves a fast signal propagation with high precision, and at the same time minimize the metabolic costs for the generation of activity [164].

At the mesoscopic scale, the brain is organized into hierarchically arranged circuits [102, 296, 126]. The neocortex is a very illustrative example for this hierarchical organization. Neurons in this brain region are arranged in vertical patches, called *cortical*

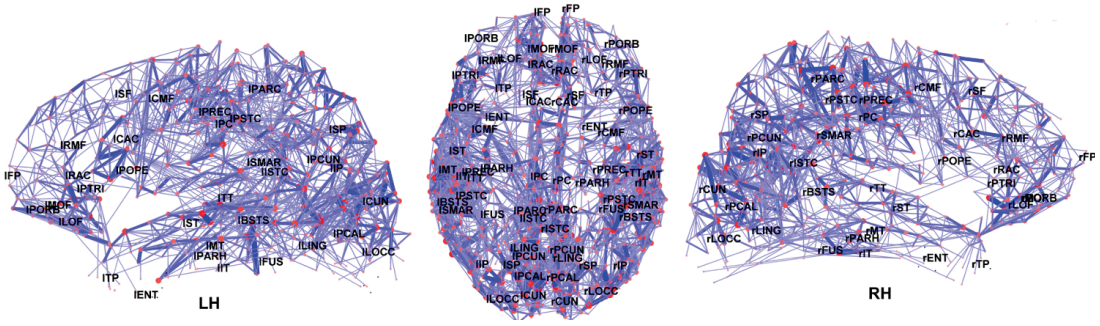

Figure 1.7. Connectivity backbone of the human brain from diffusion spectrum MRI, plotted in anatomical coordinates [126]. Nodes are regions of interest and links represent the fiber densities between the regions. Lateral view (left and right picture, LH = left hemisphere and RH = right hemisphere) and dorsal view (middle picture).

columns of about 10^5 neurons, which could be identified as the basic functional units for information processing [151]. These separate circuits are highly coupled so that activity can be transmitted through successive stages of a processing pathway. The local circuitry of the columns can be divided into three main classes,

- feedforward, where activity is transmitted to a region at later stages of the processing pathway,
- recurrent, where neurons are coupled within the same stage of processing,
- top-down, where signals are sent back to earlier stages.

Examples for a feedforward, recurrent and top-down network are shown in Figure 1.6. Recurrent neuronal networks are particularly interesting, because their recurrent activity resembles a feedback mechanism that enables the neuronal population to preserve its functional state, which is particularly important for memory processes. All three neuronal circuits are increasingly used in the design of artificial intelligence [139, 140, 175, 230].

At the macroscale, the brain is organized into various modules that differ in their function and cytoarchitecture [247]. Graph-theoretical analysis at this level reveals a structural core of central hub regions that are strongly connected to each other. Since these hub regions link together all major structural modules [126], they likely play an important role in the integration and processing of information [3, 250, 271]. Figure 1.7 shows an exemplary graph representation of the macroscale brain architecture that has been obtained with diffusion spectrum MRI [126]. The graph exhibits groupings of highly connected regions that are located along the cortical surface.

1.3 Modeling neuronal activity

How does complex brain activity emerge from the interaction of many spiking neurons? This question is well-suited for theoretical and numerical modeling. A wide spectrum of models are available that range from highly abstract binary neurons to highly detailed neuron models that take into account specific features at the molecular level [118, 85, 216, 49]. Models of neuronal activity have to integrate two components, the description of activity of single neurons (or populations of neurons) and rules for spreading the activity through the network of their synaptic connections. The level of complexity has to be chosen with care, since a more detailed model does not necessarily provide more insight into the system of interest for several reasons. First, despite large efforts, the exact network structure of the mammalian brain is still not known, so that one has to rely on guessed parameters. Second, complex activity patterns already emerge in relatively simple systems [53, 118, 223] so that a model of increased complexity does not necessarily provide additional insight, but it certainly is more difficult to implement and interpret. Third, the level of detail a model can provide is limited by computational resources and time.

However, it is meaningless to model the spiking dynamics of a neuronal network without being able to interpret the activity patterns of the neurons. This requires a basic mathematical concept of neuronal spiking as a coding mechanism, which we introduce in the next section.

1.3.1 The neural code

The way everyone of us perceives reality may be highly individual, but the underlying mechanism is remarkably similar: Our experience of the world is essentially an interpretation of the spike trains sent to our brain by our sensory nerves. For example, patterns of light falling onto the retina are converted into patterns of spikes, which are sent to our visual cortex by the optical nerve, and our brain interprets these spiking patterns as a colored image. Not only sensory information is encoded in spike trains, also computations and decision processes are based on these activity patterns. In fact, neurons use spikes as a primary signal to communicate with each other and if we want to make sense of the neuronal activity, we need to understand how their spiking patterns encode information.

As a first approach it is meaningful to search for universal principles of spiking that apply to the majority of neurons. Some of the most important principles were established by Adrian et al. in the early 30s [4, 5]. First, he proposed the so-called *all-or-none law*, which states that neurons encode information in a binary way - either they produce a spike or they do not. Although the spikes (also called action potentials) vary in shape, duration and amplitude, they are commonly treated as identical

events because their characteristics appear to be far less relevant in neural coding than the timing of their occurance [85]. Most computations in the brain are mediated by spikes, although in some regions the neurons primarily communicate with each other via graded potentials (e.g. in the retina) [151]. Second, Adrian observed that the rate of spikes emitted by a sensory neuron correlates with the intensity of a stimulus applied to the corresponding sensory region. Later, this rule was generalized to the concept of *feature selectivity*, stating that the response of a neuron is maximized for a certain set of parameters, e.g. a pattern of light for retinal neurons.

Rate coding or temporal coding?

Adrians observation made a strong point for the concept of *rate coding*, which claims that the mean firing rate of a neuron conveys most of the relevant information [4, 22]. However, it is also possible that information is encoded directly in the precise timing of each spike, which is known as *temporal coding*. This mechanism has been shown to play a significant role in brain functions where fast processing is important, e.g. in the visual cortex [277, 262, 61], auditory cortex [77], or the hippocampus [144]. In these networks, the temporal resolution of the neural code is of the order of a few milliseconds, which is roughly the duration of a single action potential [177]. Whether most information is carried by rate coding or temporal coding is a hotly discussed topic within the neuroscience community. However, a clear distinction between the two coding schemes is rather difficult, since the ensemble-averaged firing rate of several neurons can also change on very small timescales [85, 118].

A different view on this problem has been proposed by Dayan and Abbott [85]. They suggested to ask whether information is encoded independently by each action potential or if correlations between spikes of a neuron are important. If one assumes that neuronal spiking is uncorrelated, then all information is carried by the firing rate, which would indeed classify as rate coding. On the other hand, additional information may be carried by correlations between the timing of spikes that would go missing if one assumed independent spiking. One example of this strategy is the encoding of information in the interspike intervals between action potentials [74, 173].

Correlations may also exist between spikes of different neurons. In Figure 1.8 we show some examples of spiking correlations across a population of neurons. If the neurons spike independently of each other as illustrated in Figure 1.8A, the mean firing rate $\hat{r}(t)$ of the population conveys all the relevant information. One example of a possible correlation coding mechanism is the synchronous activity of two or more neurons, which means that they fire spikes at similar times (Figure 1.8B). The synchronous firing appears in the mean population firing rate as sharp peaks, but the exact information about which neurons synchronize goes missing if one only regards the population mean.

Another mechanism for a correlation code involves oscillatory activity of the popula-

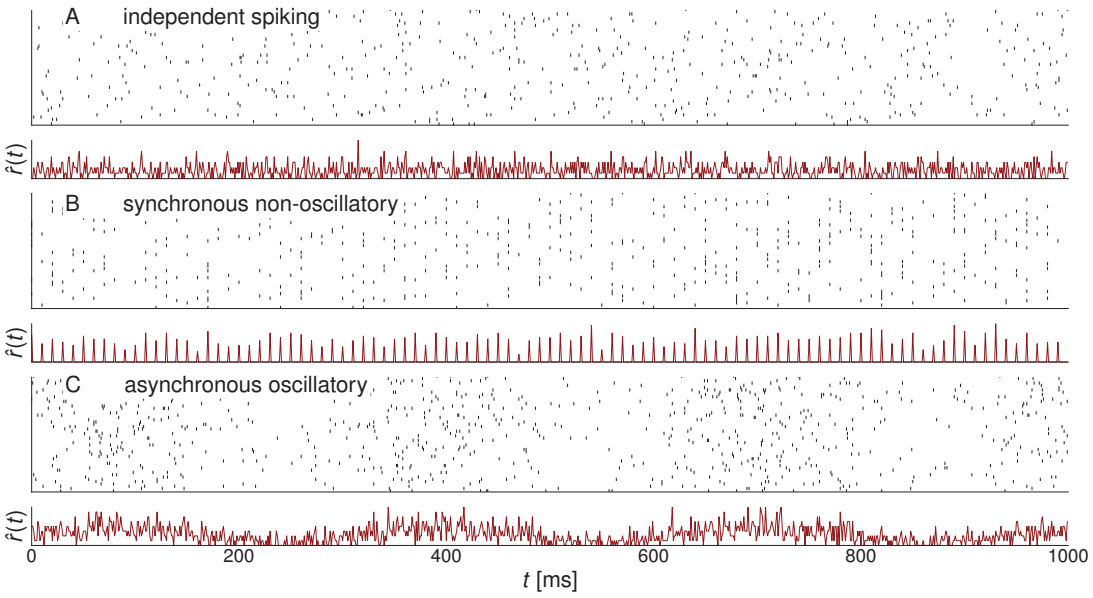

Figure 1.8. Raster plots of spikes for a population of neurons. Below each raster plot we show the ensemble-averaged firing rate $\hat{r}(t)$ of the neurons, which we calculated by sorting the spikes into bins of 1 ms.

tion due to similar variations in the firing rate of the neurons (Figure 1.8C). Additional information may be carried by the spike timing of individual neurons in relation to the oscillatory population activity. This correlation mechanism has been shown to play a role in the rat hippocampus, where so-called *place cells* encode information about the spatial location of the animal by producing spikes with respect to the phase of the global oscillation [269]. Although synchronization [256, 111, 110] and oscillations [125, 257, 63] have been frequently observed in neuronal activity, it is often not clear whether these correlations also carry significant additional information [85].

Stochastic description of spike trains

A precise and universal formulation of the neural code requires a mathematical description of the spiking patterns. If we neglect the relatively short duration of an action potential (about 1 ms) we can represent a sequence of m spikes, e.g. the spike train of a single neuron, by a sum of infinitely narrow Dirac delta functions [85]

$$f_R(t) = \sum_{i=1}^{m} \delta(t - t_i), \tag{1.14}$$

where $f_R(t)$ is called the response function, and t_i is the time at which the i-th action potential occurs. The response function can then be used to express the recording of a spike train over a time-period T as an integral

$$\int_0^T dt' h(t') f_R(t') = \sum_{i=1}^{m} h(t_i), \tag{1.15}$$

where $h(t)$ can be a function of choice to model the individual response of a neuron to the spike train: For example, by setting $h(t_i) = J$ we could describe a series of equal voltage-jumps J that were measured in a patch-clamp recording of a neuron's membrane potential. Using the response function (1.14), we can define the instantaneous rate $r(t)$ of a spike train as

$$r(t) = \lim_{\Delta t \to 0} \frac{1}{\Delta t} \int_t^{t+\Delta t} dt' f_R(t'). \tag{1.16}$$

In real experimental recordings, the firing rate of a neuron can be estimated by counting the number of spikes within a small time window Δt and dividing that number by the window size. The above definitions set the mathematical basis for quantifying the response of a neuron to a given stimulus.

In experiments it has been observed that neuronal spiking is highly irregular: Different trials involving the same stimulus yield different responses [243, 85]. It is not resolved whether these irregularities carry significant amounts of information [243, 235, 236, 118], but for convenience they are often considered as *noise*. Consequently, the spiking patterns can be described as a stochastic processes, which often considerably simplifies their analysis [118, 174, 85, 223].

The Poisson process. The simplest stochastic process that generates sequences of spikes is the *Poisson process*. It is based on the assumption that the probability for a spike to occur is independent from all preceding activity. Poisson processes have been widely used to approximate stochastic neuronal firing, because they are particularly simple to handle mathematically [85]. Due to the lack of correlations the process is sufficiently described by the instantaneous firing rate $r(t)$. If the firing rate is constant over time the process is called the *homogeneous* Poisson process. The *inhomogenous* Poisson process is characterized by a time-dependent firing rate. For very small time-periods we can approximate the inhomogeneous Poisson process by a homogeneous Poisson process.

A spike train that is generated by a homogeneous Poisson process can be characterized as follows. Since the firing rate does not change over time, we can set $r(t) = r$. The probability to find n spikes during a time-window Δt is given by the Poisson

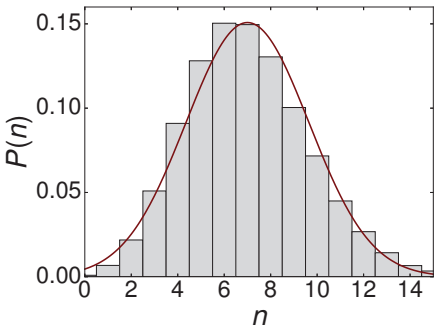

Figure 1.9. Poisson distribution. Probability to find n spikes during the time period Δt for which $r\Delta t = 7$ (bars), according to the Poisson distribution $P(r\Delta t, n)$ of Equation (1.17). The red line is the corresponding Gaussian approximation (1.20).

distribution

$$P(r\Delta t, n) = \frac{(r\Delta t)^n}{n!} \exp(-r\Delta t). \tag{1.17}$$

If the time-window is small ($r\Delta t \ll 1$), we can approximate the probability to find a spike during Δt as

$$P(r, \Delta t) \simeq r\Delta t. \tag{1.18}$$

This mechanism is particularly easy to generate on a computer. For each time-step Δt one simply draws a random number uniformly between 0 and 1 and generates a spike if this random number is smaller than $r\Delta t$. From Equation (1.17) it is easy to calculate the mean $\langle n \rangle$ and variance σ_n^2 of the spike count in the time window Δt,

$$\langle n \rangle = r\Delta t, \quad \text{and} \quad \sigma_n^2 = \langle n^2 \rangle - \langle n \rangle^2 = r\Delta t, \tag{1.19}$$

which are both equal. The fraction between the variance and mean of the spike count is called *Fano factor*. For a homogeneous Poisson process the Fano factor takes the value one. The superposition of two independent Poisson processes with rates r_1 and r_2 is again a Poisson process with rate $r = r_1 + r_2$. Assuming that a neuron receives Poissonian input from several independent sources, this means that its total input can be described as a single Poisson process whose rate is the sum of rates of the individual inputs.

For large $r\Delta t$ the Poisson distribution can be approximated by a Gaussian distribution

$$P(r\Delta t, n) \simeq \frac{1}{\sqrt{2\pi r\Delta t}} \exp\left(-\frac{(n - r\Delta t)^2}{2r\Delta t}\right). \tag{1.20}$$

In Figure 1.9 we show an exemplary plot of a Poisson distribution $P(n)$ for $r\Delta t = 7$

and the Gaussian approximation (1.20). Although Poisson processes and their Gaussian approximations have been widely used to describe neuronal activity, there is also much evidence that spiking activity in the brain is correlated [173, 14, 118, 242]. It is possible to deal with this problem by considering generalized stochastic processes that generate correlated spiking activity. These processes can be roughly divided into two categories: *renewal processes*, where the current spiking activity depends only on the immediately preceding event and *nonrenewal processes*, where the dependency goes back several events, up to the complete history of activity. The Poisson process is a special form of a renewal process, since the current activity does not depend on any of the preceding events.

1.3.2 Spiking neuron models

Nerve cells are highly specialized for the task of processing and transmitting electrical and chemical signals. Although they greatly vary in shape, size and molecular properties, their function rests upon similar electrochemical principles that are known in great detail. Based on these principles it is possible to develop models of neuronal activity. Typically, a neuron consists of a cell body (the soma) that is connected to an axon and a highly branched structure of dendrites (Figure 1.5). The dendrites allow the neuron to receive synaptic input from many other neurons, and its axon conducts electrical signals away from the cell body. Synaptic input arriving at the dendrites is transmitted to the soma, where it is integrated by internal molecular processes. Additionally, the neuron can receive electrical input from others through *gap junctions*, which are ion channels made of connexin proteins [35, 90, 153] that join neighboring neurons, allowing for small currents to flow between them.

Since the soma is responsible for the integration of the input and the process of generating spikes, its electrophysiological properties are a central part of most spiking neuron models. In the following we will give a brief description of its functional principle that is mimicked by the models. The soma is made of a closed cell membrane that separates the fluid inside the cell body from the fluid outside. Since the cell membrane is essentially impermeable to most charged molecules, it acts as a capacitor by separating the charges lying inside and outside of the cell body. Various ion conducting channels embedded in the membrane allow currents to flow across it (Figure 1.10A), and ion pumps expend energy to transfer charges across the membrane to maintain a specific concentration inside and outside of the soma. Most of these ion pumps are specialized for moving a particular type of ion into and out of the cell. The most important ions used for the electrochemical processes in the neuron are sodium (Na^+), potassium (K^+), calcium (Ca^{2+}) and chloride (Cl^-). In homeostasis, the ion concentrations generate a voltage difference between the interior of the soma and its surrounding, which is about -70 mV, if the neuron is not active. For convenience the potential of the surrounding

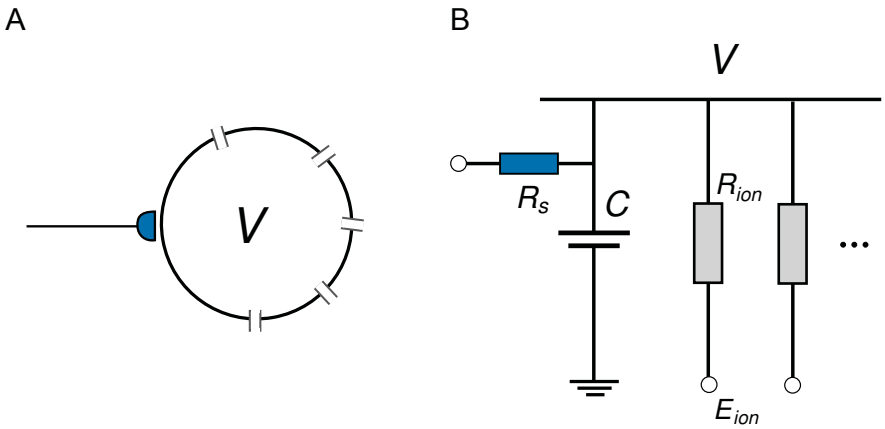

Figure 1.10. (**A**) Schematic representation of a neuron and a synapse connected to it. Embedded in the cell membrane are various channels and ion pumps that allow charged molecules and ions to be transferred into the cell and out of it. (**B**) RC circuit that represents the electrical properties of the neuron. The capacitance C corresponds to the cell membrane separating the charges in the soma from the charges outside of it and the resistances R_{ion} represent membrane channels that allow currents to flow across the cell membrane. The potentials E_{ion} are the corresponding reversal potentials. Synaptic input is modeled as a current flowing through the resistance R_s.

medium is defined as 0 mV, so that the potential V inside the cell (called the *membrane potential*) takes the value -70 mV.

Positive charge flowing into the cell decreases the voltage difference, a process that is called *depolarization*, and negative charge increases the difference, which is termed *hyperpolarization*. The current flowing through the membrane can be expressed for each ion type (labeled with index *ion*) in terms of the *Nernst potential* E_{ion} that accounts for the bias of the current due to the concentration gradient. Hence, the total current flowing through the membrane for an ion type is

$$I_{ion} = \frac{1}{R_{ion}}(V - E_{ion}), \tag{1.21}$$

where R_{ion} is the total resistance for the ion-type *ion*. For $V = E_{ion}$ the membrane current for this type of channel is zero. If V passes through E_{ion} the membrane current changes its sign, therefore E_{ion} is also called the *reversal potential* of an ion type.

Ions flowing through the channels accumulate in the cell and charge it, which is reminiscent of charging a capacitor. Hence, we can represent the soma by an RC circuit (Figure 1.10B), where the capacitance C corresponds to the cell membrane that separates the interior potential from the exterior potential. Several resistances $R_{ion} \equiv R_1, R_2, \ldots$ represent the conducting channels that allow currents to flow across the cell membrane. Synaptic input arriving at the soma can be modeled by a separate

current I_s flowing through an additional resistance R_s. According to the RC circuit the rate of change of the membrane potential is proportional to the sum of the input currents,

$$C\frac{dV}{dt} = I_s - \sum_{ion} I_{ion} = I_s - \sum_{ion} \frac{1}{R_{ion}}(V - E_{ion}), \tag{1.22}$$

where the negative sign before the sum follows from the convention to describe the membrane ion currents as positive-outward and the synaptic input as positive-inward. In real neurons the resistances R_{ion} change over time, and they also depend on the difference between voltage and reversal potential. However, some parts contributing to the total current can be treated as relatively constant so that they can be 'lumped' into a single term, called the *leakage current* $I_L = \frac{1}{R_L}(V - E_L)$. The reversal potential E_L for the leakage current is usually a free parameter that is adjusted to the resting potential of the cell [85].

Integrate-and-fire model. If one assumes that *all* resistances R_{ion} are constant, then it is possible to account for the sum of all ion channel currents by a single leakage current I_L. Then, the reversal potential E_L equals the resting potential of the neuron. This is the basis of the so-called leaky integrate-and-fire (LIF) model, originally introduced by Lapicque [161, 54]. Remarkably, Lapique constructed this model in 1907 long before the mechanisms responsible for generating action potentials were known. Nevertheless, this model is widely used in neuroscientific modeling because it captures important features of the neuron dynamics and due to its simplicity, it can be easily implemented and analyzed. The LIF model simplifies the membrane voltage equation (1.22) to

$$C\frac{dV}{dt} = -I_L + I_s = -\frac{1}{R_L}(V - E_L) + I_s. \tag{1.23}$$

Other versions of the integrate-and-fire model use slightly different voltage equations, e.g. the *perfect* IF model neglects the leakage current I_L in Equation (1.23). For convenience, Equation (1.22) is often multiplied by R_L, and the term $R_L C$ is replaced by the time-constant τ that describes how quickly the neuron recovers to its resting potential in the absence of synaptic input,

$$\tau\frac{dV}{dt} = -(V - E_L) + R_L I_s. \tag{1.24}$$

This equation can be further simplified if one only regards the difference between the membrane potential and the resting potential by setting $E_L \equiv 0$ so that

$$\tau\frac{dV}{dt} = -V + R_L I_s. \tag{1.25}$$

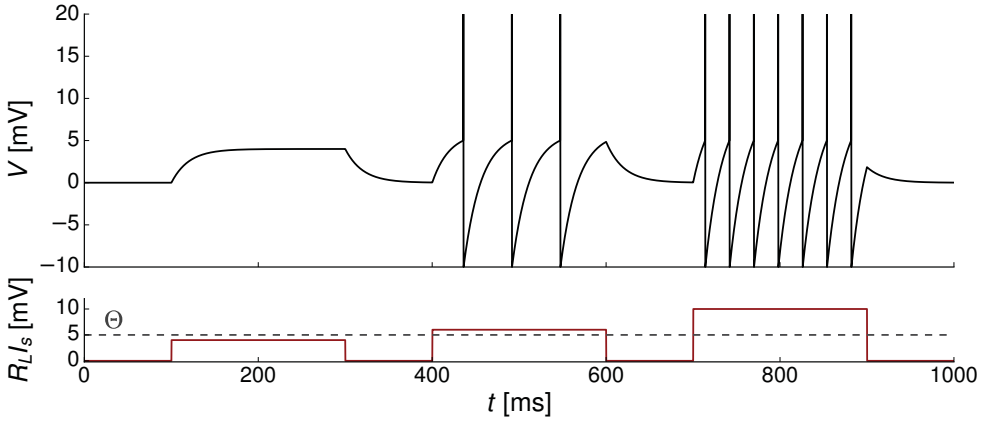

Figure 1.11. Voltage response of a LIF neuron (upper panel) to a synaptic input current (lower panel). The neuron is modeled with Equation (1.25) using following parameters: $\Theta = 5$ mV, $\tau = 20$ ms, $V_\mathrm{r} = -10$ mV, $V_\mathrm{peak} = 20$ mV.

If a neuron becomes sufficiently depolarized, it creates an action potential, which is a sharp increase of its voltage followed by a sudden drop to a value that is usually below the resting potential. This behavior is emulated by the LIF model in the following way. When the depolarization V of the neuron reaches a threshold potential Θ, the neuron generates an action potential and immediately after that, the voltage is set to a reset potential V_r. The shape and duration of the action potential is not considered in the LIF model, but for illustration purpose the voltage can be set to a peak-voltage V_peak before it is reset to V_r.

Sometimes one implements an additional 'hard-coded' refractory time τ_ref during which the neuron voltage stays at V_r to account for the duration of the action potential. After the reset, the voltage relaxes exponentially to the resting potential, if the neuron receives no input. Figure 1.11 shows the voltage response of a LIF neuron to brief current injections I_s of increasing strength. If the current is large enough to drive the voltage above Θ the LIF neuron generates a sequence of action potentials. According to Equation (1.25) the minimum current that is needed to drive the neuron to spiking is given by $R_L I_s = \Theta$.

If the input current is constant, the times between spikes (called the *interspike intervals*) are also constant, since Equation (1.25) is deterministic. In this case we can calculate the constant interspike interval and the corresponding spike rate from (1.25). The derivation is shown in [85], giving following result for the spike rate

$$r = \left[\tau \ln\left(\frac{R_L I_s - V_\mathrm{r}}{R_L I_s - \Theta}\right)\right]^{-1}. \tag{1.26}$$

In a more realistic scenario the neuron receives input from a large number of other neurons in form of spike trains that we expressed in Section 1.3.1 as sums of delta functions. In its simplest form, the total input current to the neuron can be modeled as a superposition of the spike trains, where each arriving spike induces an instantaneous voltage jump J in the soma,

$$R_L I_s(t) = \tau J \sum_j \sum_l \delta(t - t_j^l), \tag{1.27}$$

where J is also called the *synaptic strength*. The first sum goes over all afferent neurons j and the second sum goes over all action potentials from neuron j arriving at the soma at times t_j. According to the above definition each action potential arriving at the neuron induces a voltage jump $V \to V + J$ in its soma at time t_j^l, which can be proven by integrating Equation (1.25) with Equation (1.27) inserted.

If the neuron receives a large number of independent spike trains, the total input resembles a Poisson process [122]. However, it has been shown that the sum of many spike trains with non-Poissonian statistics may exhibit temporal correlations that are often neglected [172, 72].

Other neuron models. Although the LIF model and its variants may appear as simplified 'caricatures' of a real neuron, they have been proven successful in modeling the dynamics of small and large-scale neuronal networks [118, 60, 223]. However, there certainly are problems for which the integrate-and-fire model is not applicable, e.g. when details of the underlying electrophysiological processes are important, or the shape and duration of the action potential play a role.

More detailed models take into account specific ion channel currents that are involved in the process of generating action potentials and in the sub-threshold voltage dynamics. One of the most famous models is the Hodgkin Huxley (HH) model that was introduced in 1952. Based on measurements on the squid giant axon the researchers developed the first model capable of simulating the electrophysiological mechanisms responsible for the initiation and propagation of action potentials [136]. However, the HH model is costly in terms of computational resources, since it requires to solve a large number of equations for each time-step and a high temporal resolution.

Many other spiking neuron models are based on a reduction of the HH-model to a simplified set of equations describing the voltage dynamics of a neuron. Among the most important are the Morris-Lecar model, [194], the Izhikevich model [148] and the FitzHugh-Nagumo model [105]. Besides the aforementioned, there are many other spiking neuron models that have specific weaknesses and strengths [118, 85, 146]. The optimal choice of the model strongly depends on the context of the problem. Complex models such as the HH model are often used to simulate single neurons and small neuronal networks, whereas simple models such as the IF model are suited for the simulation of large-scale neuronal networks because of their simplicity and small parameter

space. All of these models have in common that they describe the membrane potential V of the neuron as a single variable, hence they are called *single-compartment* models. Multi-compartment models additionally consider spatial variations in the membrane voltage by splitting the neuron into separate regions that are described by different sets of variables and equations [85].

Finally, there are other types of neuron models that completely neglect the spike generation mechanism by mapping the input of a neuron directly to its firing rate. These *rate models* are particularly useful for describing the collective activity of a great many neurons, since their reduced description of the neuron's dynamics allows to efficiently explore the behavior of the large-scale system at the expense of electrophysiological accuracy.

2 Population activity of degree-correlated neuronal networks

In this chapter we investigate the dynamics of large-scale neuronal networks with complex topology. Given the large number of neurons in such a network it is useful to apply some type of coarse-graining in the description of the network activity. An effective approach is to group neurons with similar properties into neuronal *populations* and describe the average activity of these groups rather than the spiking of individual neurons. The collective activity of the neurons in such populations provides the basis for neuronal processing in many brain areas [214, 14].

Our main focus lies on the influence of two basic statistical properties of the network structure on the neuronal activity, namely structural heterogeneity and degree correlations. Both are fundamental characteristics of large-scale neuronal networks [247], but a thorough understanding of how they influence the global spiking dynamics is still lacking. To aim at this problem, we consider a large number of excitatory leaky integrate-and-fire (LIF) neurons that are synaptically coupled to form a recurrent neuronal network with degree correlations and we systematically examine the influence of the network topology on the neuronal spiking activity. The LIF model is a simple, yet very relevant spiking neuron model that allows us to analyze the global dynamics of the system with a mean-field model [118, 60]. The mean-field model provides a coarse-grained description of the spiking activity in terms of average population firing rates, which can be used to explore the behavior of the network without having to simulate each neuron explicitly.

So far, mean-field models have not been able to take into account strongly heterogeneous network structures and degree correlations, therefore we develop a modified mean-field framework that inherently handles these features. With this framework and numerical simulations we examine the firing response of an exemplary complex neuronal network to varying stimulus levels. The resulting *stimulus/response relationship* depends on recurrent activity (Figure 2.1A), which is shaped by the connectivity structure of the network. Then, we quantify the signal transmission capability of the network by measuring the mutual information between stimulus and response. Main attention is paid to the influence of assortative degree correlations on the sensitivity of the network to weak stimuli. Results of this work have been published in [227] and [228].

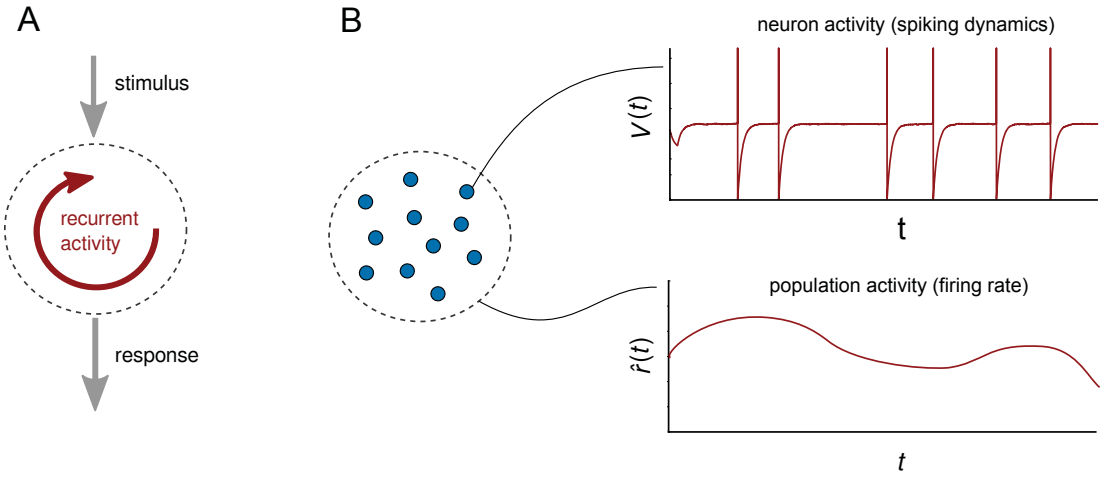

Figure 2.1. (**A**) Schematic of a recurrent neuronal network, which receives and processes a stimulus. The network response is shaped by the combination of stimulus and recurrent activity of the network. (**B**) Neuronal population, where the spiking activity of individual neurons is governed by a threshold process, e.g. the LIF model, and the population activity is described by the ensemble firing rate of neurons in this population.

2.1 Population coding

Computations in the brain take place at many scales, from the microscopic scale of single neurons and small neuronal circuits up to the macroscopic scale of cortical regions and information pathways [185, 46, 150, 249]. Higher cognitive functions and ultimately, consciousness, arise from the hierarchical integration of these computations [96, 267]. Across the scales, information processing is based on the collective activity of the interconnected neurons in form of spiking patterns. How do these patterns encode information and how are they influenced by the connectivity structure of the underlying network? An important observation in this regard is the irregularity of neuronal spiking in in-vivo measurements [243]. Whether these irregularities carry significant amounts of information or simply resemble noise is not resolved to date [243, 235, 236, 118, 62]. The assumption of 'noisy neurons' has been widely applied in neuroscience, since it allows for a simplified stochastic description of their spiking patterns [223, 85, 118]. If neuronal spiking is indeed noisy, a single spike train is not very informative and it is the combined activity of many neurons that matters [214, 14]. This so-called *population coding* has been found to play a major role in many sensory and motor areas of the brain.

A well-known example for population coding is the detection of visual stimuli in middle temporal visual area (MT) of the macaque monkey [184]. Specific neurons in

the MT fire noisy spike trains with rates that are bell-shaped in function of the speed of a moving object in a preferred direction. Reliable information about the visual stimulus could be retrieved only by taking into account the collective activity of a large population of neurons. Similar coding strategies have been observed for the control of eye [166], arm movements [117] and in the auditory system [88]. Note, that the term *population* refers to a selection of neurons within a patch of nervous tissue and does not necessarily include all neurons in a given neuronal network. The strategy of population coding possesses some significant advantages. First, it reduces uncertainty in the information, which occurs due to noise in the spiking activity of individual neurons, or the variability of their intrinsic properties. Second, it is very robust against failure of activity or neuronal loss, because the information is shared across a large number of neurons. Third, population activity can encode information with higher temporal resolution than single neurons, because collectively they produce a large number of spikes during a small time-window, in which individual neurons may fire only few spikes.

How does the brain use population coding strategies to carry out computations and how does it modify the architecture of neuronal connections to optimize the efficiency of the processing? The cortex is organized towards functional specialization: Different processing tasks are executed locally in distinct brain areas with a specialized connectivity structure [268]. Therefore, an important step towards revealing the neural code is to understand how the activity pattern of a population of neurons is shaped by the topology of the underlying network.

Recent advances in visualizing the structural and functional connectivity at the scale of large cortical regions down to single neurons allow to statistically characterize the structure of cortical networks. Brain networks are far from random and exhibit complex network properties such as small-world features [26, 56, 253], modularity [284], large variability in structural [253, 56] and functional [97] connectivity, and hub-neurons that are strongly connected and highly active [3, 250, 271]. How are these network properties related to the population dynamics of the connected neurons? This question is very well suited to computational and theoretical modeling. Although the impact of network parameters on neuronal dynamics has been subject to a large number of theoretical and numerical studies [53, 34, 278, 275, 224, 295, 209], the relevance of complex network characteristics such as heterogeneity and higher order statistics of the connectivity structure have been investigated only recently [224, 66, 295, 275, 209]. A common finding is that heterogeneous network topologies induce heterogeneous activity patterns, e.g. a broad distribution of neuronal firing rates [224, 66, 209]. Indeed, neocortical activity is highly variable: A large proportion of neurons fires at very low rates, whereas a small subset of strongly connected neurons is highly active [181, 43, 143, 290].

Heterogeneity of the network structure and neuronal activity are assumed to be important for information processing tasks such as the detection of weak stimuli [290, 187, 209, 275, 64]. A remarkable example in this regard is the barrel cortex of rodents, which

can sense very small inputs down to a few single spikes to a single neuron [142]. Subsets of strongly connected and highly active neurons in this region could play a significant role in encoding the sensory information, since their high-frequency output can convey relatively large amounts of information [290]. We are interested in the relevance of heterogeneity and correlations in the connectivity structure for the amplification of small inputs. Besides the degree distribution, degree correlations are the most basic statistical property of a network and they have been shown to influence its structural and functional characteristics, such as its resilience to damage [197, 289, 287, 276, 123, 229] or its synchronizability [279, 13]. Recently, assortative degree correlations have been observed in neuronal cultures [260, 87] and cortical networks [97, 271, 211].

2.2 The mean-field approach

How do complex activity patterns emerge from the interaction of many spiking neurons in a neuronal population? It is sensible to approach this question from *bottom-up*, which requires integrating the spiking activity of individual neurons into a description of their population dynamics. A very useful method in this regard is the mean-field framework, which uses concepts from statistical physics and has a long history going back to pioneer works more than half a century ago [37]. Since then, the model has been continuously modified to account for more complex features of the neuron dynamics and network structure [155, 10, 119, 2, 12, 156, 205, 53, 204, 118, 60, 89, 223, 66, 187, 291]. With the mean-field approach one coarse-grains the spiking activity of statistically similar neurons and describes their ensemble-averaged activity, e.g. the mean firing rate of a patch of nervous tissue (Figure 2.1B). Hence, this method is well-suited to complement experiments that measure meso- and macroscale brain activity, such as the electroencephalogramm (EEG) or magnetoencephalogramm (MEG). The reduced rate-dynamics can be used to explore the parameter space of the model, since one can quickly analyze the dynamical behavior of the system. Of particular interest are stable states (attractor states) of the system, which can be found by bifurcation analysis of the reduced equations. The coarse-graining of neuronal activity has much in common with the kinetic theory, originally used in thermodynamics, where the collective motion of single gas molecules is averaged and integrated to obtain meso-scale variables such as temperature and pressure.

Starting from the description of the spiking dynamics of individual neurons one derives equations for the average activity of a population of many statistically similar neurons. This is achieved by applying the mean-field approximation: The temporally averaged depolarization of a single neuron is replaced by the momentary ensemble-averaged depolarization of the neuronal population [223, 118]. Therefore, the mean-field approximation is based on the hypothesis of ergodicity, which states that the time-averaged activity of an individual neuron has the same statistical properties as the

ensemble-averaged activity of many neurons. An important prerequisite for ergodicity is that the neurons are independent of each other [107]. One observes, that the system undergoes transient changes in activity until it is, in most cases, attracted to a steady-state. We can express these steady-states in terms of self-consistent rate equations of the form [219]

$$\hat{r} = \phi(\hat{r}, s), \tag{2.1}$$

where ϕ is called the population *transfer function*, $\hat{r}$ is the mean stationary firing rate of the neuronal population and s is the rate of the stimulus. We use the caret in $\hat{r}$ to denote the ensemble-average over all neurons in the population. The mean population firing rate can be obtained by counting the number of spikes $n_{\text{spikes}}(t, t+dt)$ that occur during a small time-window dt. The mean population rate is then

$$\hat{r}(t) = \lim_{dt \to 0} \frac{n_{\text{spikes}}(t, t+dt)}{N_{\text{pop}} dt}, \tag{2.2}$$

where N_{pop} is the number of neurons in the population. [15] The majority of existing mean-field studies on neuronal dynamics are based on the integrate-and-fire (IF) neuron model, since its one-dimensional voltage equation is simple enough to allow for rigorous analytical treatment [118, 60, 223]. Moreover, the IF model has a small parameter space, which is easy to explore in comparison to other neuron models. Another advantage is its low computational cost per integration time, which permits numerical simulations of large networks over long time periods. Recently, mean-field models have also been developed for higher-dimensional neuron models, e.g. the Izhikevich neuron [202], or the Hodgkin-Huxley and FitzHugh-Nagumo model [17].

The leaky integrate-and-fire (LIF) model, which we apply in our study, uses only two variables to describe the intrinsic dynamics of an individual neuron, its depolarization $V(t)$ and the time since it has emitted the last action potential, $T(t)$. Spikes arriving at the dendrites of the neuron, coming from external sources or from afferent neurons in the network, are modeled as a capacitive current $I(t)$ going into the neuron. These three quantities are sufficient to represent the dynamical state of a neuron in the network at any given time. From a mathematical perspective, these variables span a three-dimensional phase space, where the state of a neuron i corresponds to a point $\mathcal{A}_i = \{V_i, I_i, T_i\}$ [223, 89]. A large population of statistically similar neurons can now be described by an ensemble density $p(\mathcal{A}, t)$, which expresses the probability density for each point in the phase space.

The dynamics of the system is then captured by the time-evolution of $p(\mathcal{A}, t)$, which we describe with the well-known Fokker-Planck equation. By using the Fokker-Planck formalism, we are able to take into account fluctuations of the spiking input to a neuron, which may result from noisy external stimulation or from fluctuating recurrent

activity in the network. We consider sparse networks, where each neuron has a fixed number of afferent connections with the same synaptic strength, which ensures a fixed mean degree of the network regardless of its size.

The mean-field approximation allows us to simplify the Fokker-Planck equation by expressing it in terms of the ensemble firing rate of the neurons, so that we can derive self-consistent rate equations of the form of Equation (2.1). This approximation is valid in the limit of large network size, so that any 'finite-size effects' are neglected, e.g. fluctuations of the global activity due to the finite number of neurons [53]. In sparse networks with constant mean connectivity the fluctuations from the finite voltage-jumps are maintained [53, 204, 89]. Apart from sparse network connectivity, several mean-field studies have examined networks with simple all-to-all coupling, where the number of input connections per neuron goes to infinity in the limit of large network size [33, 2, 47, 204, 238]. Accordingly, the synaptic strength is divided by system size to achieve realistic firing rates so that the size of the spike-induced voltage jumps goes to zero in this limit. In this case, the input to a neuron becomes a fluctuationless continuous stream that can be described by a mean current. If neuronal spiking is mainly driven by the mean of the neuronal input current, then the network is said to be *mean-driven*.

On the other hand, population models that take into account fluctuations allow for the possibility of input fluctuations as the main driver of network activity, which is denoted as the *fluctuation-driven* regime. This regime arises when the mean input current to the neurons is insufficient to drive them to spiking and fluctuations are necessary for promoting activity, e.g. in networks with balanced exhibition and inhibition, where the mean input to a neuron becomes very low [53, 118]. Apart from the Fokker-Planck formalism, alternative approaches to deal with fluctuations in the neuronal input have been proposed. One approach is based on the Boltzmann equation [65, 66] that takes into account higher-order statistics of the neuronal input fluctuations. A Fokker-Planck equation can be derived from the Boltzmann equation by expanding it for small synaptic strengths and keeping only terms up to the second order [66]. Another approach deals with the derivation of a master equation that governs the time-evolution of the population spiking activity [55, 48]. Finite-size effects have also been examined with both approaches [48, 66].

The method of describing the population activity of neurons in terms of probability densities is called *population density approach* and has been successfully applied to single populations of identical neurons [155, 10, 119, 2, 12, 156, 205, 53, 118, 60, 89, 223] and neurons with heterogeneous characteristics [187, 291]. Diverse types of neurons in the network can be grouped into distinct populations so that each population consists of statistically similar neurons [204, 118, 89, 223, 66]. Each population is then described by a separate probability density $p_k(\mathcal{A}_k, t)$. In our study, we use the probability density approach to describe networks with heterogeneous connectivity structure. To this aim,

we divide the network into populations of neurons with equal in-degree k, which we call *k-populations*, and describe the dynamics of each k-population with a separate probability density p_k. Moreover, we take into account in-degree correlations of the network structure, which are captured by the average connectivity between different k-populations. Using the Fokker-Planck formalism and the mean-field approximation we calculate the transfer function ϕ_k and the corresponding rate equation for the steady-state of each population. Network statistics, such as the degree distribution and degree correlations, enter the equations in form of a joint-in-degree distribution $N_{kk'}$, which is the average number of connections from neurons with in-degree k' to a neuron with in-degree k. We show that this joint-in-degree distribution can be calculated analytically for some networks in the limit of large network size.

2.3 Rate equations for degree-correlated networks

In this section, we derive population rate equations of the form of Equation (2.1) for LIF networks with heterogeneous degree distributions and degree correlations. Let us begin with a mathematical description of the neuronal spiking dynamics.

Assume N excitatory LIF neurons, which are interconnected in a heterogeneous network. Figure 2.2 shows a simplified schematic of such a network for the uncorrelated case (Figure 2.2A) and the assortative case (Figure 2.2B). To stimulate collective neuronal activity, each of the neurons gets injected an independent Poisson spike train with rate s, which quantifies the stimulus strength. A single LIF neuron can be driven to

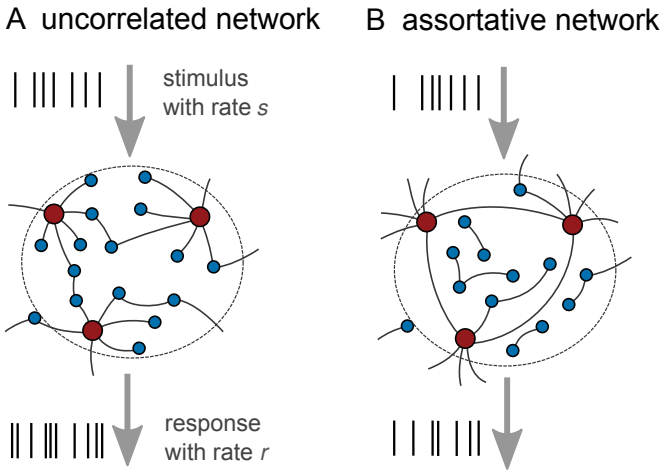

Figure 2.2. Simple schematic of a heterogeneous network of LIF neurons. Large red dots illustrate neurons with high degree and small blue dots depict neurons with low degree. (**A**) Uncorrelated network, where neurons are connected randomly, regardless of their degree. (**B**) Assortative network, where neurons with similar degree are connected preferably. The network is stimulated by injecting independent external Poisson spike trains with rate s into each neuron. The network response r is quantified by the average stationary firing rate of n randomly chosen neurons of the network. This figure has been modified from [228].

firing in the absence of recurrent input, if the stimulus rate exceeds a threshold value ν_{thr}, as discussed previously in Section 1.3.2. Following Brunel [53], we normalize s by this value, so that for $s \geq 1$ every neuron in the network is driven to firing by the stimulus, even in the absence of recurrent activity. Conversely, for $s < 1$ the stimulus by itself is not sufficient to drive neuronal spiking, and neurons become active only if they receive sufficient synaptic input from afferent spiking neurons in the network. If the stimulus strength decreases in this *subthreshold* regime, neuronal spiking increasingly depends on recurrent input, so that the population activity becomes more sensitive to the architecture of the recurrent network.

Real neuronal circuits, e.g. cortical columns, project their output to another stage of the information pathway for further processing. Since the axonal projections originate at a finite number of neurons, the network response is pooled from a finite sample of neuronal firing rates, so that it exhibits some variability, or sampling noise'. In order to account for this variability, we quantify the network response r as the mean firing rate of a fixed number of n randomly selected neurons in the network. The sampling from a limited number of randomly chosen neurons results in a variability of r, which depends on the distribution of firing rates of the neurons in the network.

Since neuronal networks with synaptic connections are directed, we distinguish between the in-degree k and out-degree j of a neuron. In-degrees and out-degrees are distributed according to the in-degree distribution $P^{\text{in}}(k)$ and the out-degree distribution $P^{\text{out}}(j)$, respectively. Possible mixing patterns of neuronal connectivity are (i) correlations between in- and out-degree per neuron and (ii) correlations of synaptic connections between neurons. The latter constitute correlations between in-degrees (in-in) and out-degrees (out-out) of connected neurons, and correlations between in- and out- degrees (in-out and out-in). As a first step in the analysis of degree correlations and neuronal activity, we focus on correlations of the in-degrees of connected neurons, because the firing rate of a neuron is closely related to its number of inputs. Moreover, for most parts of this study, we assume that each neuron has the same number of inputs and outputs, $j = k$. Strong correlations between in- and out-degree per neuron considerably simplify the network topology, and this assumption is supported by similar findings for the neural system of *C. Elegans* [274].

The dynamics of a LIF neuron in the network is governed by the differential equation

$$\tau \frac{dV_i(t)}{dt} = -V_i(t) + RI_i, \tag{2.3}$$

where V_i is the membrane potential of the i-th neuron in the network, τ is the membrane time constant, R is the membrane resistance and I_i is the input current, which is the sum of recurrent input and stimulus input to the i-th neuron. Each neuron fires an action potential, if its voltage V_i reaches a threshold value Θ and immediately after that, the membrane potential is reset to a refractory voltage V_{r} for a constant time period τ_{ref}. This 'hard-coded' refractory period limits the maximum firing rate of each neuron to $1/\tau_{\text{ref}}$ and prevents unrealistically large network activity. The input current to the i-th neuron is modeled as a delta spike train

$$RI_i = \tau J \sum_{j=1}^{N} a_{ij} \sum_{l} \delta(t - t_j^l - D_{ij}), \tag{2.4}$$

where J is the synaptic coupling strength and a_{ij} is the adjacency matrix of the network. The second sum on right hand side can be read as follows: all spikes l emitted at times

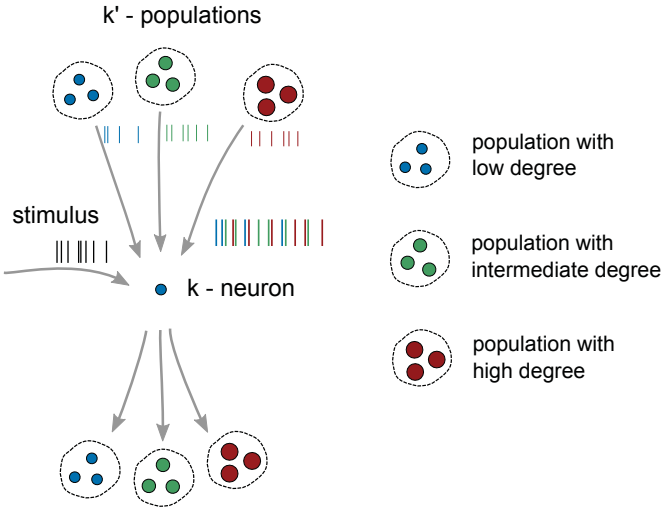

Figure 2.3. Schematic representation of a k-neuron, which receives uncorrelated input from the stimulus and from neurons within various k'-populations. The input spike trains from the stimulus (black spike train) and from neurons within the k'-populations (colored spike trains) are summed to make up the total input to the k-neuron. Conversely, the output spike train of the neuron is distributed to several k'-populations.

t_j^l by the j-th neuron arrive at the i-th neuron after a synaptic delay D_{ij}. Each spike arriving at neuron i increases its membrane voltage by J. Throughout this chapter we use parameters that resemble typical values found in the cortex: $\tau = 20$ ms, $\tau_{\mathrm{ref}} = 2$ ms, $J = 0.1$ mV, $N = 10^5$ [53]. We consider networks of sparse connectivity, so that any two neurons are unlikely to share common input. The delays D_{ij} are drawn uniformly at random between 0 ms and 6 ms and then fixed for each connection. We included the delays to prevent cascading synchronous firing of the neurons, which is discussed in [195]. Importantly, random delays do not alter the stationary firing rates of the neurons.

We now distinguish the neurons in the network by their in-degree k and denote them as *k-neurons*. The set of all k-neurons in the network is a *k-population*. The synaptic input to an individual neuron is a superposition of all incoming spike trains. Since any two neurons are unlikely to share common input, we can assume that the incoming spike trains are independent. This allows us to approximate their sum as a Poisson process whose rate is the sum of rates of the individual spike trains [122]. A k-neuron receives synaptic input from the stimulus with rate $s\nu_{\mathrm{thr}}$ and recurrent input from afferent neurons in the network. Here, $\nu_{\mathrm{thr}} = \frac{\Theta}{J\tau}$ is the threshold frequency used to normalize the stimulus [53]. The recurrent input going into the k-neuron can be divided into contributions from each k'-population in the network (Figure 2.3). On average, the input from a k'-population is of rate $N_{kk'}\hat{r}_{k'}(t)$, where $N_{kk'}$ is the average number of k'-neurons that connect to a k-neuron and $\hat{r}_{k'}(t)$ is the ensemble-averaged firing rate of the k'-population. We denote $\hat{r}_{k'}(t)$ as the *population firing rate* and $N_{kk'}$ as the *joint-in-degree distribution*. This distribution describes the coupling between the different populations and conveys all relevant information about the network topology. It can be calculated from the total number of directed links $E_{kk'}$ in the network that

go from k'-neurons into a k-neuron

$$N_{kk'} = \frac{kE_{kk'}}{\sum\limits_{k''} E_{kk''}}. \tag{2.5}$$

2.3.1 Stochastic description of the population activity

We consider a regime in which each neuron is bombarded by a large number of input spikes within its integration time τ, and each voltage jump is small compared to the firing threshold: $J \ll \Theta$. In this regime we can apply the *diffusion approximation* and describe the total input current $I_i^{(k)}$ of a neuron i in a k-population by a Gaussian process [218, 118, 174]

$$RI_i^{(k)}(t) = \mu_k(t) + \sigma_k(t)\sqrt{\tau}\xi_i^{(k)}(t), \tag{2.6}$$

with a mean part $\mu_k(t)$ and fluctuating part with intensity $\sigma_k(t)$. Here, $\xi_i^{(k)}(t)$ is Gaussian white noise of zero mean and unitary variance

$$\langle \xi_i^{(k)}(t) \rangle = 0, \quad \langle \xi_i^{(k)}(t)\xi_i^{(k)}(t') \rangle = \delta(t - t'). \tag{2.7}$$

The mean and variance of the input current can be expressed in terms of the momentary population firing rates

$$\mu_k(t) = J\tau \left(\nu_{\text{thr}} s + \sum_{k'} N_{kk'} \hat{r}_{k'}(t) \right) \tag{2.8}$$

and

$$\sigma_k^2(t) = J^2\tau \left(\nu_{\text{thr}} s + \sum_{k'} N_{kk'} \hat{r}_{k'}(t) \right). \tag{2.9}$$

The above expressions are derived in the Appendix, A.2, where we also provide a mathematical definition of the diffusion approximation.

Using Equation (2.6) we can rewrite the differential equation for the neuron voltage, Equation (2.3), to describe the voltage evolution for a neuron i in a k-population by

$$\tau \frac{dV_i^{(k)}(t)}{dt} = -V_i^{(k)}(t) + \mu_k(t) + \sigma_k(t)\sqrt{\tau}\xi_i^{(k)}(t), \tag{2.10}$$

which is a Langevin equation. In fact, the system (2.10) represents a set of Langevin Equations that are coupled by the population firing rates in the mean and variance of

the respective input current as defined in Equations (2.8) and (2.9).

Each Langevin equation in (2.10) is a stochastic differential equation that governs the dynamics of each neuron in a k-population. Because of its stochastic nature, we turn to a statistical description of the population dynamics. A statistical description of the k-population activity can be given by a probability density $p_k(v_k, t)$, which expresses the probability of a k-neuron i to have a membrane potential in the interval $[v_k, v_k + dv_k]$

$$p_k(v_k, t)dv_k = \text{Prob}\left\{V_i^{(k)}(t) \in [v_k, v_k + dv_k]\right\}. \tag{2.11}$$

Each probability density p_k contains the distribution of neuronal states in a k-population at time t. Since we assume that the neurons in a population are statistically indistinguishable, we can apply the mean-field assumption and interpret $p(v_k, t)$ as the fraction of neurons in the k-population that have a membrane potential in $[v_k, v_k + dv_k]$. Hence, we replace the probability density for the membrane potential of a single k-neuron by the density of membrane potentials in the k-population, which is valid in the limit $N \to \infty$. This allows us to discard the index i in (2.11) and (2.10), which enables us to proceed with a stochastic description of the ensemble-averaged population activity.

The time-evolution of each probability density is described by the Fokker-Planck Equation, which corresponds to the respective Langevin Equation (2.10) [221]

$$\frac{\partial p_k(v_k, t)}{\partial t} = \frac{\partial}{\partial v_k}\left[\left(\frac{v_k - \mu_k(t)}{\tau}\right) p_k(v_k, t)\right] + \frac{\partial^2}{\partial v_k^2}\left[\frac{\sigma_k^2(t)}{2\tau} p_k(v_k, t)\right]. \tag{2.12}$$

The first term on the right-hand side of Equation (2.12) describes the deterministic time-evolution of the probability density, which is driven by the mean input current to the neurons. It simply shifts the probability density $p_k(v_k, t)$ to higher voltages without changing its shape. The second term describes the stochastic broadening of p_k, which is driven by the fluctuations of the input current. If the voltage of a LIF neuron reaches the threshold value $V_i^{(k)} \geq \Theta$, it is reset to the refractory value V_r. Hence, the probability density must be zero for $v_k > \Theta$. We are interested in the number of k-neurons per time that cross the threshold Θ, which is given by the *probability current* at the threshold. The probability current can be found by rewriting the Fokker-Planck equation in a conservation-of-probability form

$$\frac{\partial p_k(v_k, t)}{\partial t} + \frac{\partial J_k(v_k, t)}{\partial v_k} = 0, \tag{2.13}$$

where the probability current is defined as

$$J_k(v_k, t) = -\frac{v_k - \mu_k}{\tau} p_k(V_k, t) - \frac{\sigma_k^2}{2\tau}\frac{\partial p_k(v_k, t)}{\partial v_k}. \tag{2.14}$$

We now discuss the behavior of the stationary solution $p(v_k)$ at the boundaries $v_k = \Theta$ and $v_k \to -\infty$. First of all, the stationary probability density must vanish at the threshold

$$p_k(\Theta) = 0, \tag{2.15}$$

and the probability current at the threshold corresponds to the stationary population firing rate

$$J_k(\Theta) = \hat{r}_k. \tag{2.16}$$

The above equation gives together with Equation (2.14)

$$\frac{\partial p_k(\Theta)}{\partial v_k} = -\frac{2\tau \hat{r}_k}{\sigma_k^2}. \tag{2.17}$$

For $v_k \to -\infty$ the probability density has to vanish fast enough to be integrable

$$\lim_{v_k \to -\infty} p_k(v_k) = \lim_{v_k \to -\infty} v_k p_k(v_k) = 0. \tag{2.18}$$

Finally, we account for the neurons, which leave the threshold at time t and are reinjected after the refractory time τ_{ref} with the reset voltage V_{r}, by rewriting Equation (2.13) as

$$\frac{\partial p_k(v_k, t)}{\partial t} + \frac{\partial}{\partial v_k}\left[J_k(v_k, t) + \hat{r}_k(t - \tau_{\mathrm{ref}})\mathrm{H}(v_k - V_{\mathrm{r}})\right] = 0, \tag{2.19}$$

where $\mathrm{H}(\cdot)$ is the Heaviside function. The stationary solution of Equation (2.19), satisfying the boundary conditions, Equations (2.15,2.17,2.18), is

$$p_k(v_k) = \frac{2\hat{r}_k \tau}{\sigma} \exp\left(-\frac{(v_k - \mu_k)^2}{\sigma_k^2}\right) \int_{\frac{v_k - \mu_k}{\sigma_k}}^{\frac{\Theta - \mu_k}{\sigma_k}} \mathrm{H}\left(x - \frac{V_{\mathrm{r}} - \mu_k}{\sigma_k}\right) e^{x^2} dx. \tag{2.20}$$

Normalization of the probability density requires

$$\int_{-\infty}^{\Theta} p_k(v_k) dv_k + \hat{r}_k \tau_{\mathrm{ref}} = 1, \tag{2.21}$$

where the second term corresponds to the fraction of neurons that are refractory. Solving Equations (2.20,2.21) for $\hat{r}_k$ leads to self-consistent equations for the stationary

population firing rate [219]

$$\begin{aligned}\hat{r}_k &= \left[\tau_{\mathrm{ref}} + \tau\sqrt{\pi}\int_{(V_{\mathrm{r}}-\mu_k)/\sigma_k}^{(\Theta-\mu_k)/\sigma_k} e^{x^2}(1+\mathrm{erf}(x))dx\right]^{-1} \\ &= \phi_k(\hat{r}_{k_{\min}},\ldots,\hat{r}_{k_{\max}},s), \quad k_{\min}\leq k\leq k_{\max},\end{aligned} \tag{2.22}$$

where $k_{\min}$, $k_{\max}$ are the minimum and maximum in-degree in the network, $\phi_k(\hat{r}_{k_{\min}},\ldots,\hat{r}_{k_{\max}},s)$ is the population transfer function, and $\mathrm{erf}(x)$ is the error function

$$\mathrm{erf}(x) = \frac{2}{\sqrt{\pi}}\int_0^x e^{-y^2}dx. \tag{2.23}$$

The input mean and variance μ_k and σ_k in the boundaries of Equation (2.22) couple the equations across all different populations, because they depend on the stationary firing rates $\hat{r}_{k'}$

$$\mu_k = J\tau\left(\nu_{\mathrm{thr}}s + \sum_{k'} N_{kk'}\hat{r}_{k'}\right), \tag{2.24}$$

$$\sigma_k^2 = J\mu_k. \tag{2.25}$$

Therefore, the rate equations (2.22) must be solved self-consistently for all k-populations in the network.

Although we derived the transfer function in Equation (2.22) for a stationary process, it can be used to describe the approximate rate dynamics of the network [118, 85, 223]. First, we rewrite the transfer function in a time-dependent form

$$\phi_k(\hat{r}_{k_{\min}}(t),\ldots,\hat{r}_{k_{\max}}(t),s). \tag{2.26}$$

The time-dependent population firing rates can be written in vector form as

$$\hat{\mathbf{r}}(t) = \{\hat{r}_{k_{\min}}(t),\ldots,\hat{r}_{k_{\max}}(t)\}. \tag{2.27}$$

Then, we can rewrite the coupled transfer function $\phi_k(r_{k_{\min}},\ldots,r_{k_{\max}},s)$ in a generalized time-dependent form $\mathbf{\Phi}(\hat{\mathbf{r}}(t),s) = \{\phi_{k_{\min}},\ldots,\phi_{k_{\max}},s\}$. With this notation, the approximate dynamics of the neuronal network can be described by the differential equation [118, 85, 223]

$$\tau_x\frac{d}{dt}\hat{\mathbf{r}}(t) = -\hat{\mathbf{r}}(t) + \mathbf{\Phi}(\hat{\mathbf{r}}(t),s), \tag{2.28}$$

where τ_x is a time-constant of appropriate choice, as discussed in [118].

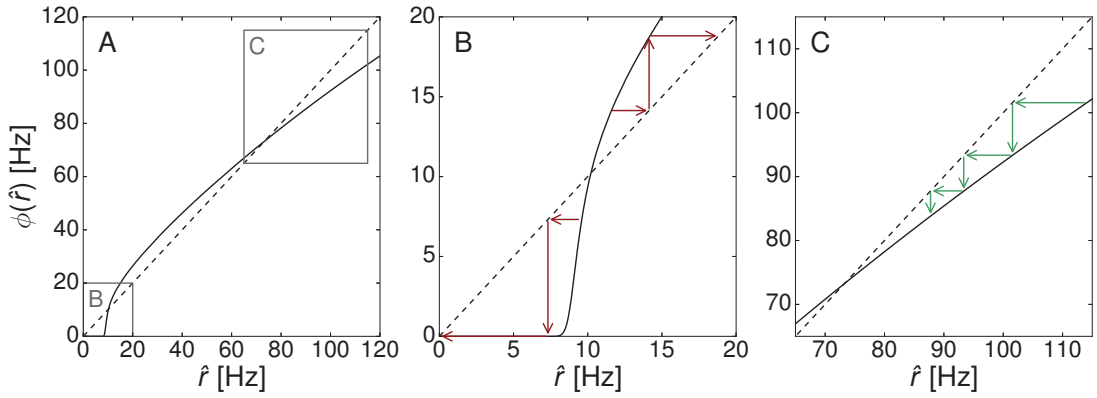

Figure 2.4. Stability of solutions for the one-dimensional self-consistent equation $\hat{r} = \phi(\hat{r})$. The dashed line shows unity $\phi(\hat{r}) = \hat{r}$. (**A**) The transfer function over the mean firing rate reveals two fixed points at the intersections with the unity function. (**B**) Unstable fixed point of the system. Red arrows indicate the iterative integration of Equation (2.28), which diverges. (**C**) Stable fixed point with green arrows illustrating the convergence of iterating Equation (2.28). The transfer function shown here corresponds to Equation (2.22) for a LIF network with neurons of equal in-degree $k = 100$ and stimulus $s = 0.9$.

Stationary solutions $\hat{\mathbf{r}} = \mathbf{\Phi}(\hat{\mathbf{r}}, s)$ are fixed points of Equation (2.28). Stable fixed points can be found by numerical integration of Equation (2.28). Unstable fixed points are more difficult to obtain, since the system does not converge to these states. In the one-dimensional case it is possible to plot the stationary transfer function $\phi(\hat{r})$ over $\hat{r}$ for a specific value of s, where intersections with the unity function $\phi = \hat{r}$ represent fixed-point solutions (Figure 2.4). We focus on the stable rate solutions of our system, which can be obtained by numerical integration. Stability conditions for high-dimensional systems are discussed in the Appendix, A.1. Multistability can lead to hysteretic behavior, since the network jumps between different stable solutions, depending on the actual state of the system. Hysteretic behavior of the rate-solutions is discussed extensively in [159, 66] for one-dimensional systems. For full LIF simulations we obtain the network activity by injecting a super-threshold stimulus $s > 1$ and then reducing the stimulus to a subthreshold value. In order to integrate Equation (2.28), we need to evaluate the network topology in form of the joint-in-degree distribution $N_{kk'}$. In principle, the distribution $N_{kk'}$ can always be computed numerically from the adjacency matrix of the network by averaging the number of links going into k-neurons and originating at at k'-neurons. We can rewrite $N_{kk'}$ in terms of the probability $f(k, k')$ that a random input to a k-neuron originates at a k'-neuron

$$N_{kk'} = kf(k, k'). \tag{2.29}$$

Normalization requires

$$\sum_{k'} f(k,k') = 1, \qquad \sum_{k'} N_{kk'} = k. \tag{2.30}$$

In the next section, we derive expressions for $N_{kk'}$ for some generic random networks in the limit of large N.

2.3.2 Influence of the network topology

In the previous section we derived reduced rate equations for the population dynamics of the system, which depend on a reduced description of the network topology in terms of the joint-in-degree distribution $N_{kk'} = kf(k,k')$. This distribution can be approximated for generic random networks in the limit of large N. In some cases, it takes a particularly simple form, which helps to illustrate the role of network heterogeneity and degree correlations in shaping the population dynamics. In the following we will calculate $N_{kk'}$ for two network types, which differ in the correlations between in- and out-degree per neuron. It is important to apprechiate that these in-out correlations *per neuron* are different from the in-degree correlations of connected neurons, as described in Section 1.1.1.

The first network type has no correlations between in- and out-degree per neuron, which we refer to as an *IOU network*, for in-out uncorrelated. Moreover, we assume no in-degree correlations of connected neurons for this network type. These networks are interesting, because their topology is only constrained by the choice of the in- and out-degree distributions, so that the connectivity structure is highly random. However, in most parts of the study we will focus on a second network type in which each neuron has equal in- and out-degree (*IOE network*, for in-out equal). Similar correlations have been found for the neuronal network of *C. Elegans* [274].

We first derive $N_{kk'}$ for IOU networks without in-degree correlations and then, we focus on IOE networks with different in-degree correlations.

(1) Uncorrelated IOU networks

Consider a directed random network with fixed in- and out-degree distributions $P^{\text{in}}(k)$ and $P^{\text{out}}(j)$, respectively. Let us assume that the connections are drawn at random, so that there are no correlations between in-degrees of connected neurons and no correlations between the in- and out-degree per neuron. In this case, the probability $f(k,k')$ of a random input to a k-neuron to originate at a k'-neuron is independent of k and equals the fraction of links in the network that originate at k'-neurons

$$f(k,k') = \frac{E_{k'}}{E}. \tag{2.31}$$

Here, $E_{k'}$ is the total number of links originating at k'-neurons and $E = N\langle k\rangle = N\langle j\rangle$ is the total number of links in the network. We calculate $E_{k'}$ by summing up all outgoing links of all k'-neurons as in the following. The total number of k'-neurons in the network is $NP^{\text{in}}(k')$. Since there are no correlations between in- and out-degree per neuron, a fraction $P^{\text{out}}(j')$ of the k'-neurons has out-degree j' and the number of outgoing links of that fraction is

$$j' P^{\text{out}}(j') N P^{\text{in}}(k'), \tag{2.32}$$

which is the number of outgoing links from neurons with in-degree k' and out-degree j'. Summing up the total number of outgoing links of all k'-neurons with out-degree j', we obtain the total number of links that originate at neurons with in-degree k'

$$E_{k'} = NP^{\text{in}}(k') \sum_{j'} j' P^{\text{out}}(j') = N \cdot P^{\text{in}}(k')\langle j'\rangle. \tag{2.33}$$

Inserting the above result in Equation (2.31), we obtain for the joint-in-degree distribution

$$N_{kk'} = k f(k, k') = k P^{\text{in}}(k'), \tag{2.34}$$

and for the input mean and variance of Equations (2.24, 2.25)

$$\mu_k = J\tau \left(\nu_{\text{thr}} s + k\hat{r}\right), \tag{2.35}$$

$$\sigma_k^2 = J\mu_k, \tag{2.36}$$

where $\hat{r}$ is the mean stationary firing rate of the network

$$\hat{r} = \sum_k P^{\text{in}}(k)\hat{r}_k. \tag{2.37}$$

We observe, that the self-consistent equations (2.22) for the stationary population firing rates decouple to

$$\hat{r}_k = \phi_k(\hat{r}), \tag{2.38}$$

and that we can obtain a one-dimensional equation for the mean stationary firing rate $\hat{r}$ of the whole network

$$\hat{r} = \sum_k P^{\text{in}}(k)\phi_k(\hat{r}). \tag{2.39}$$

Note, that this equation is independent of the out-degree distribution $P^{\text{out}}(j)$ of the network, which results from the high level of randomness in the connectivity structure.

(2) Uncorrelated IOE networks

Consider a network, where in-degrees of the neurons are randomly drawn from $P^{\text{in}}(k)$, and the out-degree of each neuron is set equal to its in-degree, giving $P^{\text{out}}(j) = P^{\text{in}}(k)$ for $j = k$. We will see that the positive in-out correlations prevent a decoupling of the self-consistent rate equations. First assume no in-degree correlations in the network so that again the probability of a random input into a k-neuron to originate at a k'-neuron is equal to the fraction of links in the network that originate at k'-neurons

$$f(k, k') = \frac{E_{k'}}{E}. \tag{2.40}$$

We count the number $E_{k'}$ of outgoing links from all k'-neurons

$$E_{k'} = k' N P^{\text{in}}(k'), \tag{2.41}$$

which gives together with Equation (2.40) for the joint-in-degree distribution

$$N_{kk'} = k f(k, k') = k \frac{k'}{\langle k \rangle} P^{\text{in}}(k'). \tag{2.42}$$

Inserting the above expression into Equations (2.24, 2.25), we obtain following input mean and variance

$$\mu_k = J\tau \left(\nu_{\text{thr}} s + \frac{k}{\langle k \rangle} \sum_{k'} k' P^{\text{in}}(k') \hat{r}_{k'} \right), \tag{2.43}$$

$$\sigma_k^2 = J \mu_k. \tag{2.44}$$

The above result shows that for uncorrelated IOE networks the input means and variances are coupled across all populations via the stationary population firing rates $\hat{r}_{k'}$. We find that the contribution of each k'-population in the sum of Equation (2.43) is multiplied by k' in comparison to an uncorrelated IOU network. We can interpret this result as a generic effect of the 'in-out assortativity' per neuron on the network dynamics: Neurons with high in-degree also have high out-degree, so that their spiking activity is mediated by a larger number of outgoing connections.

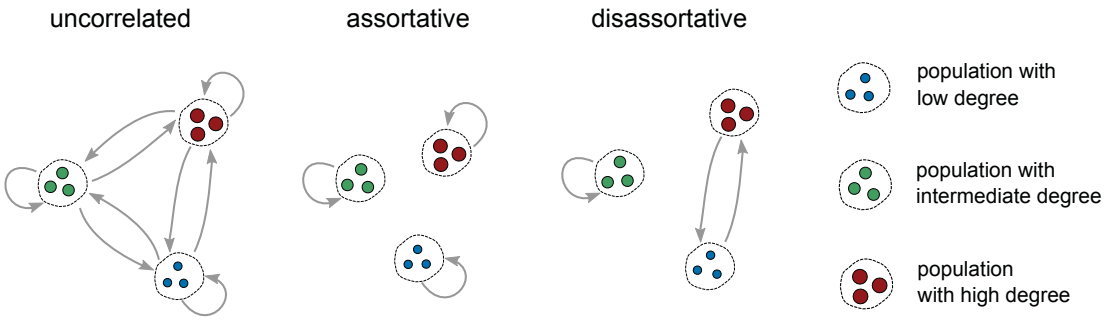

Figure 2.5. Schematic of the coupling between distinct populations for networks with different in-degree correlations. In an uncorrelated network all populations are interconnected and each population also has recurrent connectivity. Strongly assortative networks segregate into decoupled populations with recurrent connectivity. Strongly disassortative networks segregate into subnetworks with strongly coupled high-degree and low-degree populations, and populations of intermediate degree with recurrent connectivity.

(3) Correlated IOE networks

In-degree correlations dramatically alter the coupling between distinct populations, which is reflected by altered joint-in-degree distributions. In Figure 2.5 we illustrate how the coupling patterns differ for different in-degree correlations. In assortative IOE networks, neurons connect preferably to others with similar in-degree and the connection probability $f(k, k')$ can in principle depend nontrivially on the in-degree distribution. Exact expressions for $f(k, k')$ have been calculated for undirected networks in [287]. We here focus on a particularly simple case of a fully assortative IOE network, where neurons of equal in-degree are connected exclusively. This network segregates into disconnected k-populations and

$$f(k, k') = \delta(k, k'), \tag{2.45}$$

where $\delta(k, k')$ is the Kronecker delta. The equal in- and out-degree per neuron in an IOE network assures that the sum of outgoing links of a k-population equals the sum of incoming links. In networks, where these numbers do not match, the populations cannot be entirely disconnected.

In disassortative IOE networks, high-degree neurons preferably connect to low-degree neurons and vice-versa. Consequently, neurons of moderate degree likely connect to other neurons with moderate degree. In the process of constructing a maximally disassortative network, at first neurons of highest in-degree will be connected to neurons of the lowest in-degree. Depending on the in-degree distribution of the network, either the outgoing links of high-degree neurons will be used up first, or the incoming links of low-degree neurons, respectively. In the former case, neurons of the second high-

est in-degree will begin to connect to neurons of the lowest in-degree, whereas in the latter case, neurons of the highest in-degree will begin to connect to the neurons of second lowest in-degree and so on. Thus, the connection probability $f(k, k')$ depends nontrivially on the in-degree distribution of the network. For a quantitative analysis in undirected networks, see [287]. However, in simulations we observed that for the strongly disassortative IOE network, which we introduce in the next section, $f(k, k')$ can be approximated by

$$f(k, k') = \delta\left(k, \tilde{k}'(k)\right), \tag{2.46}$$

where $\tilde{k}'(k)$ is defined by the in-degree distribution of the network. Note that in the case of equal in- and out-degree per neuron (IOE networks) the occurrence of in-degree correlations implies the existence of similar correlations between out-degrees (including out-out, in-out, and out-in correlations). In the case of uncorrelated in- and out-degree per neuron (IOU network) it is possible to impose in-degree correlations as well as out-degree correlations (or in-out, out-in). However, the maximum level of correlations that can be imposed on the network depends nontrivially on the in- and out-degree distribution as well as on correlations between the in- and out-degree per neuron.

2.4 Network model

We are interested in strongly heterogeneous connectivity structures, therefore we consider a network with power-law in-degree distribution and, for simplicity, an equal out-degree distribution. Networks with power-law ('heavy-tailed') degree distribution have been subject to strong scientific interest for over two decades (see [7, 39, 20, 196] for reviews) and similar distributions have been found for anatomical [132, 170, 247] and functional [97, 3, 272] cortical networks and recently, also for neural cultures grown in-vitro [94].

We assume sparse connectivity, so that any two neurons are unlikely to share a large number of common input. In reality, a neuron has a limited number of connections, hence we use a lower and upper limit for the in- and out-degree distributions. In what follows, we first describe the method for generating correlated model networks and after that, we characterize the connectivity structure of several representative networks of interest.

2.4.1 Construction method

We use the configuration model that is described in Section 1.1.2 to construct directed graphs with the desired in- and out-degree distributions. The algorithm generates a small number of self-edges and multiedges, which we simply remove. This creates biased samples of all possible network configurations [190]. However, since the networks are large and sparse, they contain very few self-edges and multiedges, so that this bias is negligible.

We generate IOU networks, where in- and out-degrees per neuron are uncorrelated and IOE networks, where in- and out-degree are equal for each neuron. The IOU network is generated as follows. First, we create a list with N numbers that are drawn from the in-degree distribution. This list is copied, so that we have an exact replica of it. Then, we consider a set of N neurons and assign each of the neurons a target in-degree that is drawn at random from the first list and a target out-degree that is drawn at random from the second list (the entries are removed from the respective list). Links are created at random between the ingoing and outgoing stubs as described in Section 1.1.2. For generating IOE networks, we simply set the target out-degree for each neuron equal to its target in-degree.

We additionally impose assortative and disassortative in-degree correlations on the IOE networks by swapping links according to a Metropolis algorithm [289] for directed networks, which works as follows. The algorithm selects two random links i, j, which originate at nodes with in-degrees k_i, k_j and go into nodes with in-degrees m_i, m_j (Figure 2.6). The targets of both links are swapped with probability g, if the swap increases the desired in-degree correlations of the graph. Respectively, with probability $1 - g$,

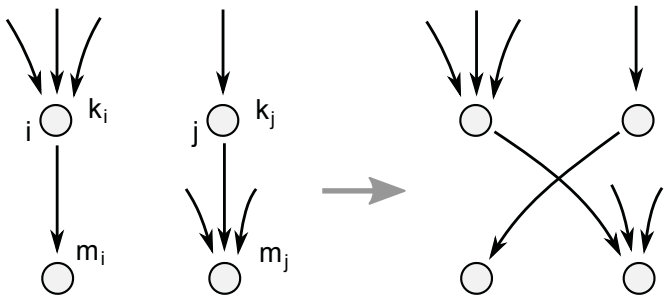

Figure 2.6. Schematic of a link swap that increases assortative in-degree correlations in the network without changing the in- and out-degrees of the nodes.

the targets are swapped at random, which randomizes the connections and decreases degree correlations. Hence, the level of assortativity or disassortativity is controlled by g, with the values $g = 0$ for maximal randomness and $g = 1$ for maximal correlations.

A swap increases assortativity, if

$$k_i m_i + k_j m_j < k_i m_j + k_j m_i. \tag{2.47}$$

A simple example for a link swap that increases assortative in-degree correlations is shown in Figure 2.6. A swap increases disassortativity, if

$$k_i m_i + k_j m_j > k_i m_j + k_j m_i. \tag{2.48}$$

The swapping procedure is repeated until the network reaches a steady-state with respect to further iterations. We found the steady-state to set in at about 10^9 iterations for a network of size $N = 10^5$ (compare Figure 2.7B). Degree correlations are quantified by the Pearson in-degree correlation coefficient p_{in} as defined by Equation (1.8) in Section 1.1.1.

2.4.2 Connectivity structure of the model

Assume a network, where in- and out-degrees are distributed according to a power-law $P^{\text{in}}(k) \sim k^{-\bar{\gamma}}$ between a minimum and maximum degree:

$$P^{\text{in}}(k) = \begin{cases} Z \cdot k^{-\bar{\gamma}}, & k_{\min} \leq k \leq k_{\max} \\ 0, & \text{else,} \end{cases} \tag{2.49}$$

with the normalization constant

$$Z = \left(\sum_{k=k_{\min}}^{k_{\max}} k^{-\bar{\gamma}} \right)^{-1}. \tag{2.50}$$

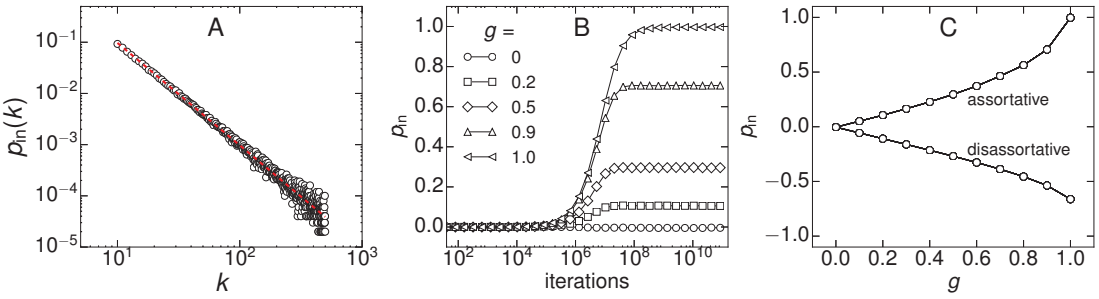

Figure 2.7. Characterization of the IOE network. (**A**) Power-law in-degree distribution $P^{\text{in}}(k) = Z \cdot k^{-2}$ between the minimum and maximum in-degrees $k_{\min} = 10$, $k_{\max} = 500$. Open symbols represent a histogram sampled from a network with 10^5 neurons and red dashed line illustrates the theoretical distribution. (**B**) Pearson coefficient after repeated iterations of the Metropolis algorithm for different swapping probabilities g in the assortative case. (**C**) Pearson coefficient after saturation (10^{10} iterations). All results are ensemble averages from 10 independent realizations of a network with $N = 10^5$.

We here choose $\bar{\gamma} = 2$, $k_{\min} = 10$, $k_{\max} = 500$. An exemplary plot of the in-degree distribution with these parameters is shown in Figure 2.7A for a network with $N = 10^5$.

For the IOE network, we impose degree correlations by applying the Metropolis algorithm for link rewiring. The dependence of the Pearson coefficient on the number of iterations of the algorithm is shown in Figure 2.7B for a network with $N = 10^5$. One observes that p_{in} saturates after 10^9 iterations at values that depend on the rewiring probability g. The saturation values for p_{in} against g range from 0 up to 1 for the assortative network, but only to about -0.66 for the disassortative network (Figure 2.7C). The reason that we cannot achieve a Pearson coefficient of $p_{\text{in}} = -1$ for the disassortative network lies in the heterogeneity of the in-degree distribution. While there is a large number of neurons with low in-degree in the network, only very few neurons with high in-degree exist. In the fully disassortative network, the neurons with lowest in-degree receive links from neurons with highest in-degree, but since there are not enough outgoing links from them, the neurons with lowest in-degree must also connect to neurons with second-highest in-degree (and lower), which results in a smaller Pearson coefficient.

In the following we will characterize the network topology for three representative cases: the uncorrelated, fully assortative and fully disassortative IOE network. The corresponding Pearson coefficients are $p_{\text{in}} = -0.004$, $p_{\text{in}} = 0.997$ and $p_{\text{in}} = -0.662$, respectively. Figure 2.8 shows the connection probabilities $f(k, k')$ that are sampled from the adjacency matrices of the networks. For the uncorrelated network (Figure 2.8A), we observe a broad coupling across all populations and a significant decrease of $f(k, k')$ for increasing k'. This decrease results from the decreased probability to find high-degree

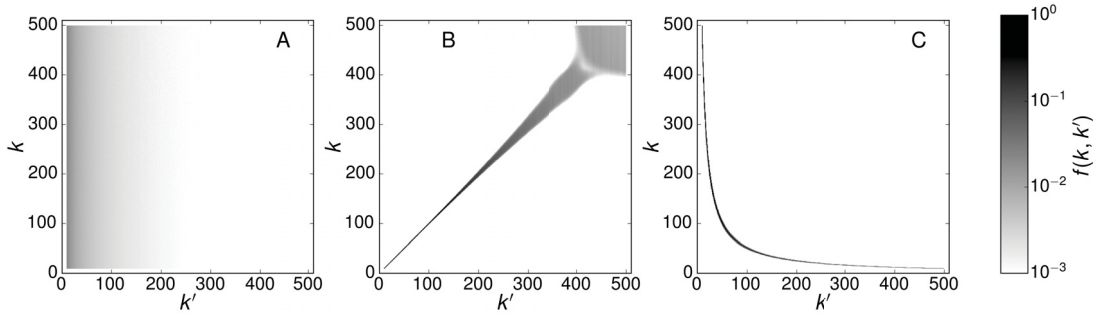

Figure 2.8. Probability $f(k, k')$ for a random input of a k-neuron to originate at a k'-neuron for IOE networks. Normalization demands $\sum_{k'} f(k, k') = 1$. (**A**) Uncorrelated network, (**B**) assortative network, (**C**) disassortative network. An ensemble of 10 independent realizations of a network with $N = 10^5$ was used for sampling of $f(k, k')$. This figure has been modified from [228].

neurons in the network. On the other hand, the assortative and disassortative networks show highly selective coupling (Figures 2.8B, C). The broadening of $f(k, k')$ for large k and k' in the assortative network (top right corner of Figure 2.8B) results from the finite size of the simulated network.

For the mean-field analysis, we use simplified expressions for $N_{kk'} = kf(k, k')$, which were acquired in Section 2.3.2. These can now be evaluated using the specific degree distribution (2.49). For the uncorrelated network we use Equation (2.42) for $f(k, k')$, which gives with the distribution (2.49)

$$f(k, k') = \frac{k'}{\langle k \rangle} P^{\text{in}}(k') = \frac{Z}{\langle k \rangle} k'^{-1}. \tag{2.51}$$

The inverse dependency $f(k, k') \sim k'^{-1}$ in the above equation explains the strong decrease of $f(k, k')$ in Figure 2.8A for increasing k'. For the assortative network, we find that Equation (2.45)

$$f(k, k') = \delta(k, k') \tag{2.52}$$

gives a good approximation of the peaks in Figure 2.8B. Finally, for the disassortative network, we find

$$f(k, k') = \delta(k, \tilde{k}'), \tag{2.53}$$

where $\tilde{k}'(k) = \frac{k_{\min} k_{\max}}{k}$ is given by a fit of the peak positions in Figure 2.8C.

On a final note, a random network model typically refers to the ensemble of all configurations of a graph that conform to certain topological characteristics, e.g. the

degree distribution of nodes [41, 200, 199, 196]. Accurate numerical results are obtained by averaging over many realizations of a random graph model. Unfortunately, this can be computationally expensive, if the networks are subject to long-term dynamics as in our study. Therefore, we use ensemble averages of the graphs for statistical network analysis in this section and single graphs for each simulation of the stochastic network dynamics in the next section, where neuronal spiking is monitored over long time-periods.

2.5 Population activity of the network model

In this section we explore the population dynamics of networks with in- and out-degree distributions according to (2.49). For this purpose, we employ the rate equation (2.28), which again reads

$$\tau_x \frac{d}{dt}\hat{\mathbf{r}}(t) = -\hat{\mathbf{r}}(t) + \mathbf{\Phi}(\hat{\mathbf{r}}(t), s), \tag{2.54}$$

where $\hat{\mathbf{r}}(t)$ is the vector of population firing rates, $\mathbf{\Phi}(\hat{\mathbf{r}}(t), s)$ is the vector of transfer functions as defined in Equation (2.26) and the time-constant τ_x is set to 3 ms as suggested by [187, 118]. All population rates are initialized with 500 Hz and then evolve according to (2.54). For all networks we show that the population firing rates approach stationary values for several different stimuli and then, we examine the stationary population activity for varying stimulus levels. Moreover, we compare the stationary solutions of Equation (2.54) to full numerical simulations of large-scale LIF networks.

First, we focus on random networks without in-degree correlations and compare the dynamics of an IOU network (in-out uncorrelated) and an IOE network (in-out equal). After that, we explore the dynamics of correlated IOE networks.

2.5.1 Uncorrelated IOU and IOE networks

Let us examine the approximate time-dependent population rate dynamics of the IOU and IOE network using Equation (2.54). Figure 2.9 shows the time-evolution of several population firing rates for three different levels of the stimulus, $s = 1.2$, $s = 0.85$ and $s = 0.5$ (solid lines). Additionally, we plot the mean firing rates of the networks (dashed lines). For both networks, the population firing rates quickly approach stationary values for high input ($s = 1.2$, top row in Figure 2.9), with increased firing rates for populations with higher k. The mean firing rates of the networks (dashed lines) are proximate to the firing rates of the low-degree populations, since low-degree neurons make up a large proportion of the networks. The population firing rates in the IOE network are increased in comparison to the IOU network, which results from larger recurrent activity

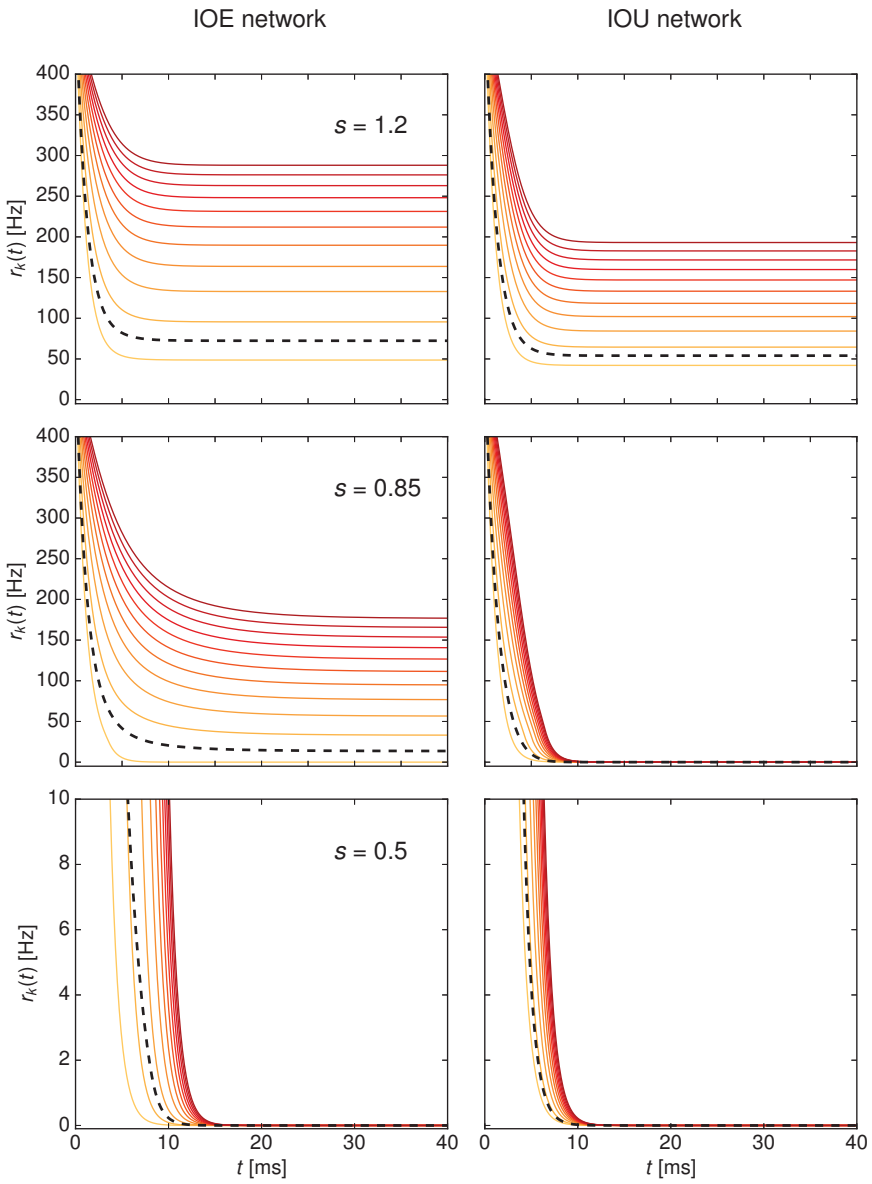

Figure 2.9. Population rate dynamics of uncorrelated IOE and IOU networks. Time evolution of several population firing rates (straight lines) and the mean firing rate (dashed line) for three different levels of s. Population firing rates are shown for $k = 10, 59, 108, \cdots, 451, 500$ (from yellow to red).

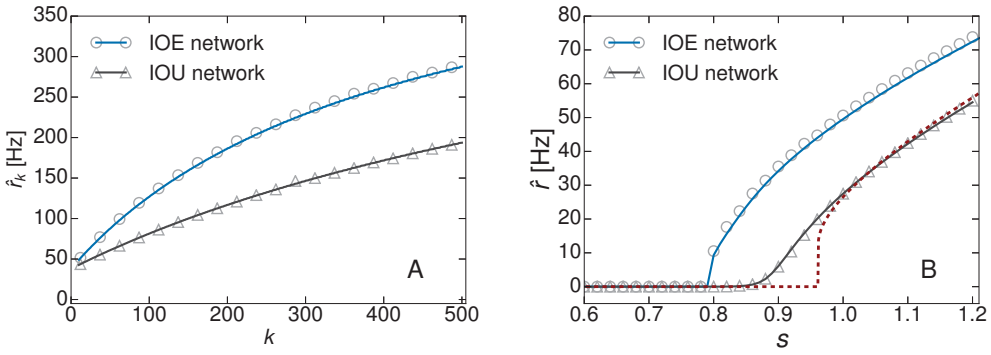

Figure 2.10. Stationary activity of uncorrelated IOE networks. (**A**) Population firing rates for $s = 1.2$. (**B**) Mean firing rate of the network for different stimuli s. Lines represent theoretical predictions from solving the self-consistent equations (2.22) and open symbols are results from full IF simulations ($N = 10^5$). The red dashed line results from the mean-field prediction (2.55) which neglects network heterogeneity and takes into account only the mean degree of the network.

due to the larger proportion of links originating at highly active neurons with high in-degree. For a stimulus slightly below threshold ($s = 0.85$, middle row in Figure 2.9), all population rates in the IOU network go to zero, whereas only the populations with small k fail to sustain activity in the IOE network. This indicates that the elevated recurrent activity in the IOE network prevents the strongly connected neurons from failure of firing for this stimulus level. Finally, for a low level of the stimulus ($s = 0.5$, bottom panel in Figure 2.9), all population firing rates quickly approach zero in both networks, since there is not enough recurrent activity to compensate for the low stimulus input.

Figure 2.10A shows the stationary population firing rates for both networks for $s = 1.2$. Open symbols represent simulation results and lines are mean-field predictions. Theory and simulation results agree very well. We observe a nonlinear increase of $\hat{r}_k$, which can be explained as follows. Neurons with larger in-degree k receive a higher mean input μ_k. However, for large μ_k the population transfer function (2.22) approaches the constant value $1/\tau_{\mathrm{ref}}$. Roughly speaking, neurons with more inputs fire closer to their maximum rate so that for increasing k the firing rate increases by smaller amounts until it saturates at $1/\tau_{\mathrm{ref}}$. Interestingly, the stationary population rates in the IOE network are substantially elevated in comparison to the IOU network only for large k, which can be explained as follows. The total input current to a neuron is the sum of recurrent input from afferent spiking neurons and stimulus input. The recurrent input is proportional to the in-degree k and the stimulus input is constant for each neuron. For neurons with lowest in-degree ($k = 10$), the recurrent input is relatively small compared to the stimulus current with a ratio of roughly $\frac{k\hat{r}}{\nu_{\mathrm{thr}} s} \simeq 0.05$ for the IOU network (see Equation (2.35)), whereas the ratio for neurons with highest in-degree

($k = 500$) is about 2.5. Hence, the input of neurons with low in-degree is almost independent of recurrent activity, whereas the input of neurons with high in-degree is strongly affected by a raise of recurrent activity.

How do the networks respond to varying stimulus levels? Figure 2.10B shows the stationary mean firing rates of the networks for increasing s from mean-field theory (lines) and from simulations (open symbols). Additionally, we show a mean-field curve that is based on the mean degree $\langle k \rangle$ of the network (red dashed line), which is obtained by solving the simplified rate equation

$$\hat{r} = \phi_{\langle k \rangle}(\hat{r}), \tag{2.55}$$

where $\phi_{\langle k \rangle}$ is the transfer function for a single population with in-degree $\langle k \rangle$.

We observe a similar behavior for both networks: The mean firing rate is zero for $s < 0.8$ and transitions towards sustained firing at a critical stimulus s_c (the 'transition point'). The solution of Equation (2.55) gives a good approximation for the curve of the IOU network for stimuli above the threshold ($s > 1$), but strongly deviates in the subthreshold regime. For $s < 1$, the curve $\hat{r}(s)$ for the IOU network appears to be smoothed. This effect is similar to the smoothing of the response curve of IF neurons due to noise [151], but here results from the heterogeneity of the in-degree distribution. In comparison, the firing rate curve of the IOE network shows a relatively sharp increase at $s \simeq 0.8$ and is shifted to the left as a result from the increased recurrent activity in the network.

2.5.2 Degree-correlated IOE networks

Let us now turn to IOE networks with in-degree correlations. We focus on a fully assortative and fully disassortative network with Pearson coefficients $p_{\text{in}} = 0.997$ and $p_{\text{in}} = -0.662$, respectively, and compare them to an uncorrelated network that has $p_{\text{in}} = -0.004$. The time-evolution of several population firing rates is shown for all networks in Figure 2.11 (straight lines) for three levels of the stimulus, $s = 1.2$, $s = 0.85$ and $s = 0.5$. Dashed lines in Figure 2.11 represent the mean firing rates of the networks. Assortativity increases the firing rates of high-degree populations and decreases the firing rates of low-degree populations, as we can observe for $s = 1.2$ in the top row of Figure 2.11. Disassortativity has the opposite effect. In the assortative network, strongly connected neurons fire close to their maximum rate of $1/\tau_{\text{ref}} = 500$ Hz, whereas in the uncorrelated and dissasortative networks these neurons fire at much lower rates.

For a stimulus slightly below the threshold ($s = 0.85$, middle row in Figure 2.11), an interesting effect occurs. In the assortative network, the firing rates of populations with lowest k approach zero, whereas populations with high k sustain firing at almost equal rates as for $s = 1.2$. In the disassortative network, on the other hand, all populations fail to sustain activity. These effects can be explained as follows. The assortative

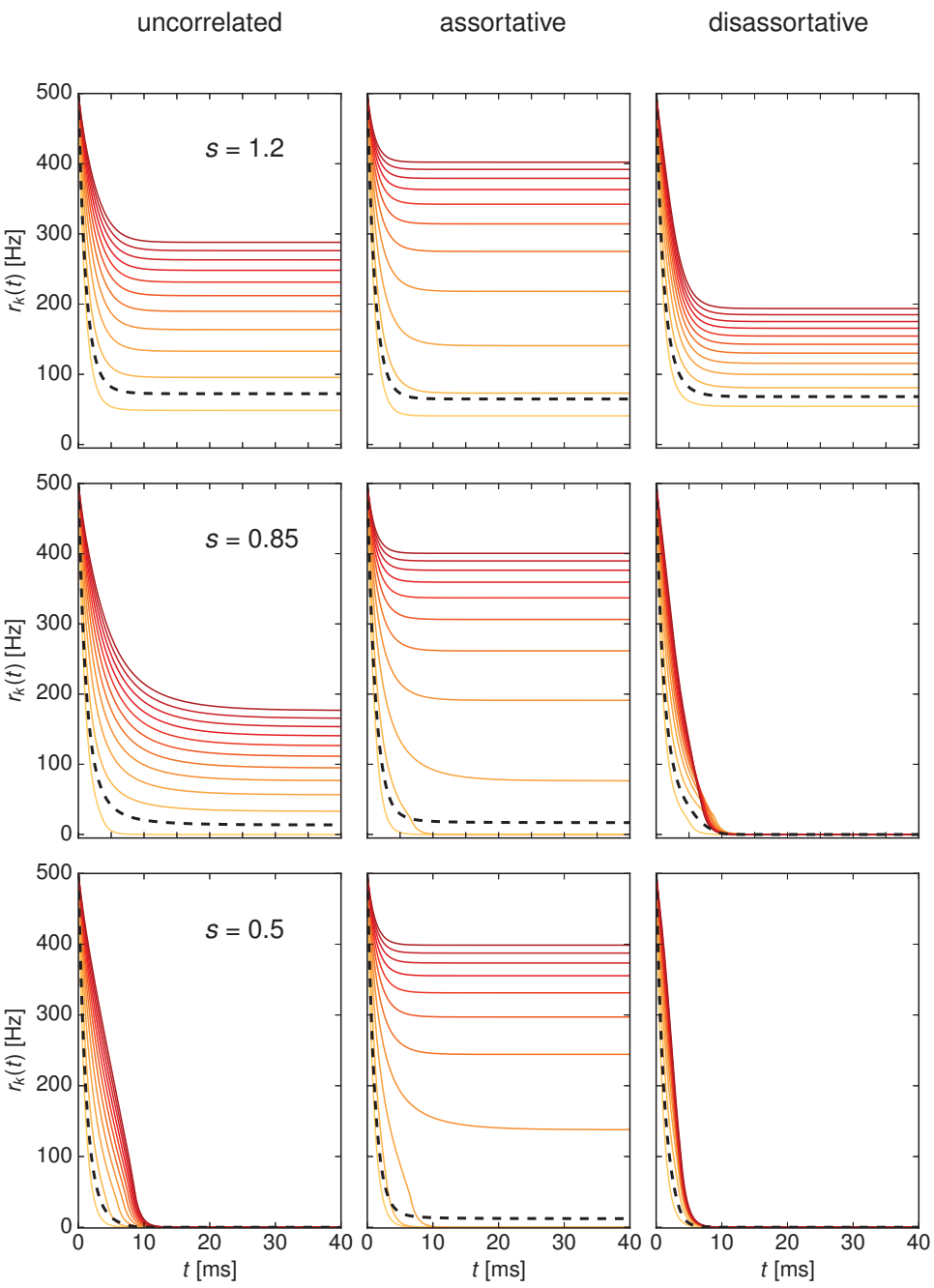

Figure 2.11. Population rate dynamics of correlated IOE networks. Time evolution of several population firing rates (straight lines) and the mean firing rate (dashed line) for three different levels of s. Population firing rates are shown for $k = 10, 59, 108, \cdots, 451, 500$ (from yellow to red).

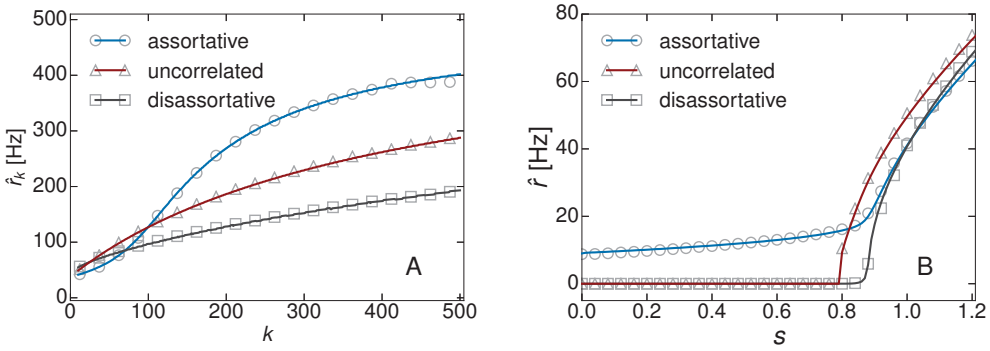

Figure 2.12. Stationary activity of correlated IOE networks. (**A**) Population firing rates for $s = 1.2$. (**B**) Mean firing rate of the network for different stimuli s. Lines represent theoretical predictions from solving the self-consistent equations (2.22) and open symbols are results from full IF simulations ($N = 10^5$).

network is segregated into subnetworks of neurons with similar degree so that distinct populations are only weakly coupled. Due to the weak coupling, a decrease of activity of weakly connected neurons has just a small effect on the activity of stronger connected neurons. Thus, weakly connected neurons that receive low input fail to fire, whereas strongly connected neurons sustain activity for lower levels of s. The disassortative network, on the other hand, is segregated into subnetworks, in which strongly connected neurons receive input from weakly connected neurons and vice-versa, so that failure of firing of weakly connected neurons leads to failure of firing of strongly connected neurons: Since the total input current of weakly connected neurons is almost exclusively made up from the stimulus, these neurons fail to fire at $s = 0.85$. Consequently, the strongly connected neurons lack their spiking input and fail to sustain their activity as well.

For a low level of the stimulus ($s = 0.5$, bottom row in Figure 2.11), all population firing rates in the uncorrelated and disassortative network go to zero. In contrast, the firing rates of high-degree populations in the assortative network approach nonzero values. This indicates that the extremely well connected hub neurons in the assortative network receive sufficient recurrent input from afferent spiking hub neurons so that they can sustain firing for very low stimuli.

In Figure 2.12A we show the stationary population firing rates of the networks for $s = 1.2$. We again observe that assortativity decreases the rates of low-degree populations and increases the rates of high-degree populations. Disassortativity has the opposite effect. The curves $\hat{r}_k$ for the assortative and disassortative network intersect at $k \simeq 70$. Hence, we assume that the population with $k = 70$ in the disassortative network is almost exclusively recurrently coupled. This is confirmed by the peak for

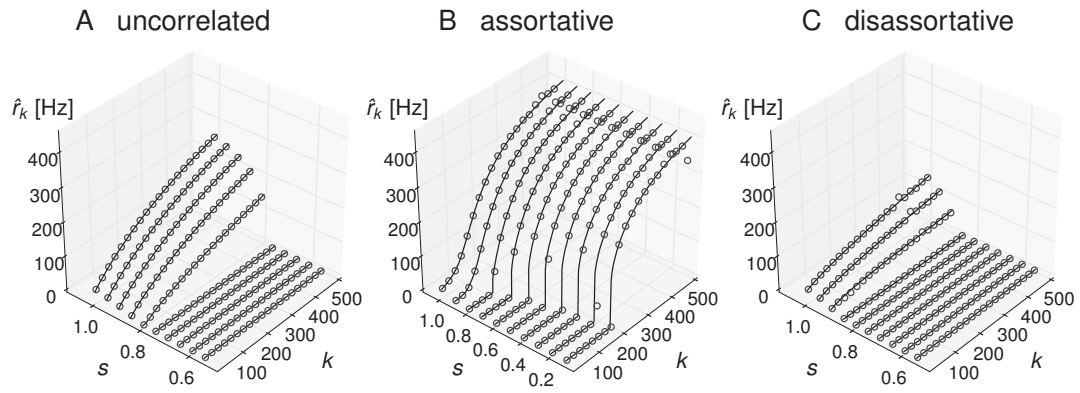

Figure 2.13. Stationary k-population firing rates of the correlated IOE networks for subthreshold stimuli. Open symbols are results from full LIF simulations ($N = 10^5$) and lines are theoretical predictions from mean-field theory. This figure has been modified from [228].

the probability matrix $f(k, k')$ at $k = k' = 70$ in Figure 2.8.

Degree correlations also strongly affect the stationary average firing rates of the networks for varying levels of the stimulus as we can see from Figure 2.12B. The firing rate curves of the uncorrelated and disassortative network exhibit a sharp transition towards sustained firing at $s_c \simeq 0.8$, whereas the assortative network sustains activity for very weak stimuli down to $s = 0$. The transition point of the disassortative network is slightly above the one for the uncorrelated network, indicating that the disassortative network is slightly less sensitive to weak stimuli. On the other hand, the global activity of assortative networks is extremely robust against decreasing stimulus levels, because strongly connected neurons receive sufficient recurrent input from other strongly connected neurons so that they can sustain firing.

To illustrate this effect, we show the stationary population firing rates of the three networks for decreasing s in Figure 2.13. In the uncorrelated network (Figure 2.13A), the stationary firing rates of all different populations decrease in a similar way until they transition to zero at the same threshold $s \simeq 0.8$ due to the strong coupling of activity across all populations: At first, the weakly connected neurons fail to sustain spiking, since they receive the smallest amount of total input current. Their failure of firing leads to a decrease of recurrent input to adjacent neurons in the network. This decrease in input results in failure of firing of stronger connected neurons, which further decreases the recurrent activity in the network, and so forth. This cascading failure of firing of stronger connected neurons produces an abrupt decrease of the mean firing rate of the network when the stimulus decreases below the transition point.

In the assortative network (Figure 2.13B), populations with large k sustain their activity for very low inputs. As s decreases we observe an increasing number of popu-

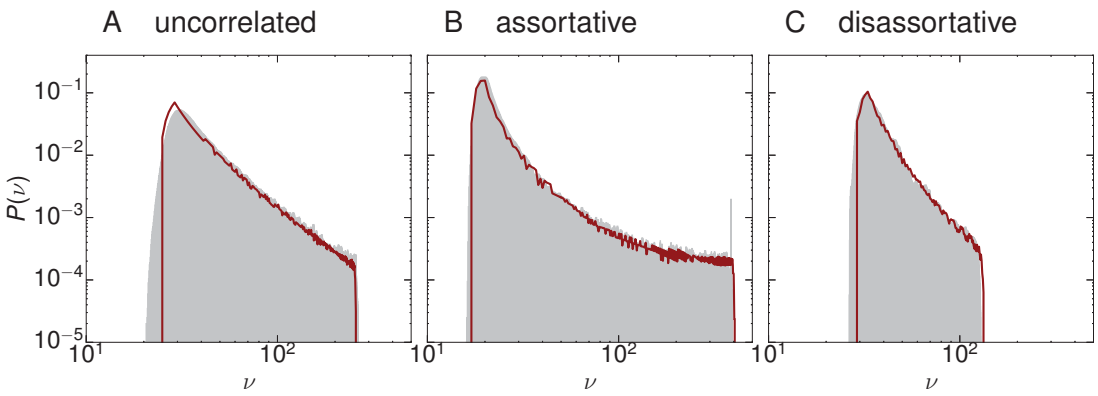

Figure 2.14. Distribution of stationary firing rates of individual neurons for an IOE network for $s = 1.2$ and $N = 10^5$. Gray area represents simulation data and solid red lines correspond to theoretical predictions (see text). Assortativity broadens the firing rate distribution and disassortativity narrows it. Note, that the distributions of firing rates appear to be power-law tailed for the disassortative and uncorrelated network, but more skewed in the assortative network.

lations with small k that fail to sustain firing. The strongly connected neurons receive high recurrent input so that they fire close to their maximum rate of 500 Hz and their frequency of firing stays almost constant for decreasing s. Finally, in the disassortative network (Figure 2.13C), all population firing rates are very low and they quickly transition to zero for a decreasing stimulus.

Can we use the mean-field model to predict the distribution $P(\nu)$ of individual neuron firing rates? Apparently, we can estimate $P(\nu)$ from the mean population rates, if we neglect variations of the firing rates within each population. In this case, all k-neurons are assumed to fire with equal rates and each rate $\hat{r}_k$ occurs $NP^{\text{in}}(k)$ times in the network. This distribution can be binned and normalized to estimate the actual firing rate distribution. In Figure 2.14 we show $P(\nu)$ for the stationary activity of the three networks for $s = 1.2$ from simulations of large-scale LIF networks (gray area) and we observe that the estimate from the population rates (red lines) gives a good approximation of the real distribution. Assortativity broadens the distribution and disassortativity narrows it, according to the broadening and narrowing effect for the distribution of population firing rates.

Our finding that assortativity increases the persistence of the network activity for weak stimulus levels is consistent with recent studies showing that assortative networks are robust against random failure of nodes or links [197, 280, 198, 289, 287, 40, 276, 203, 123, 229]. In our model, a neuron in the network fails to sustain firing, if the sum of the stimulus and recurrent input drops below a threshold value. Therefore, our system can be related to a *bootstrap percolation* model, where nodes in a network are

activated if their input exceeds a threshold [27, 11]. Baxter et al. [27] found that for degree distributions with finite first moment $\langle k \rangle$, but diverging second moment

$$\langle k^2 \rangle = \sum_{k_{\min}}^{\infty} k^2 P(k), \tag{2.56}$$

the network becomes active if an infinitely small fraction of its nodes is active. However, their results are not directly comparable to the ones in our study, because they apply to infinite networks, where hub-nodes have extremely large in-degrees. Neurons in our model network have a maximum in-degree of $k_{\max} = 500$, so that the second moment of the in-degree distribution does not diverge. Moreover, the maximum firing rate of the neurons is restricted by the refractory period τ_{ref}, which limits the influence of extremely well connected neurons on the global dynamics. Nevertheless, our results are in good agreement with the finding of Baxter et al., since we find that the heterogeneous in-degree distribution allows the network to sustain activity for lower levels of s in comparison to a network where each node has equal in-degree (see the response curve for the uncorrelated IOU network in Figure 2.10). Our main conclusion is, however, that the resilience of a heterogeneous network is further enhanced by assortative degree correlations. Based on these findings, we predict a strong effect of assortative degree correlations in a bootstrap percolation model, which may be confirmed or rejected by further studies.

2.6 Information transfer of the stimulus/response relation

In the previous section we showed that degree correlations strongly influence the mean response of a network to small inputs. A central result is that assortative networks sustain activity for very weak stimulus levels, where the uncorrelated and disassortative networks would not fire. This can be interpreted as an improved ability of the assortative networks to sense and amplify weak stimuli. In this section we explore how the network could possibly transmit information about these stimuli and how the quality of the signal transmission is influenced by assortativity. To this aim, we successively increase the amount of assortative degree correlations and examine how the stimulus-response relationship is affected. Increasing assortativity implies stronger segregation of the network into subnetworks of neurons with similar in-degree, which corresponds to a more selective coupling between the populations, see Figure 2.15.

2.6.1 Stimulus/response relation of assortative IOE networks

Recall that we consider the network response $r(s)$ to be the average stationary firing rate of n randomly chosen neurons in the network. Since this response is pooled from

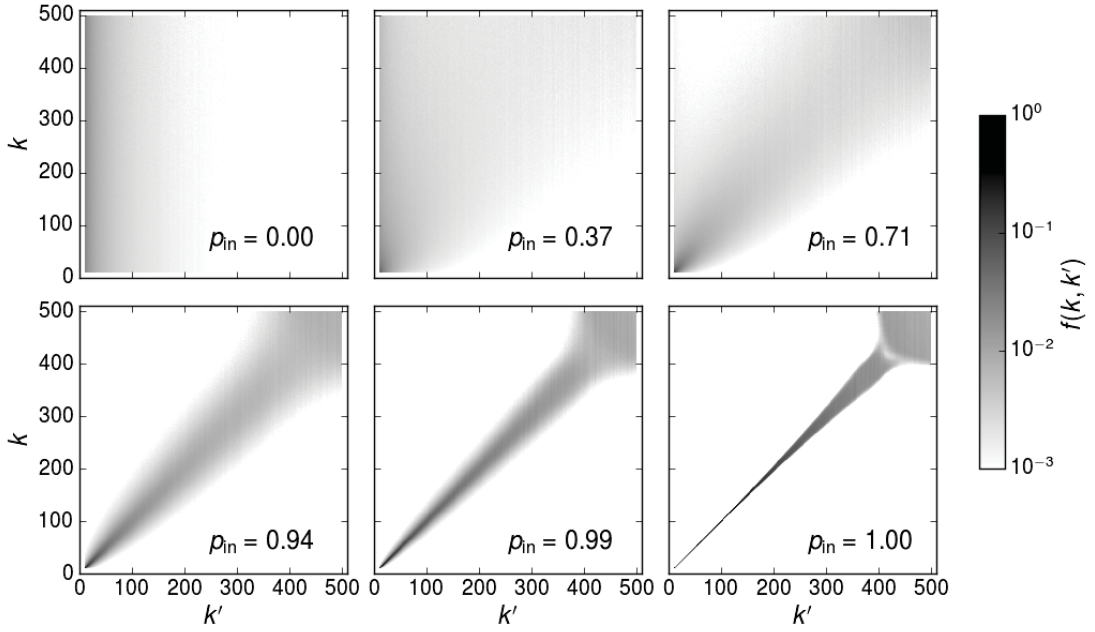

Figure 2.15. Probability $f(k, k')$ for a random input of a k-neuron to originate at a k'-neuron for IOE networks of increasing assortativity. Networks of increasing assortativity exhibit stronger segregation into subnetworks of neurons with similar degree, characterized by more selective coupling between the populations (sharper peaks of $f(k, k')$).

a heterogeneous distribution of individual neuron firing rates (Figure 2.14), it is noisy with respect to multiple samplings. Assume that we conduct multiple trials where we apply the same stimulus s to the network and measure the respective network responses. Due to the sampling noise the responses will be distributed around the mean value $\hat{r}(s)$. For large n this distribution[1] $p(r|s)$ can be approximated by a Gaussian distribution with mean $\hat{r}(s)$ and variance $\sigma^2(s)/n$, where $\sigma^2(s)$ is the variance of the distribution $P(\nu)$ of individual neuron firing rates for a stimulus s. The Gaussian distribution reads

$$p(r|s) = \frac{1}{\sqrt{2\pi\sigma^2/n}} \exp\left(\frac{[r - \hat{r}(s)]^2}{2\sigma^2(s)/n}\right). \tag{2.57}$$

Figure 2.16 illustrates the noisy response curves of increasingly assortative IOE networks from simulations of $N = 10^5$ neurons (left panel) and mean-field calculations (right panel). The black lines correspond to the mean response curves $\hat{r}(s)$ and the thick light red lines indicate ± 1 standard deviation (SD) of the noise of the output

[1] We here refer to the distributions in form of probability densities.

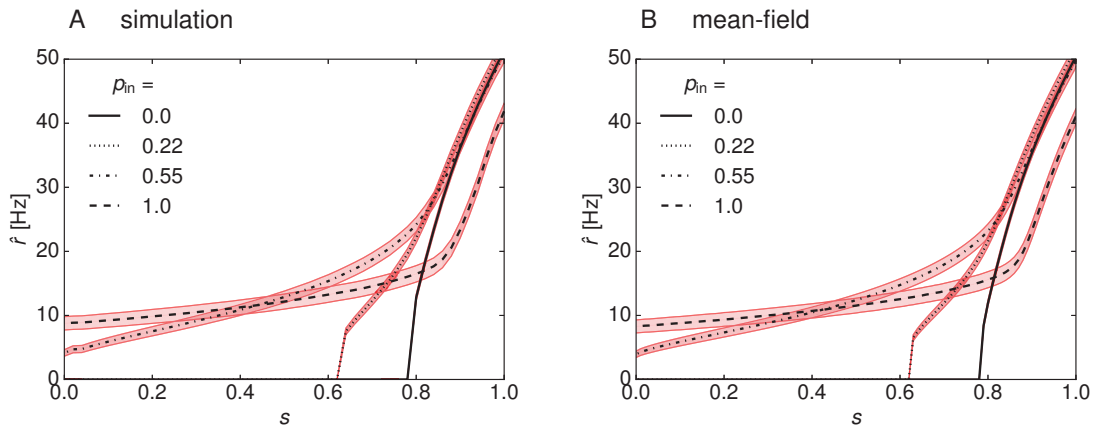

Figure 2.16. Mean stationary firing rate of IOE networks with increasing assortativity (black lines). The thick light red lines indicate ± 1 SD of the noise of the output from $n = 2500$ neurons. Full simulations of 10^5 neurons (left) and results from mean-field theory (right) agree very well. For the mean-field calculations the probabilities $f(k, k')$ were sampled from the adjacency matrices of the simulated networks. This figure has been modified from [228].

from $n = 2500$ neurons, which is given by $\sigma(s)/\sqrt{n}$. For the mean-field curves in the right panel of Figure 2.16, we obtained $\hat{r}(s)$ by solving the self-consistent equations (2.22) with $f(k, k')$ sampled from the adjacency matrix of each network. The variance $\sigma^2(s)$ was obtained by approximating the single-neuron firing rate distribution from the population means as discussed previously for Figure 2.14. Mean-field predictions and simulation results agree very well.

As we can see from Figure 2.16, increasing assortativity flattens the slope of the mean response curve for small s (black lines) and decreases the critical stimulus for sustained network activity. Therefore, assortative in-degree correlations may in principle improve the ability of the network to sense small input signals, where networks with less assortativity would not respond at all. On the other hand, assortativity also increases the sampling noise as indicated by a larger standard deviation (SD) $\sigma(s)/\sqrt{n}$ (broader red lines in Figure 2.16 for larger p_{in}), which is detrimental for signal transmission. We thus turn to a quantitative description of the information transmission capability of the networks using the mutual information of the stimulus/response relation.

2.6.2 Mutual information of the stimulus/response relation

Assume that we present a set of stimuli $p(s)$ to the network and collect a set of network responses $p(r)$ as illustrated in Figure 2.17. Obviously, the set of network responses can only provide meaningful information about the set of stimuli if $r(s)$ is different for different s. The information content of this variability of responses can be quantified

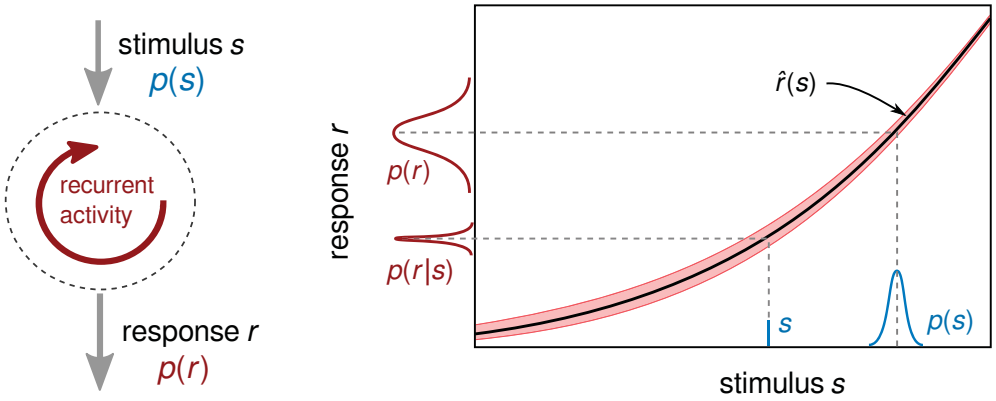

Figure 2.17. Schematic of the input/output relation for a recurrent network. The panel on the right shows the an exemplary mean response curve $\hat{r}(s)$ with red lines indicating ± 1 SD of the output noise. If a stimulus s is applied repeatedly, the network generates a distribution of responses $p(r|s)$ that is centered around the mean $\hat{r}(s)$, because the output is noisy. If the network is subjected to a distribution of stimuli $p(s)$, it generates a distribution $p(r)$ of responses that is also broadened by the output noise.

by the Shannon entropy [85]

$$H = -\int dr\ p(r) \log_2 p(r). \tag{2.58}$$

Roughly speaking, the entropy H measures in bits how much information a given set of network responses can maximally contain about the set of stimuli that evoked the responses. A large response variability (broad $p(r)$) is associated with high information value about the stimulus, because it indicates that small differences of s are mapped to large differences of r and thus, one can easily distinguish between different stimuli by analyzing the corresponding responses.

However, since the network output is noisy, repeated trials involving the same stimulus will evoke different responses. These response variations also contribute to the entropy H, but they are not correlated with changes in the stimulus. The information that is lost due to these variations can be quantified by the so-called *noise entropy* [85]

$$H_{\text{noise}} = -\int ds\ p(s) \int dr\ p(r|s) \log_2 p(r|s). \tag{2.59}$$

We can measure how much information the set of network responses conveys about the set of stimuli by subtracting the noise entropy from the full response entropy, which

gives the input-output *mutual information* [85]

$$I = H - H_{\text{noise}} = -\int dr\ p(r)\log_2 p(r) + \int ds\ p(s)\int dr\ p(r|s)\log_2 p(r|s). \quad (2.60)$$

Our goal is to evaluate the mutual information from the mean response curves $\hat{r}(s)$ and the corresponding sampling noise with variance $\sigma^2(s)/n$. To this aim, we apply a small noise approximation, following Tkačik et al. [265, 264]. With the small noise approximation we neglect the broadening of $p(r)$ due to the sampling noise, since this effect is small for small $\sigma^2(s)/n$. Thus, we replace $p(r)$ by the distribution of mean responses $p(\hat{r})$ the network would generate in the absence of noise if it is subjected to a distribution of stimuli $p(s)$. The corresponding equation for I can be found by using the Gaussian approximation of $p(r|s)$ and expanding Equation (2.60) as a power series in $\sigma/\sqrt{n}$ around $\hat{r}$, keeping only the zero-th order (for the derivation, see Appendix A.3):

$$I \simeq -\int d\hat{r}\ p(\hat{r})\log_2 p(\hat{r}) - \frac{1}{2}\int d\hat{r}\ p(\hat{r})\log_2[2\pi e\sigma^2(\hat{r})/n]. \quad (2.61)$$

The first term on the right-hand side of Equation (2.61) approximates the full response entropy H and the second term equals the (negative) noise entropy H_{noise}. The probability distribution of mean responses $p(\hat{r})$ can be sampled from $\hat{r}(s)$ by using $p(\hat{r})d\hat{r} = p(s)ds$ so that

$$p(\hat{r}) = \left(\frac{d\hat{r}(s)}{ds}\right)^{-1} p[s = s(\hat{r})]. \quad (2.62)$$

Here, $s(\hat{r})$ is the stimulus at which the mean response of the network is $\hat{r}$ and $p[s = s(\hat{r})]$ is the distribution of stimuli evaluated at $s = s(\hat{r})$. In general, the shape of the response curve $\hat{r}(s)$ could be tuned to the specific distribution of stimuli $p(s)$, if this distribution is known [264]. We simply assume that all subthreshold stimuli are equally likely, $p(s) = \text{const.}$, for $0 \leq s \leq 1$. Other choices of $p(s)$ may be also applicable and they possibly favor different shapes of $\hat{r}(s)$ for optimal signal transmission. Using Equation (2.62) we calculate $p(\hat{r})$ from the mean response curves $\hat{r}(s)$ that were shown previously in Figure 2.16. The corresponding $\sigma^2(\hat{r})$ associated with the sampling noise are obtained from the distribution $P(\nu)$ of individual neuron firing rates for each $\hat{r}$. Both quantities, $p(\hat{r})$ and $\sigma^2(\hat{r})$, can be inserted in Equation (2.61) to calculate the mutual information for each network.

We compare numerical results for simulations of large LIF networks with predictions from mean-field theory, since we can obtain $\hat{r}(s)$ and $P(\nu)$ with both methods. For the mean-field calculations, we sampled $f(k, k')$ from the adjacency matrices of the correlated networks and calculated the response curves $\hat{r}(s)$ using the coupled self-consistent

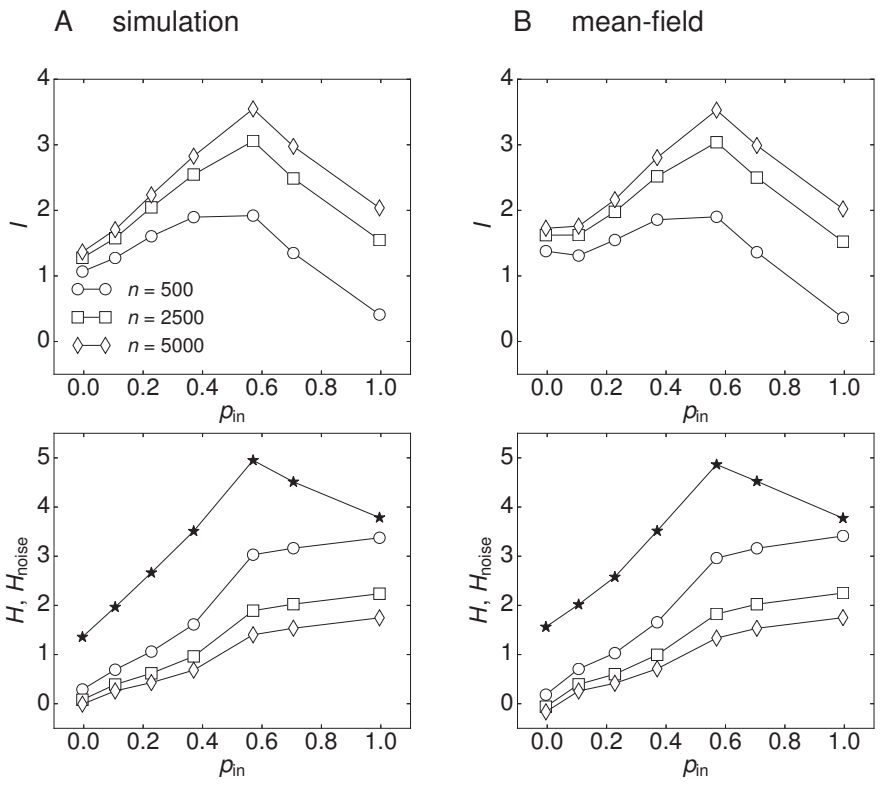

Figure 2.18. Information transfer for IOE networks with increasing assortativity. (**Top row**) Mutual information $I = H - H_{\mathrm{noise}}$ of the input/output relation. (**Bottom row**) Entropy H (stars) and noise entropy H_{noise} (open symbols) of the response. The network output is quantified by the average firing rate of n randomly chosen neurons. (**A**) Numerical simulations of networks with $N = 10^5$ neurons and (**B**) theoretical predictions with the mean-field framework, where the joint-in-degree distribution $N_{kk'}$ is sampled from the adjacency matrices of the correlated networks. This figure has been modified from [228].

equations (2.54) for the population firing rate dynamics. The variance $\sigma^2(\hat{r})$ was sampled from the distribution of mean population firing rates as previously described for Figure 2.14.

Figure 2.18 (top row) shows the input/output mutual information for networks of increasing assortativity for three different values of n. Again, simulation results (left panel) and mean-field predictions (right panel) agree very well. We immediately see that I has a maximum for an intermediate level of assortativity, $p_{\mathrm{in}} \simeq 0.55$, which can be explained as follows. While some amount of assortativity increases the network's sensitivity to small inputs by decreasing its firing threshold, an excess level of assortativity decreases the response variability due to a flattened slope of $\hat{r}(s)$ for small s. A

strongly assortative network segregates into populations of strongly connected neurons that fire close to their maximum rate and populations of weakly connected neurons that do not fire at all. In this state, the network responses to different inputs are very similar, because the strongly connected neurons fire at similar rates for different input levels so that they do not contain much information about the input. Moreover, assortativity increases the output noise, which reduces I even further due to increased H_{noise} (open symbols in Figure 2.18, bottom row) so that the mutual information drops below the initial value for uncorrelated networks.

This indicates that the network response of extremely assortative networks is too noisy to reliably encode information about the stimulus. Note that the entropy H is calculated from the mean response curves under the small noise approximation and hence, it is independent of the number of neurons n the response is pooled from (stars in bottom row of Figure 2.18). The noise entropy, on the other hand, decreases with increasing n, since the variance of the output noise is proportional to $1/n$. Thus, if the response is pooled from a larger number of neurons the mutual information is larger so that the information transmission is more reliable (see top row of Figure 2.18). The optimum level of assortativity shows a slight shift to lower values of p_{in} for increasing n, since the noise-increasing effect of assortativity is less detrimental for signal transmission if the response is pooled from a larger number of neurons.

In general, the information transmission capability of the network defined by two properties of the stimulus/response relation, firstly, the shape of the mean response curve $\hat{r}(s)$ and secondly, the response noise that arises from the variance $\sigma^2(s)$ of the firing rate distribution of individual neurons. Both properties strongly depend on the in-degree distribution and in-degree correlations of the network. A large mean degree is associated with strong recurrent activity and a small threshold at which the network begins to fire. Strong heterogeneity of the in-degree distribution causes a broad distribution of firing rates and large noise in the output. Assortative in-degree correlations decrease the firing threshold and increase the output noise and, importantly, they also change the shape of the mean response curve. For the network model analyzed in this study we find that the signal transmission is optimized for intermediate levels of assortativity. Does this result hold for other networks with different in-degree distributions?

2.6.3 Mutual information for different degree distributions

In the following we will analyze how changes in the in-degree (and out-degree) distribution affect the information transfer of the correlated networks and discuss the generality of our results. For this purpose, we compare the input/output mutual information of three model networks that differ slightly in the exponent of the power-law in-degree distribution, having $\bar{\gamma} = -2.3$, $\bar{\gamma} = -2$ and $\bar{\gamma} = -1.7$. The means and variances of the

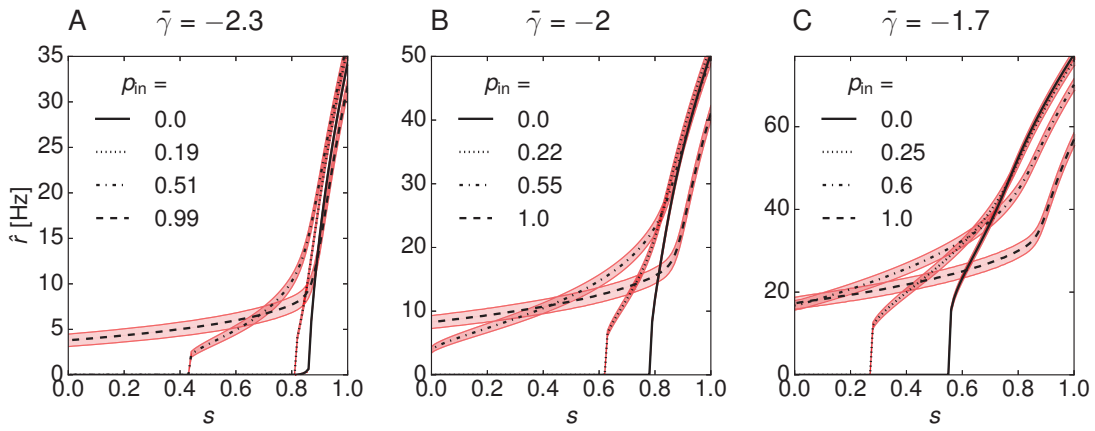

Figure 2.19. Mean response curves of three IOE networks with power-law in-degree distribution $P^{\text{in}} \sim k^{\bar{\gamma}}$ and different exponents $\bar{\gamma}$. For each network we show the mean response curves for four different levels of assortativity p_{in} (thin black lines). The thick light red lines indicate ± 1SD of the noise of the output from $n = 2500$ neurons. (**A**) Network with large negative exponent of $\bar{\gamma} = -2.3$ and small mean degree. (**B**) Network with intermediate exponent $\bar{\gamma} = -2$ and intermediate mean degree that has been previously characterized (see text). (**C**) Network with small negative exponent, $\bar{\gamma} = -1.7$ and large mean degree. This figure has been modified from [228].

in-degree distributions are shown in Table 2.1.

$\bar{\gamma}$	$\langle k \rangle$	$\sigma^2_{\bar{\gamma}}$
-2.3	29	1707
-2	38	3283
-1.7	54	6001

Table 2.1. Means and variances of the in-degree distributions $P^{\text{in}}(k) \sim k^{\bar{\gamma}}$ with minimum and maximum in-degrees $k_{\min} = 10$ and $k_{\max} = 500$.

In Figure 2.19 we show the mean response curves of the three networks (thin black lines) and ± 1 SD of the output noise, $\sigma/\sqrt{n}$, for $n = 2500$ (broad red lines). Both the response curves and standard deviations were calculated with the mean-field method, where $f(k, k')$ was sampled from the adjacency matrices of the networks. The network with large negative exponent, $\bar{\gamma} = -2.3$ and small mean degree fires at lower rates compared to the other networks (Figure 2.19A). The firing threshold for the uncorrelated network is equal to 0.8 and decreases for increasing assortativity, which corresponds to increasing sensitivity to weak stimuli. On the other hand, assortativity strongly

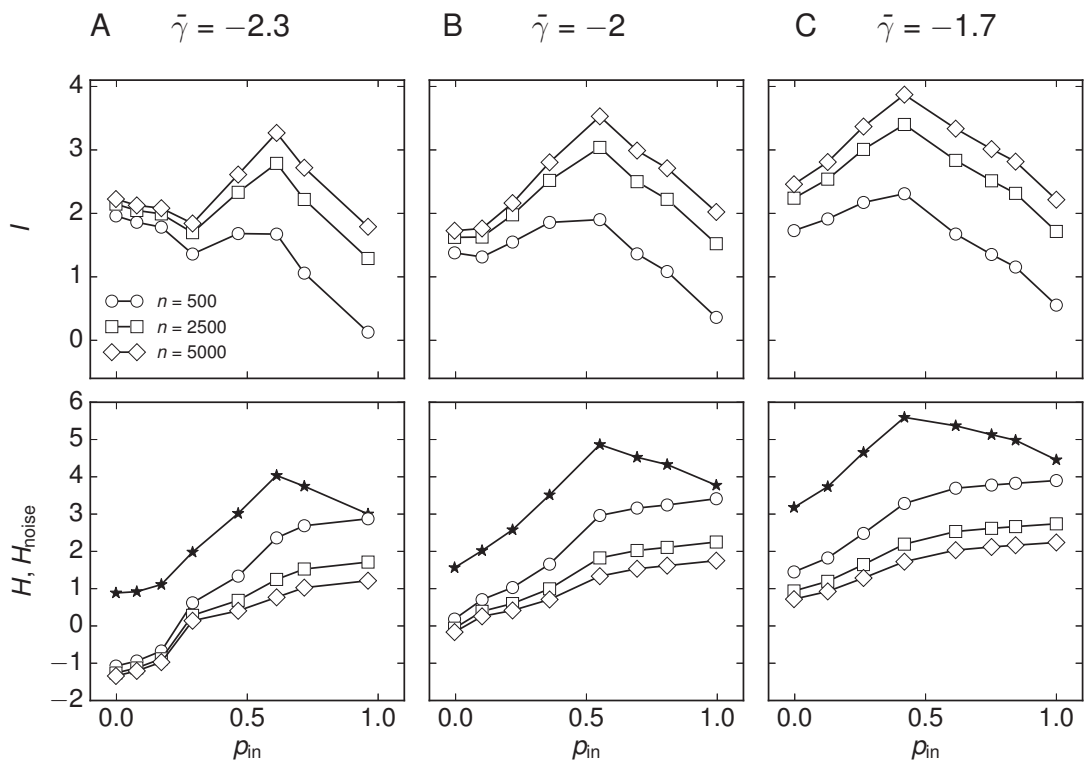

Figure 2.20. Information transfer for IOE networks with different $\bar{\gamma}$. (Top row) Input-output mutual information $I = H - H_{\text{noise}}$ of the networks. (Bottom row) Entropy H (stars) and noise entropy H_{noise} (open symbols). (**A**) The network with large negative exponent $\bar{\gamma} = -2.3$ has an optimum of I for slightly higher value of assortativity $p \simeq 0.66$ compared to the other networks. Additionally, its signal transmission capabilities are poorer which is characterized by lower values of I. The poor information transmission capability results from small entropy H due to a low mean firing rate of the network. (**B**) The network with intermediate exponent $\bar{\gamma} = -2$ has its signal transmission optimized at intermediate values of assortativity, $p_{\text{in}} \simeq 0.55$. (**C**) The network with small negative exponent $\bar{\gamma} = -1.7$ has the highest signal transmission capabilities with largest values of I. The mutual information peaks for a relatively small level of assortativity $p \simeq 0.4$, which indicates that the uncorrelated network is already quite efficient in signal transmission. This figure has been modified from [228].

increases the output noise (broad red lines in Figure 2.19A). The network with small negative exponent, $\bar{\gamma} = -1.7$ and large mean degree fires at higher rates and has a comparatively low firing threshold of $s_c \simeq 0.55$ for $p_{\text{in}} = 0$. For this network, even small levels of assortativity shift the firing threshold to zero. For all three networks assortativity significantly reshapes the response curve and increases the output noise.

Let us compare the input-output mutual information of the three networks, which is shown in Figure 2.20. The maximum mutual information increases with increasing $\bar{\gamma}$ (top row in Figure 2.20), which results from the elevation of firing rates due to larger recurrent activity. This effect can be interpreted as a stronger amplification of the input signal due to increased recurrent connectivity for increasing $\bar{\gamma}$, which corresponds to a larger entropy H of the output (stars in Figure 2.20, bottom row). However, the distributions with larger $\bar{\gamma}$ are also characterized by a larger variance and increased output noise, which corresponds to larger values of H_{noise} (open symbols in Figure 2.20, bottom row). In consequence, the net effect is a slight increase of the mutual information for increasing $\bar{\gamma}$. Moreover, we observe a negative shift of the peak position for I as $\bar{\gamma}$ increases (Figure 2.20, top row). This indicates, that networks with larger mean and variance of the degree distribution have their information transfer optimized by smaller levels of assortativity, since their sensitivity to small inputs is already enhanced by larger recurrent activity.

We conclude that assortativity optimizes the information transfer for a range of network configurations, but the optimal level of assortativity and the corresponding maximum mutual information depend on the specific in-degree distribution. For significantly lower (higher) $\bar{\gamma}$ as well as other in-degree distributions we found that the optimum vanishes and assortativity monotonically increases or decreases the information transfer. We propose that a network is susceptible to optimization by assortativity if it cannot sustain firing for low inputs for $p_{\text{in}} = 0$. Moreover, its in-degree distribution has to be broad enough so that the firing rates of individual neurons are highly variable. Then, in-degree correlations can have a significant effect on the network activity. For networks with in-degree distribution of small variance such as the standard Erdős-Rényi network, we expect that in-degree correlations have only a small effect on the population firing rates and information transfer.

2.7 Discussion

How neuronal networks sense and process information is a central question in neuroscience. The brain is structurally segregated into different regions that are specialized in certain processing tasks, which likely optimizes the overall computational performance with respect to limited resources of space and energy [113, 247]. Therefore, it is reasonable to assume that the topology of a neuronal network is strongly affiliated with its specific function. Many parts of the nervous system are recurrently connected so that neuronal spiking is driven by external input in combination with feedback through recurrent links [93]. In particular, excitatory recurrent activity is thought to play a major role in neuronal computations [93] and one of its most fundamental functions is the amplification of small input signals.

In this chapter we examined how the sensitivity of a neuronal network to small input signals depends on the topology of the recurrent connections. Main attention was paid to two basic statistical properties of the network, namely structural heterogeneity in terms of a broad degree distribution and degree correlations. For this purpose, we developed a novel mean-field method to calculate the activity of large neuronal networks with these properties, assuming independent spiking of the neurons. Our model is based on dividing the network into populations of neurons with equal in-degrees and solving coupled self-consistent equations for their steady-state firing rate. The network structure is captured by the joint-in-degree distribution $N_{kk'}$ which is the average number of links that originate at neurons with in-degree k' and go into neurons with in-degree k. The influence of the connectivity structure on the population dynamics can be conveniently assessed by examining the joint-in-degree distribution. The model is applicable to degree-correlated random networks with arbitrary in- and out-degree distributions under the condition that they have a maximum in- and out-degree and that they are large and sparse enough so that neurons can be assumed to share no inputs and fire uncorrelated spike trains.

We applied our mean-field model to a neuronal network with power-law in- and out-degree distribution and found that the stationary firing rates of the neuronal populations are well described by this theory. The stationary mean firing rate of the network differs from 'simple' mean-field predictions that neglect the network structure. For subthreshold inputs the network sustains firing through recurrent activity that is strongly dependent on the connectivity structure and in this region we found that assortative in-degree correlations have the largest impact on the network activity. Assortative networks respond to weak input levels, where disassortative and uncorrelated networks would not fire. This result is reminiscent of percolation, where assortativity has been shown to increase the network robustness to random failure of nodes or links [197, 280, 198, 289, 287, 40, 276, 203, 123, 229]. More specifically, our model can be related to a bootstrap percolation model, where nodes in a network are activated if

their input exceeds a threshold [27, 11]. In terms of bootstrap percolation theory it has been shown that heterogeneity in the degree distribution lowers the activation threshold of a network [27]. Our central result is that assortativity increases the ability of heterogeneous networks to sustain activity for small inputs, which complements these findings.

The improved ability of assortative networks to sustain firing for low inputs can be interpreted as an increased sensitivity to weak stimuli. We quantified the information transmission capability of assortative networks by the mutual information of the stimulus-response relationship, assuming that all stimuli are equally likely. We found that the signal transmission is optimized by an intermediate level of assortativity. The improved sensitivity of assortative networks to weak stimuli is based on a smoothing of their response curve which is similar to a smoothing by increased levels of noise [151]. Additional noise may further improve the sensitivity of the network to small inputs, but it could also be detrimental since it also increases the output noise.

In principle, the signal transmission could be improved by combination of noise and assortativity, or by increasing the mean connectivity of the network, which raises the recurrent activity. However, the strategy of increasing assortative degree correlations inherits a couple of advantages. While assortativity increases the mean firing rate of the network in response to weak stimuli, it *decreases* the firing rate for large inputs and thus, decreases the overall energy consumption of the network which is an important factor in the wiring strategy of the brain [164]. Additionally, degree correlations do not require additional links between neurons in order to increase the recurrent activity for small inputs as opposed to an increase of the mean recurrent connectivity. Moreover, since degree correlations change the shape of the mean response curve, they could be used to tune the stimulus-response relationship to the specific distribution of stimuli that is commonly presented to the network in its natural environment.

Our finding that assortativity improves the signal transmission capability of a network complements the results of recent studies showing that assortativity increases the information content in heterogeneous directed networks [211] and enhances memory in noisy conditions [86]. In contrast, assortativity has been found to decrease the synchronizability [279, 13] of complex networks and the stability of dynamical processes taking place on them [44]. This seeming contradiction to our results can be explained by the different conditions applied to the networks [86]: Assortativity improves performance in ‘bad conditions‘ such as low density of links and high noise, whereas it decreases performance in ‘good conditions’ (high density of links, low noise). In our model, the low level of external input can be regarded as bad conditions, similar to a low link density.

Moreover, we found that an excess of assortative degree correlations decreases the information transfer capability of heterogeneous networks. In this case, strongly connected neurons fire close to their maximum rate, whereas many weakly connected neu-

rons do not fire. Neurons that fire close to the maximum rate respond to different inputs with almost equal rates so that they do not contain much information about the stimulus. Moreover, assortativity increases the output noise so that the information content is reduced further. The optimum level of assortativity depends on the in-degree distribution. For networks with larger mean degree and larger variance less assortativity is needed for optimal signal transmission, whereas for networks with small mean and small variance higher levels of assortativity are needed.

In a related study, Vasquez et al. [275] found that the sensitivity and stability of the networks are optimized by disassortative degree correlations which seems contradictory to our results. This contradiction stems from differences in the network model and dynamic regime used for the simulations. Vasquez et al. assume no in-degree correlations of connected neurons, but investigate correlations of in- and out-degree per neuron, whereas our study is focused on in-degree correlations of connected neurons. We mostly use neurons with equal in- and out-degree, which corresponds to assortative correlations of in- and out-degree per neuron. Moreover, in [275] additional external input is used to increase the recurrent activity of the network, which shifts the global dynamics into a superthreshold regime. The combined effect of in-out degree correlations on a neuron level and in-degree correlations on a network level could be examined in future studies. Note that the maximum value of in-degree correlations depends on in-out-degree correlations of neurons: If the in- and out-degree is not equal for each neuron, the network may not be able to fully segregate into subnetworks of neurons with equal in-degree, because the number of outgoing links in each subnetwork does not necessarily match the number of incoming links.

We considered highly simplified model networks so that we could focus on the basic mechanisms that relate network topology and neuronal dynamics at the expense of realism and biological relevance. In the following we will discuss some of the biological features that we did not include into our model, although they may change our results quantitatively or even qualitatively.

Probably the most relevant issue is inhibition: Large parts of the neocortex are densely connected to inhibitory neurons [104], although most of the neurons are excitatory. Our model can be extended to account for inhibitory neurons by simply adding them as separate populations. However, including inhibition comes with increased complexity of the connectivity structure, since the network can be divided into subnetworks of excitatory (E) and inhibitory (I) neurons, or mixed (EI) subnetworks. One way to deal with the increased complexity is to keep the E-I connections fixed and focus on the E-E connections of the excitatory subnetwork [224]. Another method is to create a specific network structure and then simply make a random fraction of the neurons inhibitory [209]. Another possibility is to keep a fixed connectivity pattern for the E-E and I-I networks and manipulate the E-I connectivity. Since the dynamics of simple EI networks can already be quite elaborate [53], we expect a rich spectrum of activity

patterns for more complex EI networks. For now, we can only speculate about how adding inhibition to our model would affect the network dynamics. In an EI network with assortative E-E connections we expect similar effects as for a purely excitatory network due to increased recurrent activity. In a related study, Roxin [224] showed that a broad degree distribution of E-E connections in an EI network promotes oscillations. In this study a reduced rate model revealed that the higher firing rates of strongly connected neurons increase the mean effective input gain of these excitatory subnetworks. We assume that assortativity could further increase the gain for strongly connected neurons while inhibitory activity would remain at a similar level. In another study, Pernice et al. [209] examined the influence of broad degree distributions and degree correlations on the activity of EI networks, where a random fraction of the neurons are inhibitory. They found that positive degree correlations increase the firing rate of strongly connected neurons, similar to the effect in our model.

Another important issue is spike timing and synchronization. In our study we assumed uncorrelated firing so that we could focus on simple rate coding mechanisms. Synchronization of neuronal spiking was deliberately avoided by introducing random delays in our model and the precise timing of spikes was assumed to be irrelevant. In contrast, a large number of studies have found that precise timing of spikes plays a significant role in neural coding [277, 262, 61]. One possible mechanism for encoding information in the timing of spikes is based on correlations of the inter-spike intervals [73].

Moreover, in real neuronal networks, the synaptic transmission of signals depends on the characteristics of the spiking patterns [1]. Processing of the signals in the postsynaptic neuron already takes place at the level of dendrites: Synaptic inputs are amplified or reduced, depending on their temporal correlations and the activity state of the postsynaptic neuron [116, 213, 165]. Finally, synchronized population activity and collective oscillations are also thought to play a significant role in neural coding and signal detection [241, 109, 187]. Although these studies challenge our assumption of rate coding, there is also strong support for the idea that much (if not most) information is carried by the mean firing rate of neurons as discussed in Section 1.3.1 [118, 85].

A final remark about correlations and information transfer: While in our study the network structure is degree-correlated, the neuronal activity is assumed to be uncorrelated. Research on the inverse situation, correlated activity in uncorrelated networks, also revealed advantages in information by *moderate* levels of correlations [212, 149, 240]: On the one hand, uncorrelated activity from weak recurrent excitation is too low to carry substantial amounts of information. On the other hand, highly correlated firing that occurs in networks with strong recurrent excitatory activity is also associated with decreased information content [220]. Consequently, an optimum in information transfer could be found at intermediate levels of excitability, e.g. in

networks operating at criticality [154, 28, 240]. Although our model can not be related to criticality, the fundamental principle is quite similar: For small levels of assortativity, the network response to small inputs is too weak to carry significant information, whereas in highly assortative networks the response becomes insensitive to changes in the stimulus.

3 Percolation of degree-correlated networks with spatial constraints

The previous chapter has shown that assortative degree correlations strongly influence the sensitivity of a neuronal network to small stimuli. We have concluded that this effect is reminiscent of percolation, where assortativity increases the robustness of a network to random removal of nodes or links [280, 276, 203, 123, 196]. In this chapter we turn to the problem of percolation in a random network more quantitatively. Percolation theory, originally proposed for the description of fluid flow through porous materials [50], deals with phase transitions in disordered systems [59]. In network sciences it has been used to describe the structural changes a network undergoes under successive removal of nodes or links [196] and it has been applied to a large number of systems, e.g. the internet [68, 83], immune networks [6], social networks [245], and neuronal networks [29, 45, 246, 134, 239].

In recent experiments by Soriano et al. [246], a developing cultured network of neurons was analyzed in terms of a percolation model. Synaptic connections between neurons were considered as links and avalanches of activity were associated with the connected components in the network [45, 246, 81]. The connectivity structure underlying the percolation model was chosen as an undirected Erdős-Rényi (ER) graph, based on their finding that the degree distribution of their neuronal network was Poisson-like. Interestingly, it has been shown for several neuronal cultures that the synaptic network structure also exhibits degree correlations [36, 260, 87]. Therefore, we aim to complement these experimental studies by numerically investigating how degree correlations affect the percolation behavior of an ER graph. In addition, we take into account the fact that a neuronal system is subject to metric constraints: Spatially close neurons are more likely to be synaptically coupled than distant neurons.

We use two different methods to construct spatially embedded ER networks with degree correlations: In the first method, nodes are distributed homogeneously in a two-dimensional domain and degree correlations are imposed by connecting pairs of nodes in dependence of their distance and degree. In the second method, nodes with similar degree are first placed spatially close to each other and then connected in dependence of their distance, so that degree correlations emerge with increasing locality of links. Results of this study have been published in [229].

3.1 Percolation theory

Consider a liquid that is poured on top of a porous material. Will the liquid seep through to the bottom by percolating through a conjunction of small pores? Percolation theory deals with this question mathematically by analyzing the geometric characteristics of the connected pores forming small and large clusters [255].

The porous material can be modeled by a grid of cavities that are connected by passable channels as shown in Figure 3.1A in two dimensions. A simplified representation of this model is given by a square lattice with N nodes, where each node corresponds to a cavity and each link to a permeable channel (Figure 3.1B). Since we do not know the exact structure of the material, we make the simplifying assumption that any two neighboring cavities are connected by a permeable channel at random with probability q, which quantifies the porosity of the material. Equivalently, in the square lattice, each of the possible links is present with probability q or missing with probability $1-q$. The quantity q is called the *occupation probability*, or sometimes *concentration*, because it is an intrinsic parameter that defines the abundance of links in the lattice.

For $q = 0$ the lattice consists entirely of isolated nodes with no links connecting them. As q grows, connected neighbors will begin to form clusters of increasing size until, at a specific concentration, a spanning cluster emerges that connects the top and bottom row of the grid. In the above example, the fluid poured on top of the material could then pass through successive channels (a path in the grind) through to the bottom, hence the system is said to 'percolate'. Percolation theory is concerned with the properties of these clusters and specific attention is given to the critical probability $q = q_c$ at which a spanning cluster first appears, the so-called *percolation threshold*. The percolation threshold is particularly interesting, because it separates two qualitative distinct states of the system: the non-percolating ($q < q_c$) and the percolating ($q > q_c$) phase. In physics terminology the system is said to undergo a *phase-transition* from a sub-critical to a super-critical state [255, 59]. Consequently, the system is considered to be at criticality right at the percolation threshold.

The origins of percolation theory go back to Flory and Stockmayer, who described how branched-chain polymers transition from liquid to a gel [106, 258]. This phenomenon, called *gelation*, is very analogous to the above described percolation process: Small branching molecules form chemical bonds and assemble to larger and larger macromolecules, until a spanning cluster extends across the whole system. A similar phenomenon occurs if one boils an egg; above a critical temperature, the protein contained in the egg denatures and becomes solid.

A more mathematical description of several generic percolation processes was introduced 1957 by Broadbent and Hammerslay, who also coined the term 'percolation' in reference to the classical problem whether a fluid or gas could percolate through a porous medium [50]. Since then, percolation theory has been studied intensively

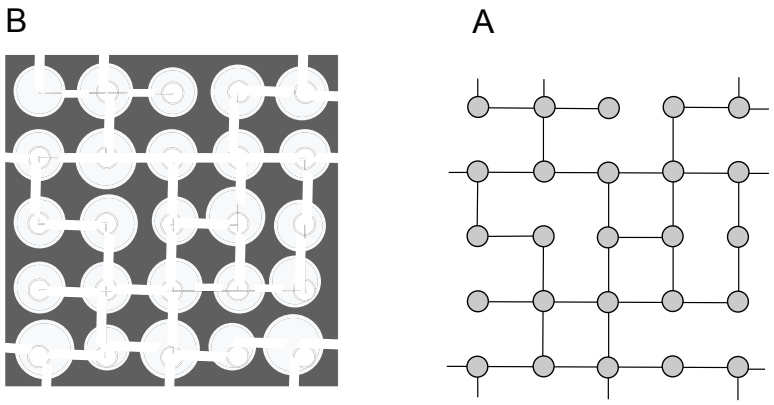

Figure 3.1. Simplified model of a porous medium. (**A**) The medium is represented by a two-dimensional grid of cavities that can be connected by passable channels. (**B**) Simple graph representation of the same model as (A) with nodes as cavities and edges as permeable channels.

by mathematicians and physicists and it has become one of the best characterized problems in statistical physics with applications across various fields of research [244, 255, 59, 225]. For example, percolation theory is used to estimate the accessibility of oil resources in porous reservoirs. The porous reservoir can be modeled as a simple percolation lattice, where the average concentration of oil or gas is quantified by q. Companies are interested in maximizing the amount of oil they can harvest by a single drilling, which corresponds to hitting a large cluster of connected pores. For this purpose, they take small probes with diameter of a few centimeters and examine their porosity to estimate the concentration q. With finite-size scaling methods one can extrapolate the amount of oil they can expect to harvest at larger scales with diameters of a few kilometers [255].

The process we described so far corresponds to the so-called *bond percolation*, where nodes in the lattice are fixed and bonds are added or removed. Alternatively, one can define a percolation process in terms of passable or occupied nodes, which is denoted as *site percolation*. The occupation probability q is then defined analogously by the probability of a node to be passable and the probability $1 - q$ to be blocked or removed. Clusters are then formed by neighboring passable nodes. In fact, the theory of percolation was first introduced in terms of site percolation [106, 50, 255]. The site percolation behavior is similar to the behavior of bond percolation, although it differs quantitatively. For example, the concentration $q = q_c$ where a spanning cluster first appears for site percolation is always larger or equal to the one for bond percolation [128].

Classical percolation theory can be applied to various types of lattices that are embedded in two-, three-, or higher dimensional space. Prominent examples besides the

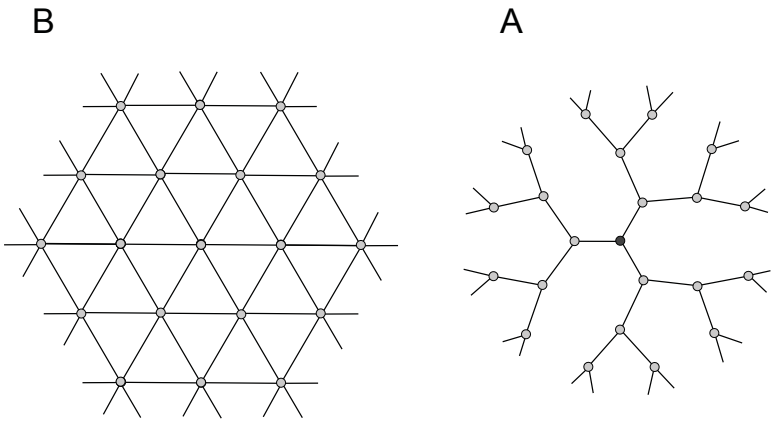

Figure 3.2. Schematic of a triangular lattice (left) and a Bethe lattice (right), respectively. The Bethe lattice is defined as a connected cycle-free graph where each node is connected to z neighbors. The Bethe lattice shown in (B) has $z = 3$.

square lattice are the triangular lattice and the Bethe lattice (Figure 3.2). The triangular lattice is widely used as a basis for modeling isotropic activity because of its rotational symmetry. The Bethe lattice is a particularly interesting example of a cycle-free graph, which is referred to as a *tree*. Moreover, the Bethe lattice can be associated with the origin of percolation theory, since it was the first lattice for which an exact analytical solution for the percolation threshold was found [106, 258, 255]. All of the lattices differ quantitatively in their percolation properties, but they show a similar qualitative behavior: There is always a concentration $q = q_c$ that separates the non-percolating phase from the percolating phase.

So far, we have neglected an important subtlety in the definition of q_c. Finite lattices that are simulated on a computer generally do not have a sharply defined percolation threshold [255]. Since the system is of limited size N, there is always at least some small probability to find a spanning cluster for each occupation probability $q > 0$. An exact definition of q_c can only be given in the limit of infinite size of the lattice so that for $q < q_c$ the probability to find a spanning cluster is zero and for $q > q_c$ it is one. Exact solutions for q_c in the limit $N \to \infty$ can be found for bond or site percolation, depending on the lattice type. However, in many cases a rigorous mathematical proof of the results is incredibly hard to obtain, especially for high-dimensional lattices [100, 129, 152, 255] so that most of the studies on percolation problems are based on computer simulations. The correct percolation threshold must be carefully extrapolated from numerical simulations of finite lattices, because many characteristics of a percolation transition depend on the lattice size [255].

If we plot the probability to find a spanning cluster (P_{conn}) over the concentration q, we find that this probability sharply increases in the region around the percolation

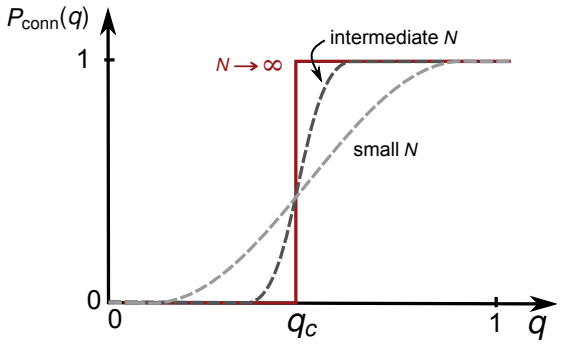

Figure 3.3. Schematic of the probability $P_{\mathrm{conn}}(q)$ that a spanning cluster exists in a lattice of size N. For small N, the curve smoothly increases around the percolation threshol q_c and for $N \to \infty$ it approaches a step function.

threshold q_c. This increase becomes more sudden as the lattice size increases, so that the curve approaches a step function for $N \to \infty$ (Figure 3.3). One approach to deal with the problem of the system size dependence is the *finite-size scaling theory* [255], which is discussed in the Appendix, A.4. With this theory one can calculate the percolation properties of infinite systems by considering the behavior of the clusters for different system sizes.

Classical percolation theory on lattices has been found useful to characterize the structural and dynamical properties of various disordered systems, including diffusion processes [226, 32, 208], fragmentation of fluids [70, 69], composite materials [58] and evolution processes [182, 217].

3.1.1 Percolation of complex networks

While classical percolation theory deals with various lattice types, it can also be applied to complex networks: Nodes or edges are randomly removed from an initially well-connected network until it disintegrates into smaller components that are disconnected from each other. The *robustness* of the network then describes how quickly it disassembles within this process, and a network is said to be resilient against random failure if it has a low percolation threshold [196]. It turns out, however, that it is difficult to find a sharp criterion for the percolating phase of complex network, since there is no clear definition of a spanning component. Since a random network is not necessarily embedded in space, it has no sides which a spanning cluster could possibly connect to. Therefore, the definition of a spanning cluster has to be generalized in a sensible way and the following definition by Kesten et al. [152] has been widely used in this regard. A cluster in the network is said to be a spanning component (also called the *giant component*), if the fraction between the number of nodes within this cluster and the number of nodes in the whole network is larger than zero as the network size goes to infinity. One then defines the percolation threshold q_c as the concentration of nodes or links where the giant component appears for the first time in the infinite network. Since lattices are a subgroup of complex networks, this definition of the giant

component has to satisfy the requirements for the percolating cluster in infinite lattices, which it does [152].

Percolation in complex networks has been first studied by Erdős and Rényi in 1959 [98], and their random network model (ER graph) remains one of few examples for which the phase transition could be characterized analytically with rigorous mathematical proof. Since then, percolation theory of complex networks has been receiving increasing attention in various fields. Percolation network models have been used to characterize the robustness of the internet [68, 83], immune networks [6], social networks [245], and neuronal networks [29, 45, 246, 134, 239]. Recently, methods from percolation theory were used in an experimental study to characterize a developing network of cultured neurons [45, 95, 246, 81, 11, 206]. In their experiments, Soriano et al. [246] successively decreased the synaptic connectivity of the neuronal culture by applying increasing doses of a neurotransmitter antagonist, which corresponds to random removal of links in the network. Avalanches of spontaneous activity percolating through the system were then measured by calcium imaging. The synaptic connectivity structure could be characterized by analyzing how the disintegration of the synaptic network affected the size distribution of these avalanches [45, 266, 81].

The concept of phase transitions and criticality has received increasing interest in the neuroscientific field over the last decade. Observations of power-law distributions of event-sizes in various neuronal tissues have been associated with criticality, leading to the hypothesis that some parts of the brain might self-organize to operate at a critical state [29, 75, 127, 28, 134]. We discuss criticality and power-law scaling in Section 3.1.2. Theoretical studies have shown that the critical state might provide advantages in information processing by optimizing the dynamic range of a neuronal network [154, 127, 28, 30]. Since these studies deal with dynamical processes on functional brain networks, they often describe the problem in terms of a *branching process* that models the reproduction of activity. In a branching process the states of nodes or links in a network evolve over time, independently of their past activity. The exact relation between branching processes and percolation processes is described in [130].

Much effort has been spent to understand how the resilience of a complex network is related to its topological properties. A general observation is that networks with a heterogeneous degree distribution, e.g. scale-free networks, are very robust against random failure [68, 82, 7, 196]. Moreover, degree correlations have been found to substantially influence the percolation behavior of a network [197, 280, 201, 289, 287, 40, 276, 203, 123]. Considerable attention has been paid to assortativity, which has been found to dramatically increase the resilience of a network to random failure, and in some cases to even qualitatively change the phase transition of a network [280, 276, 203, 123, 196]. With the shift of interest from percolating lattices to complex network models, the property of spatial embedding of the system has become increasingly disregarded, although it is an important feature of many real-world networks. A large number of real

networks have evolved under spatial constraints, so that their connectivity structure exhibits geometrical features. For example, the structural and functional organization of the brain must optimize the flow of information while minimizing its volume and the metabolic cost of activity, which is accounted for by connecting spatially close neurons with higher probability [191, 57, 247].

Spatial embedding has been shown to strongly influence other network properties such as the degree distribution, average path length, clustering coefficient and percolation behavior [24, 179, 288, 280], see [131, 25] for reviews. Since the topology and geometry of a network are related to each other, it is difficult to address each of them individually. A popular way of modeling a spatially embedded random network is to make the connection probability between the nodes dependent on their Euclidian distance. This dependency is often chosen as a power-law, because such distributions of link lengths have been found empirically in many real networks, e.g. in social networks [160, 51, 171], the internet [292] and air transportation networks [38, 23].

3.1.2 Important quantities

In the following we introduce some important measures and approaches that are useful for a quantitative description of the percolation process on a network. We here define the concentration q as the number of links divided by system size

$$q = E/N, \tag{3.1}$$

where N is the number of nodes in the network. In classical percolation of lattices, the system size is usually measured in terms of side lengths L of the lattice. A lattice that is embedded in d-dimensional space has $N = L^d$ nodes. The inverted relation $L = N^{\frac{1}{d}}$ is useful for the application of measures from classical percolation theory to complex networks.

Connected component. A connected component, or cluster, is defined as a subnetwork of nodes that are connected to each other such that a path exists between any two nodes within the cluster. A cluster that contains a finite fraction of the nodes of the network for $N \to \infty$ is called the giant component. Recall that the emergence of a giant component separates the non-percolating phase of a network from the percolating phase. Unfortunately, the giant component is defined only for infinite networks so that we lack an appropriate definition of the percolation transition in a finite network. That being said, a finite network still undergoes an abrupt structural change as q increases, which can be associated with a phase transition. To overcome this problem, Cohen et al. [83] proposed to use the largest cluster (largest component) of a network as a generalization of the giant component to deal with percolation in finite networks. Then,

we can use the *largest cluster density*

$$G(q) = \frac{\text{number of nodes in the largest cluster}}{N} \tag{3.2}$$

to characterize the percolation behavior of the network in the region around q_c. Equivalently, $G(q)$ is the probability that a randomly chosen node belongs to the largest cluster. The *mass* of the largest cluster refers to its absolute size, $NG(q)$. The quantity $G(q)$ is very analogous to the probability $P_{\text{conn}}(q)$ to find a spanning cluster in a lattice. In an infinite network, the largest cluster becomes the giant component if its density is larger than zero. Thus, we can separate the non-percolating phase from the percolating phase in terms of the largest cluster density as follows for $N \to \infty$. For $q < q_c$ the largest cluster density is zero and for $q > q_c$ it is larger than zero. With this formulation we can give a precise definition of the percolation threshold,

$$q_c = \sup\{q : G(q) = 0\}, \quad N \to \infty. \tag{3.3}$$

Finite clusters. We consider any cluster in the network besides the largest component as a *finite cluster*. At minimum, an isolated node can be regarded as a cluster of size one. Let us define the *cluster number* $n_s(q)$ as the number of clusters of size s in the network divided by network size

$$n_s(q) = \frac{\text{number of finite clusters of size s}}{N}. \tag{3.4}$$

A randomly chosen node in the network belongs to a finite cluster of size s with probability $sn_s(q)$. A node in the network belongs either to a finite cluster with probability $\sum_s sn_s(q)$ or to the largest cluster with probability $G(q)$ so that

$$G(q) + \sum_s sn_s(q) = 1. \tag{3.5}$$

Mean cluster size. The next quantity is defined on the remaining part of the network after removing the largest cluster from it. Then, a randomly chosen node belongs to a cluster of size s with probability

$$w_s(q) = \frac{sn_s(q)}{Z}, \tag{3.6}$$

where $Z = \sum_s sn_s(q)$. Hence, the average size of a cluster we are hitting if we point at a random node is

$$S(q) = \sum_s sw_s(q) = \sum_s \frac{s^2 n_s(q)}{Z}. \tag{3.7}$$

This measure is known as the *mean cluster size* and it is widely used in percolation theory. Note that it corresponds to a weighted average by cluster size as opposed to a simple average over the set of clusters.

Both quantities, $G(q)$ and $S(q)$, play an important role in the characterization of the phase transition in a network. Often the exact transition point in the limit $N \to \infty$ cannot be calculated analytically, but it can be estimated from the behavior of $G(q)$ and $S(q)$ in finite networks as q approaches q_c. Analogous to percolation in finite lattices, the finite network shows strong finite-size effects in the region around q_c, which have to be analyzed carefully in order to interpolate the results to infinite networks. This problem is addressed explicitly by *finite-size scaling theory* for networks, which we discuss in the Appendix, A.4.

Critical exponents. In infinite networks, one observes that the largest cluster density exhibits power-law scaling as q approaches q_c from above [255, 59],

$$G(q) \sim (q - q_c)^{\beta}, \quad N \to \infty. \tag{3.8}$$

Similarly, above and below q_c, the mean cluster size scales as

$$S(q) \sim |q - q_c|^{-\gamma} \quad N \to \infty, \tag{3.9}$$

which implies that $S(q)$ diverges as q approaches the critical value, since the exponents are positive. The scaling exponents β and γ are called the *critical exponents* of the percolation transition. At criticality, the structure of the largest cluster behaves as a *fractal* [254, 178, 59], which means that it exhibits repeating patterns that are replicated on different scales. Moreover, the mass of the largest cluster scales with Euclidian distance L as [254, 178, 59]

$$NG(q) \sim L^D \sim N^{\frac{D}{d}}, \tag{3.10}$$

where D is the *fractal dimension* of the system. An important property of the critical exponents and the fractal dimension is that they neither depend on the microstructure of the system, nor on the type of percolation (node or bond), but only on the dimension d of the system.

The spatial dimension d entering Equations (A.51) and (A.60) is well-defined in geometric systems such as lattices, but its application to random networks can be problematic. Random networks with no spatial constraints have no defined length in space so that d cannot be a relevant parameter. In general, these networks are considered to have dimension $d \to \infty$. The critical behavior of complex networks without spatial embedding has been studied in terms of a mean-field model [145, 92, 168, 138]. With the mean-field approach one simplifies the topology of the network by taking into account only the mean connectivity. Consequently, this method has been

successfully applied to homogeneous networks, including the ER graph, whereas its applicability to heterogeneous networks is limited [138]. Phase transitions that can be characterized by the mean-field approach belong to the *mean-field universality class*.

However, for spatially embedded random networks, a spatial dimension d can be defined. Daquing et al. [84] showed that d can be obtained from the connectivity structure of the network and the link length distribution $P(l)$. Moreover, this definition of d is also applicable for percolation scaling arguments. Our model networks range from non-spatial networks to networks with very strong constraints that are expected to behave similar to a two-dimensional lattice. Therefore, to avoid confusion about the spatial dimension of our system, we will therefore consider only the combined expression D/d. For simplicity, we continue to refer to D/d as the fractal dimension (in rescaled form).

3.2 Network model

In this section we describe our method to generate degree-correlated spatial ER networks. It is based on the configuration model of Newman, Strogatz and Watts [200] that generates networks with a specific degree distribution (see Section 1.1.2). We first introduce the basic algorithm that constructs uncorrelated random networks with spatial constraints and the Poisson degree distribution of ER graphs,

$$P(k) = \frac{(2q)^k}{k!} e^{-2q}. \tag{3.11}$$

We employ two different methods that generate degree-correlated spatial networks at the basis of the configuration model. These methods will be described in Section 3.2.2.

3.2.1 Spatial embedding of the random network

In contrast to the original ER graph that has no spatial dimension, we distribute all nodes randomly in a two-dimensional domain of size $L \times L = 100 \times 100$, so that each link connecting two nodes can be assigned a geometric length. To impose spatial constraints on the network, we modify the configuration model as follows. First, the algorithm assigns each of the N nodes a target-degree according to the Poisson distribution (3.11). Then, it randomly selects a free stub in the network that belongs to a node i. We define the probability Π of this stub to connect to any of the remaining free stubs of a node j in the network as

$$\Pi(\text{free stub at node } j) = \frac{l_{ij}^{\alpha}}{Z}, \tag{3.12}$$

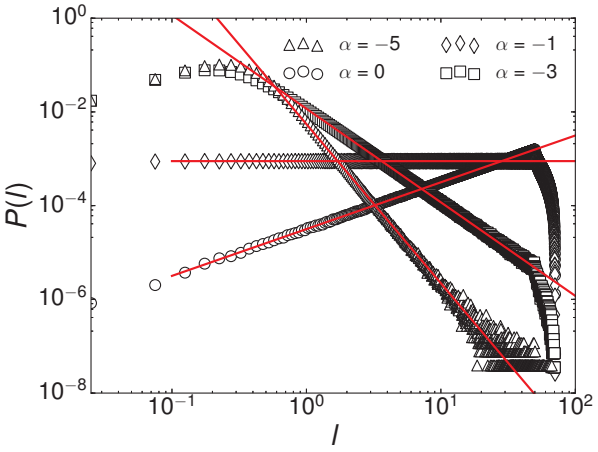

Figure 3.4. Distribution of link lengths in spatially constrained networks (open symbols). The distributions are sampled from an ensemble of 100 networks with $N = 10^5$ and $q = 2$. The tails of the distributions conform to a power law. Red straight lines show fits of the form $P(l) \sim l^{\delta}$, with $\delta = 1.0,\ 0.0, -2.0,$ and -3.4, from the largest to the smallest slope. This figure has been modified from [229].

where l_{ij} is the Euclidian distance between the nodes and $Z = \sum l_{ij}^{\alpha}$ is a normalization constant summing over all remaining stubs in the network that node i can connect to. A link is drawn according to the above distribution, whereby self-edges and multiple edges between the same pair of nodes are rejected.

The process of selecting a random stub and drawing a link is repeated until there are no free stubs left that could be connected without generating a self-edge or multiedge. The exponent α controls the strength of metric constraints on the network: For $\alpha = 0$, the network is unconstrained and conforms to the original ER network. For $\alpha < 0$, metric correlations appear: Short-range connections gradually become more probable than long-range connections as α decreases, until the majority of links connects neighboring nodes for $\alpha \ll 0$. Therefore, we will denote α as the *distance exponent*. The distribution of link lengths $P(l)$ achieved by this construction method is shown in Figure 3.4 for different values of α. For small values of $|\alpha|$, this distribution follows a power law scaling function of the form

$$P(l) \sim l^{\alpha+1}, \tag{3.13}$$

where the exponent $\alpha + 1$ originates from the ring $2\pi l \cdot dl$ in the derivation of

$$P(l)dl \sim l^{\alpha}(2\pi l \cdot dl). \tag{3.14}$$

For large negative α, the probability of long-range links is very small and $P(l)$ deviates from a power-law function, which can be explained as follows. As α decreases, nodes become more likely to connect to others in their close neighborhood. As the configuration algorithm goes on adding links to the network, increasingly many nodes reach their target-degree and have no free stub left. These nodes in the close neighbor-

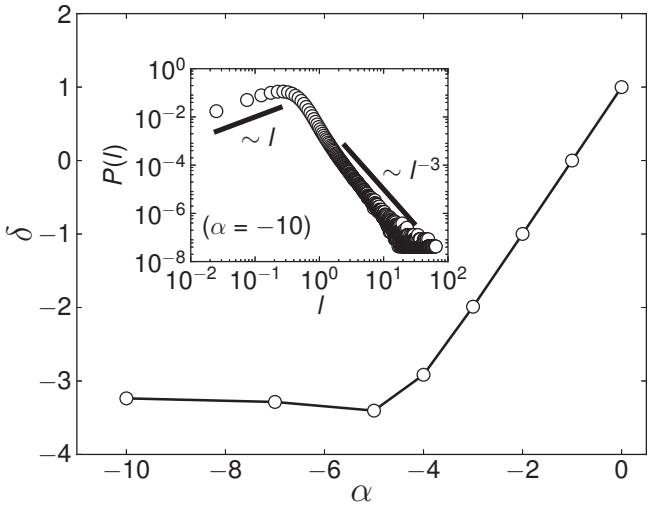

Figure 3.5. Relation between the distance exponent α and the exponent from the actual distribution $P(l) \sim l^{\delta}$ after network construction. The main plot shows that the linear relation $\delta = \alpha + 1$ is valid for small $|\alpha|$ down to $\alpha \approx -4$. For $\alpha < -4$, the exponent δ from the distribution saturates slightly below a value of -3. The inset shows the distribution of link lengths $P(l)$ for $\alpha = -10$ that is sampled from the network. The straight lines are guides for the eye to show the scaling at the limit of small and large l, according to Equation (3.23). This figure has been modified from [229].

hood are unavailable for connection so that links will have to extend to more distant areas.

We measure the link length distribution by fitting the tail of $P(l)$ with a power-law

$$P(l) \sim l^{\delta} \tag{3.15}$$

and then compare the obtained exponent δ with the distance exponent α. These fits are shown as red straight lines in Figure 3.4. We find that the equality $\delta = \alpha + 1$ is only valid for small negative values of α, and begins to deviate as α decreases. As discussed above, for large negative α the nodes almost exclusively connect to their nearest neighbors, so that the distribution $P(l)$ becomes independent of α. However, this 'saturated distribution' still has a power-law tail with an exponent of $\alpha \simeq -3$, which we estimate with a combinatorial approach as follows.

Consider the m-th iteration step of the construction algorithm for a network with $\alpha \ll 0$ so that links are mostly drawn between neighboring nodes. We assume that at this iteration step a random stub will be connected to a free stub of the nearest node available and the probability density of this connection to be of length l is given by $p_m(l)$, which reads

$$p_m(l)dl = Z(m)[1 - P_{\text{full}}(m)][P_{\text{full}}(m)]^{n(l)} l dl, \tag{3.16}$$

where P_{full} is the probability of a node to have reached its target degree, and $n(l) = c\pi l^2$ is the average number of nodes in the circle of radius l. Here, c denotes the node density that is simply the total number of nodes divided by the domain area. The prefactor

$Z(m)$ ensures normalization

$$\int_0^\infty p_m(l)dl = 1. \tag{3.17}$$

The probability of a randomly selected node to have reached its target-degree is a monotonically increasing function of the iteration step m. As a very simple estimate, we choose $P_{\text{full}} = m/M$, where M is the target number of links in the network. Inserting this assumption in Equations (3.16) and (3.17), we obtain

$$p_m(l)dl = Z(m)(1 - m/M)(m/M)^{c\pi l^2} l dl, \tag{3.18}$$

$$Z(m) = \frac{2\pi cM}{m - M} \ln(m/M). \tag{3.19}$$

The total probability density for a link to be of length l is then

$$p(l) = \frac{1}{M} \sum_{m=0}^{M} p_m(l). \tag{3.20}$$

For large M, we can approximate the sum by an integral so that

$$p(l) = \frac{1}{M} \int_0^M p_m(l)dm. \tag{3.21}$$

We insert Equations (3.18) and (3.19) in the above equation and solve the integral. The solution is

$$p(l) = \frac{4\pi lc}{(1 + \pi cl^2)^2}. \tag{3.22}$$

This yields in the limit of small and large l, respectively

$$p(l) \sim \begin{cases} l, & l \ll 1 \\ l^{-3}, & l \gg 1. \end{cases} \tag{3.23}$$

By this analysis we confirm the saturation value of $\delta \simeq -3$ for large l that occurs for large negative α (see Figure 3.5). The inset of Figure 3.5 shows an exemplary link length distribution for $\alpha = -10$, where the dependencies (3.23) are visible.

3.2.2 Modeling degree correlations

We employ two different methods to construct degree-correlated embedded networks. In the first method, correlations are imposed directly by a prefactor of the connection

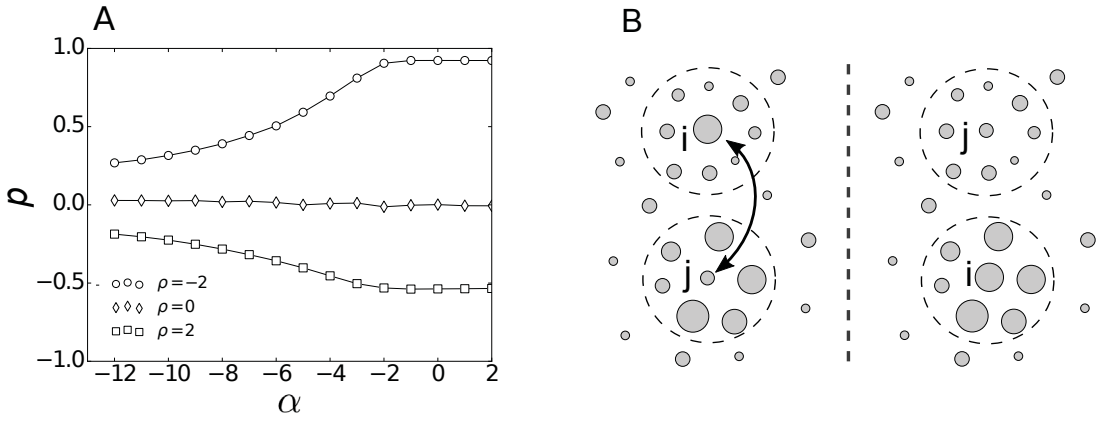

Figure 3.6. (**A**) Pearson degree correlation coefficient p for model 1 networks with 10^5 nodes and different prefactors ρ. The strength of degree correlations decreases for decreasing α which is indicated by a decrease of $|p|$. (**B**) Schematic representation of a node swap. The circles show the swapping range of radius d around nodes i and j. Gray dots represent nodes with the dot size proportional to their target-degree. The target-degrees of nodes i and j are swapped (left), which increases the difference between the average target-degree of the two neighborhoods (right). This figure has been modified from [229].

probability that depends on the target-degrees of the nodes. In the second method, nodes are first spatially redistributed such that nodes with similar target-degree are close to each other. Then, connections are drawn in the same way as in the uncorrelated case.

Model 1: degree-dependent connection probability

The first model is a modified version of the construction method for the uncorrelated network. Nodes are first randomly distributed in the spatial domain and each node is assigned a target-degree that is drawn from the Poissonian degree-distribution (3.11). Then, the algorithm selects a random stub of a node i and connects it to a free stub of node j with probability

$$\Pi(l, k_i, k_j) \sim e^{\rho|k_i - k_j|} \cdot l_{ij}^{\alpha}, \tag{3.24}$$

where k_i, k_j are the target-degrees of the nodes and ρ is a prefactor that controls the type and strength of the desired degree-correlations. For negative ρ, nodes preferably connect to nodes with similar target-degree so that the resulting graph is assortative. For positive ρ, connections between nodes with similar target-degree are avoided so that the graph becomes disassortative. We quantify the strength of the degree-correlations by the Pearson degree correlation coefficient p as defined by Equation (1.7) in Section 1.1.1.

Figure 3.6A shows the values of p for different combinations of the prefactor ρ and distance exponent α. We observe that $|p|$ becomes smaller for decreasing α, since the increasing locality of links interferes with the incentive of nodes to connect to similar (or dissimilar) nodes. In the following, we will set $\rho = -2$ for the assortative and $\rho = 2$ for the disassortative networks, respectively.

Model 2: spatial segregation of nodes

In the second model, nodes are first distributed randomly in the spatial domain and each node is assigned a target-degree from the Poisson degree distribution (3.11). Then, the nodes are spatially segregated with respect to their target-degree. This spatial segregation of nodes is realized by a swapping algorithm based on a model from Badham

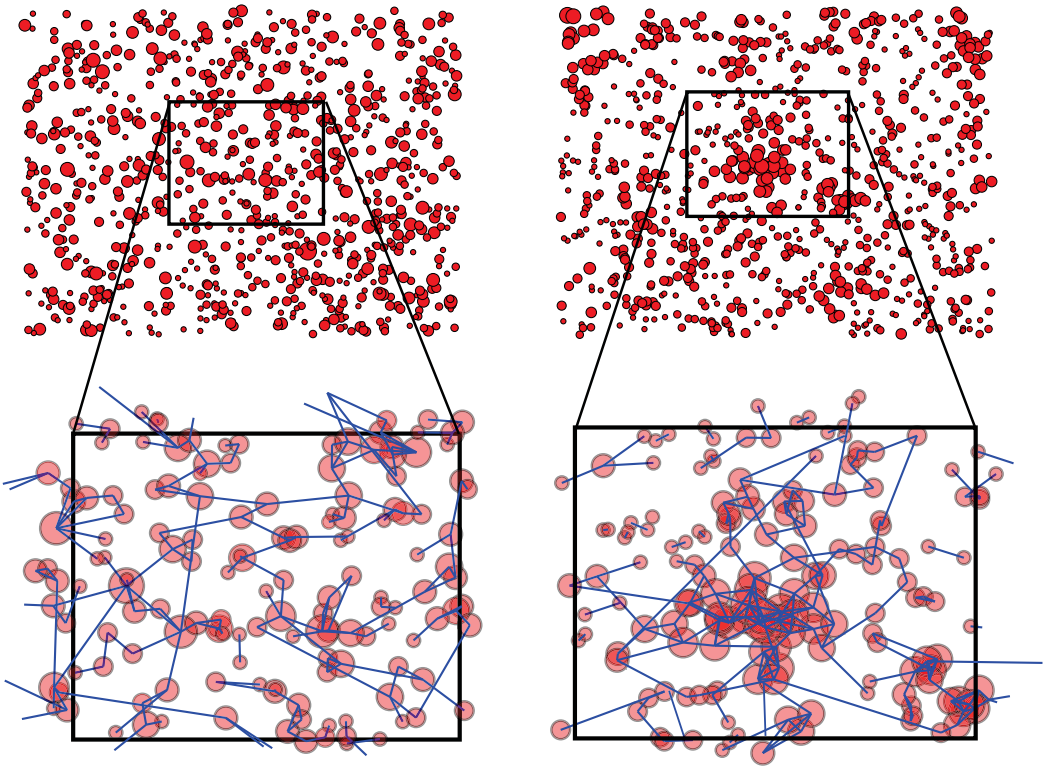

Figure 3.7. Spatial connectivity structure of a model 1 and model 2 network for $N = 10^3$ nodes (red dots) and $\alpha = -10$. Dot size is proportional to the node degree and blue lines represent links between nodes. (**A**) Model 1 network with homogeneous spatial distribution of nodes. (**B**) Model 2 network with spatially segregated nodes after 10^6 swaps. Notice the emergence of highly connected node assemblies in the model 2 network. This figure has been modified from [229].

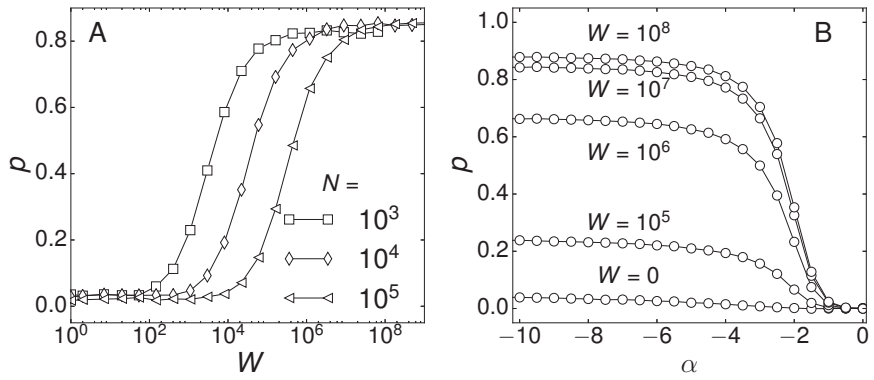

Figure 3.8. Pearson degree correlation coefficient p for model 2 networks with spatially segregated nodes. (**A**) Networks of different size with distance exponent $\alpha = -5$ after W iterations of the swapping algorithm. The Pearson coefficient saturates at about $W \sim 10^3 N$, indicating that the network is equilibrated. (**B**) Networks of size $N = 10^5$ for different α and W. Degree correlations emerge for $\alpha < 0$. This figure has been modified from [229].

et al. [16]. In short, the algorithm works as follows. First, it randomly selects two nodes i and j and calculates the mean target-degrees $\overline{k}_i, \overline{k}_j$ within a distance d of each of the nodes. The distance d is chosen such that a circle with radius d contains on average as many nodes as the larger target-degree of the nodes,

$$\pi d^2 c = \max(k_i, k_j), \tag{3.25}$$

where c is the average node density, $c = N/L^2$. Then, the target-degree of both nodes are swapped, if

$$(k_i - \overline{k}_i)^2 + (k_j - \overline{k}_j)^2 > (k_i - \overline{k}_j)^2 + (k_j - \overline{k}_i)^2. \tag{3.26}$$

Thus, the swap increases the difference of the mean target-degrees of the two neighborhoods. A schematic node swap is illustrated in Figure 3.6B. Note that the node swap does not change the spatial distribution of node positions so that the node-density is maintained. Figure 3.7 shows the spatial structure for a model 1 and model 2 network for comparison.

After repeated application of the swapping procedure the nodes are connected in the same way as for the construction of uncorrelated spatial networks with connection probability $\Pi(l) \sim l_{ij}^{\alpha}$. We find that the Pearson degree correlation coefficient saturates at about $10^3 N$ iterations of the swapping procedure, indicating that the network reached a stationary state with respect to further iterations (Figure 3.8A). We find that the level of assortativity increases for increasing locality of links (decreasing α) as

shown in Figure 3.8B, which can be understood as follows. As links become more local for decreasing α, there is a higher probability that nodes connect to other nodes in their neighborhood that have a similar degree due to the prior segregation. Note that this model only generates assortative networks and hence, we restrict the discussion of disassortativity to model 1 networks.

3.3 Percolation behavior of the model networks

3.3.1 Uncorrelated spatial networks

Let us first consider uncorrelated spatial networks. Figure 3.10 shows the giant component (GC) for four exemplary networks with distance exponents $\alpha = -2$, $\alpha = -3$, $\alpha = -4$, and $\alpha = -10$. We observe that the giant component undergoes a qualitative structural change as α decreases. For $\alpha = -2$, the giant component is made up from a large number of long-range links so that it extends across the whole spatial domain. For $\alpha = -3$ and $\alpha = -4$, the giant component is assembled from several localized subgraphs which are interconnected by a small number of long-range links. Finally, for $\alpha = -10$, almost all links are short-ranged so that the giant component is reminiscent of a two-dimensional percolating lattice.

Numerical measurements of the largest cluster density $G(q)$ are shown in Figure 3.9A for three representative networks of size $N = 10^5$ with distance exponents $\alpha = 0$, $\alpha = -4$ and $\alpha = -10$. Results are based on averages of 10^4 networks, if not stated otherwise. By qualitative inspection we see that increasing spatial constraints decrease the resilience of the graph: For $\alpha = 0$ a giant component emerges for lower density of links (smaller q) than for $\alpha = -4$ and $\alpha = -10$, respectively. This can be put another way by reading Figure 3.9A from right to left: We need to remove more links from the unconstrained graph than from the spatially constrained graphs to disassemble the giant component, hence the unconstrained graph the most robust one. The mean cluster size $S(q)$ for the same networks is shown in Figure 3.9B. The peak positions of $S(q)$

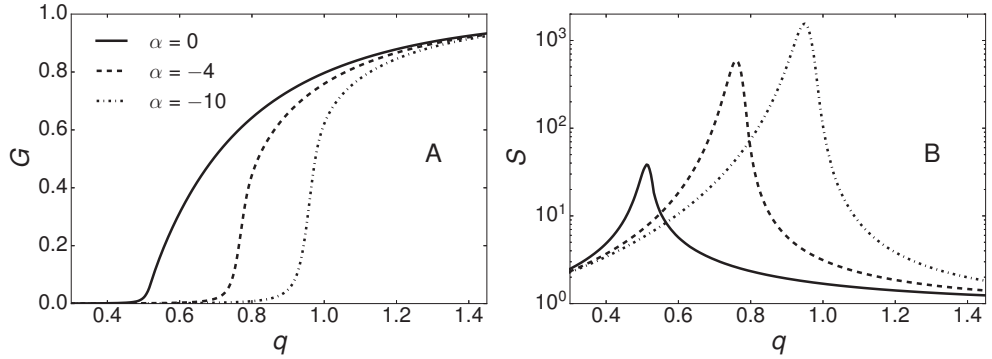

Figure 3.9. Percolation behavior of uncorrelated spatial networks of size $N = 10^5$ for three different values of α. (**A**) Largest cluster density and (**B**) mean cluster size. Both the shape of the largest cluster density curve and the mean cluster size curve are strongly affected by the value of α. Close to the percolation threshold q_c the largest cluster density G sharply rises and the mean cluster size S peaks. Both graphs indicate a shift of the percolation threshold to higher values for decreasing α.

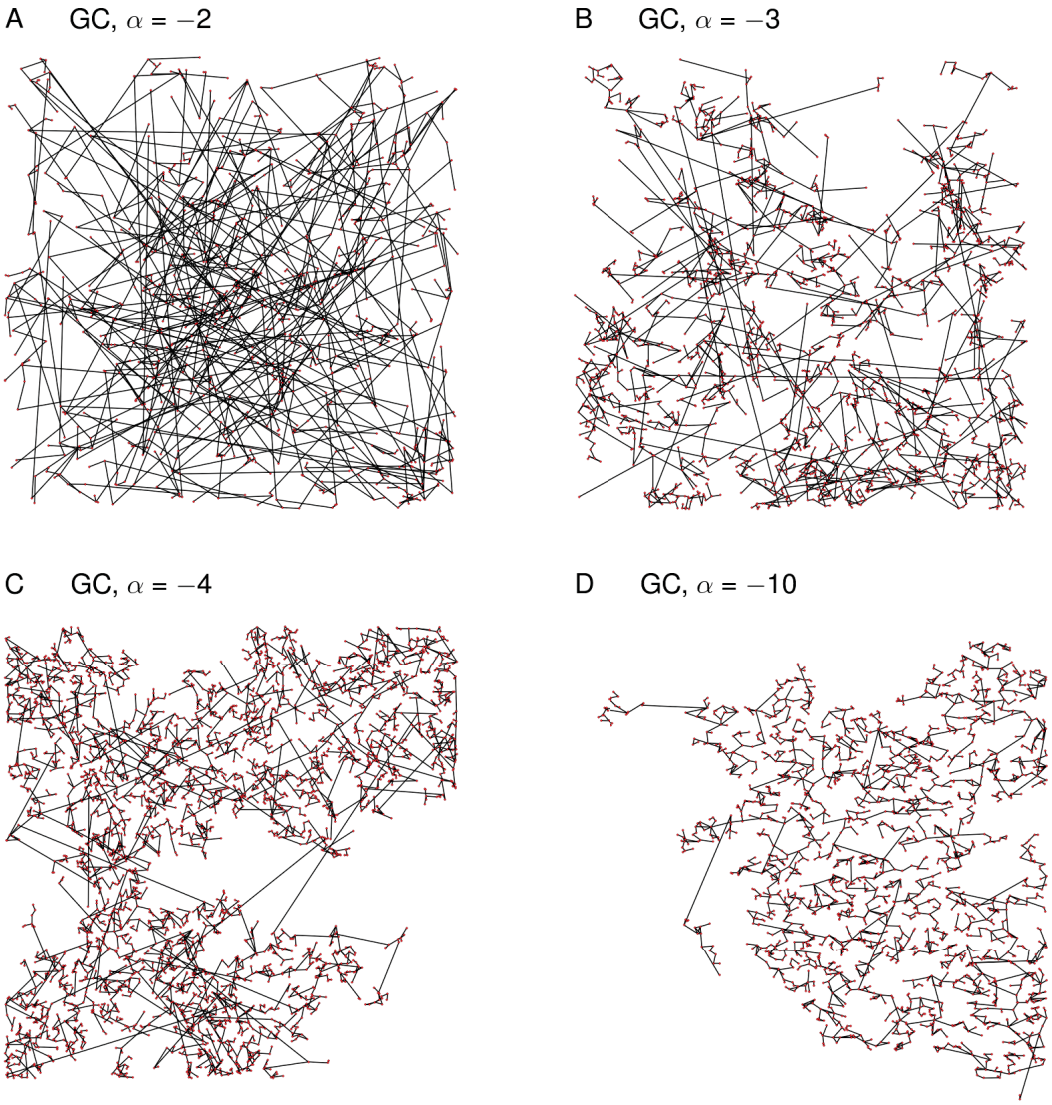

Figure 3.10. Spatial structure of the giant component (GC) for uncorrelated embedded networks of size $N = 10^4$ in the percolating phase for different distance exponents α. For decreasing α the effect of spatial embedding becomes more dominant so that the largest cluster is composed of more short-range connections and fewer long-range links. The connectivities used for construction of the networks are (**A**) $q = 0.54$; (**B**) $q = 0.62$; (**C**) $q = 0.75$; (**C**) $q = 0.9$.

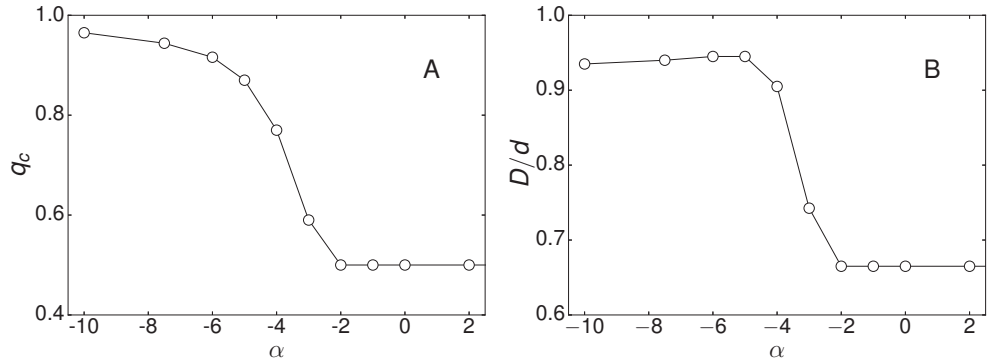

Figure 3.11. Critical behavior of uncorrelated spatial graphs. (**A**) Percolation threshold and (**B**) fractal dimension D/d at criticality for different distance exponents α. Both the percolation threshold and fractal dimension increase when α decreases below -2. The fractal dimension D/d saturates for $\alpha \leq -5$ close to the value 0.95. This figure has been modified from [229].

give a good estimate of the percolation threshold q_c of the networks and they indicate a positive shift of q_c for decreasing α.

In order to analyze the percolation transition more quantitatively, we apply the finite-size scaling method as described in the Appendix, A.4 to obtain the percolation threshold and fractal dimension for $N \to \infty$. The dependence of q_c and D/d on the distance exponent α is shown in Figure 3.11. In the regime of weak spatial constraints, $\alpha \geq -2$, we find numerically $D/d = 0.67$ and $q_c = 0.5$. These values correspond to the ones for the original ER graph, where the fractal dimension $D_{\mathrm{ER}}/d = 2/3$ belongs to the mean-field universality class and the percolation threshold takes the value $q_c = 0.5$ [98, 255, 7].

When α decreases below -2, the percolation threshold shifts to larger values (see Figure 3.11A), confirming that increasing spatial constraints decrease the resilience of the graph. In the regime of strong spatial constraints, $\alpha \leq -5$, we find $q_c = 0.95$ and $D/d = 0.945$. In this regime, the fractal dimension D/d is close to the one for regular two-dimensional lattices that takes the value $D_{\mathrm{lattice}}/d = \frac{91}{96} \backsimeq 0.95$ [59]. In the intermediate region, $-5 < \alpha < -2$, we find new percolation thresholds and exponents. We conclude that increasing spatial constraints shift the percolation transition from the universality class of random networks to the universality class of two-dimensional lattices. Li et al. [169] found a similar behavior for spatially constrained networks on a two-dimensional grid. Note that the fractal dimension D/d saturates for $\alpha \leq -5$ (Figure 3.11B), which is the region where the exponent of the link length distribution saturates (Figure 3.5). In contrast, the percolation threshold still slightly increases for decreasing α in this region, (Figure 3.11A) This indicates that for $\alpha \leq -5$ only the microstructure of the network is affected by the distance exponent, which does not

change the universality class of the percolation transition.

3.3.2 Degree-correlated model 1 network

Let us now investigate the percolation transition of model 1 networks with degree-dependent connection probability as described in Section 3.2.2. For $\rho = 0$ the model generates uncorrelated spatial networks equivalent to those in the previous section. A network with $\rho = 0$ and $\alpha = 0$ resembles the original ER graph. We examine an assortative network with $\rho = -2$ and a disassortative network with $\rho = 2$ and compare them to an uncorrelated network with $\rho = 0$. The Pearson correlation coefficients for the networks depend on the distance parameter α as shown previously in Figure 3.6A. Since maximal correlations occur for the unconstrained networks, we first consider the case $\alpha = 0$.

Figure 3.13 visualizes the connectivity structure of the giant component for the uncorrelated, assortative and disassortative network for $\alpha = 0$. The giant component of the assortative network (Figure 3.13B) is made of a strongly connected core-network with attached chains of poorly connected nodes. In contrast, the giant component of the disassortative network (Figure 3.13C) comprises assemblies of highly branched subnetworks. Finally, the giant component of the uncorrelated network (Figure 3.13A) consists of branched subnetworks as well as chains, but has no strongly connected core.

Exemplary plots of the largest component density and mean cluster size are shown in Figure 3.12 for $N = 10^5$ and $\alpha = 0$. Qualitatively, we see that assortativity significantly increases the resilience of the network and disassortativity slightly decreases it. An interesting observation is that for $\alpha = 0$ the assortative network is characterized by a non-diverging mean cluster size (dashed line in Figure 3.12B). This non-characteristic

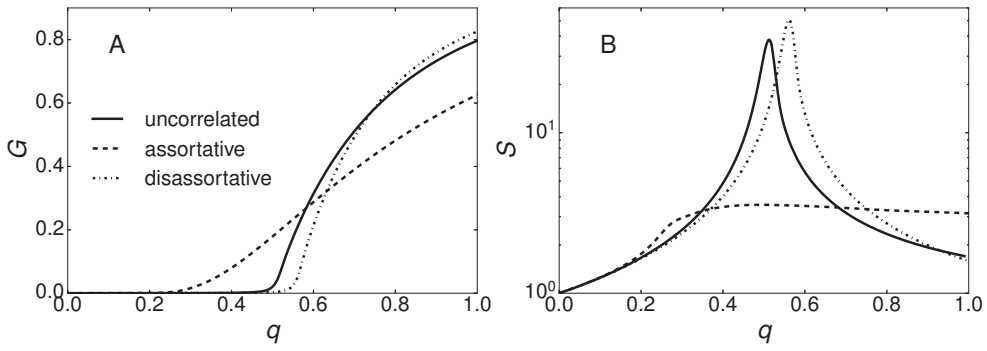

Figure 3.12. Influence of degree correlations on the percolation behavior of model 1 networks for $\alpha = 0$ and $N = 10^5$. (**A**) Largest cluster density and (**B**) mean cluster size. The corresponding Pearson coefficients $p = 0.00$ (uncorrelated), $p = 0.92$ (assortative) and $p = -0.54$ (disassortative). This figure has been modified from [229].

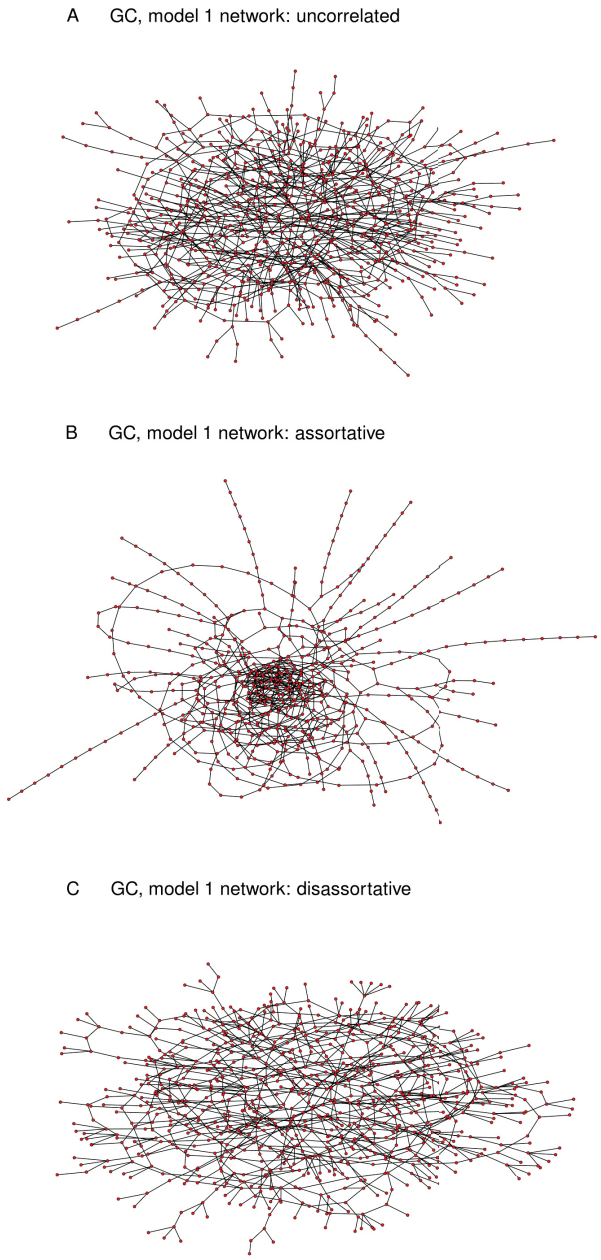

Figure 3.13. Topology of the giant component (GC) of three exemplary model 1 networks with different degree correlations for $\alpha = 0$. Nodes are *not* placed according to their position in two-dimensional space in order to better visualize the connectivity structure. Networks are of size $N = 10^4$ and connectivity $q = 1.5$.

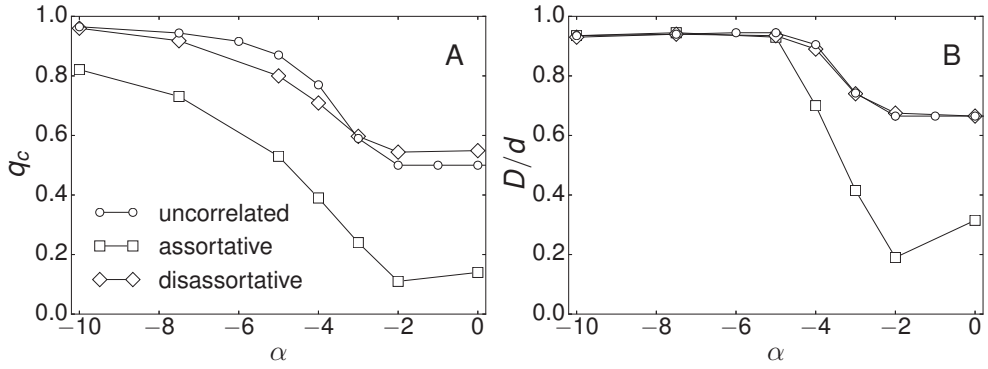

Figure 3.14. Critical behavior of model 1 networks. (**A**) Percolation threshold q_c and (**B**) fractal dimension D/d at criticality of model 1 networks for different values of α and different degree correlations: Uncorrelated networks ($\rho = 0$), assortative networks ($\rho = -2$) and disassortative networks ($\rho = 2$). This figure has been modified from [229].

percolation behavior has been previously described by Noh [203] for assortative ER networks.

Using finite-size scaling we characterize the percolation transition of the networks for $N \to \infty$. Figure 3.14 shows the percolation threshold q_c and fractal dimension D/d for different α. From Figure 3.14A we immediately see that spatial constraints persistently increase the percolation threshold in all networks and assortativity significantly lowers the percolation threshold for all α. Disassortativity, on the other hand, only slightly affects the percolation threshold. Moreover, in Figure 3.14B we see that the fractal dimension of disassortative networks is very similar to the one of uncorrelated networks. In contrast, assortativity strongly decreases the fractal dimension for $-4 \leq \alpha \leq 0$, which points to a non-characteristic percolation transition in this regime. For $\alpha \leq -5$, the percolation transition belongs to the universality class of two-dimensional lattices with $D/d \backsimeq 0.94$ as shown in Figure 3.14. An interesting result is that for $\alpha \leq -5$ the assortative and uncorrelated network have equal fractal dimensions D/d, but their percolation threshold differs significantly. A possible explanation is that in this regime only the microstructure of the network is affected by assortativity, which does not influence the universality class of the percolation transition.

To examine the mutual effect of spatial embedding and degree correlations we plot the dependence of q_c on the Pearson coefficient p and distance exponent α in Figure 3.15. The contour plot illustrates how the threshold-increasing effect of assortativity competes with the threshold-decreasing effect of spatial constraints. Assortative networks without spatial constraints ($\alpha = 0$) are very robust against random failure with a low percolation threshold (top right corner in Figure 3.15). These networks comprise a strongly connected core of high-degree nodes that extends across the whole spatial do-

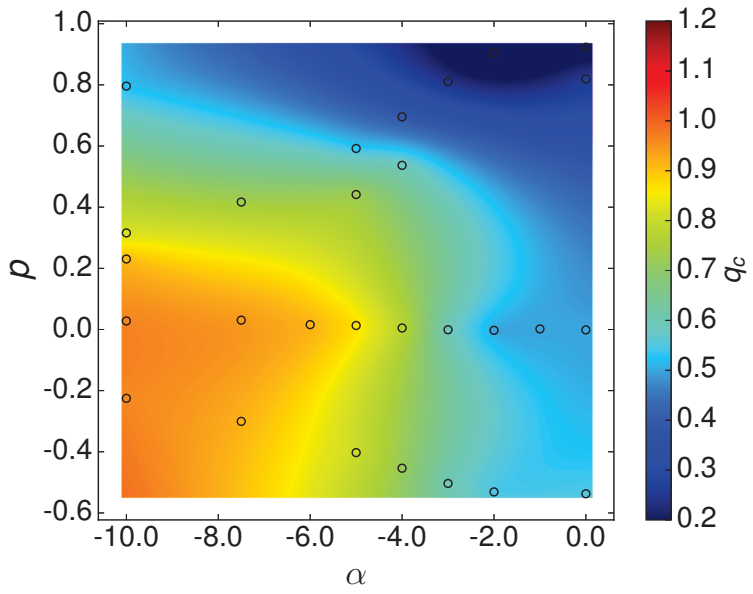

Figure 3.15. Dependence of the percolation threshold q_c on the Pearson coefficient p and distance exponent α for model 1 networks. Open symbols are actual data points that were used for linear interpolation. This figure has been modified from [229].

main and that is resilient against random removal of links. This property is conserved if we introduce weak spatial constraints ($-2 \leq \alpha < 0$) to the network, because it still contains a sufficient number of long-range connections so that the highly connected core can extend across the whole spatial domain. For increasing spatial constraints ($\alpha < -2$) the percolation threshold significantly increases, because the increasing locality of links prevents the assembly of such a strongly connected subnetwork. Disassortative networks are characterized by a high q_c that is increased even further by spatial constraints, which points to a high vulnerability of disassortative networks.

3.3.3 Degree-correlated model 2 network

In the second model, nodes are first spatially segregated according to their degree and then randomly connected in the same way as in the uncorrelated case. We here use $10^3 N$ iterations of the shuffling algorithm as described in Section 3.2.2 to maximally segregate the nodes. For $\alpha = 0$, the network conforms to the original ER graph and for $\alpha = -10$ the network is maximally correlated if the nodes are segregated (see Figure 3.8B for the corresponding Pearson coefficients). Note that the degree correlations achieved with this construction method are always positive.

We compare the resulting assortative spatial network to an uncorrelated spatial net-

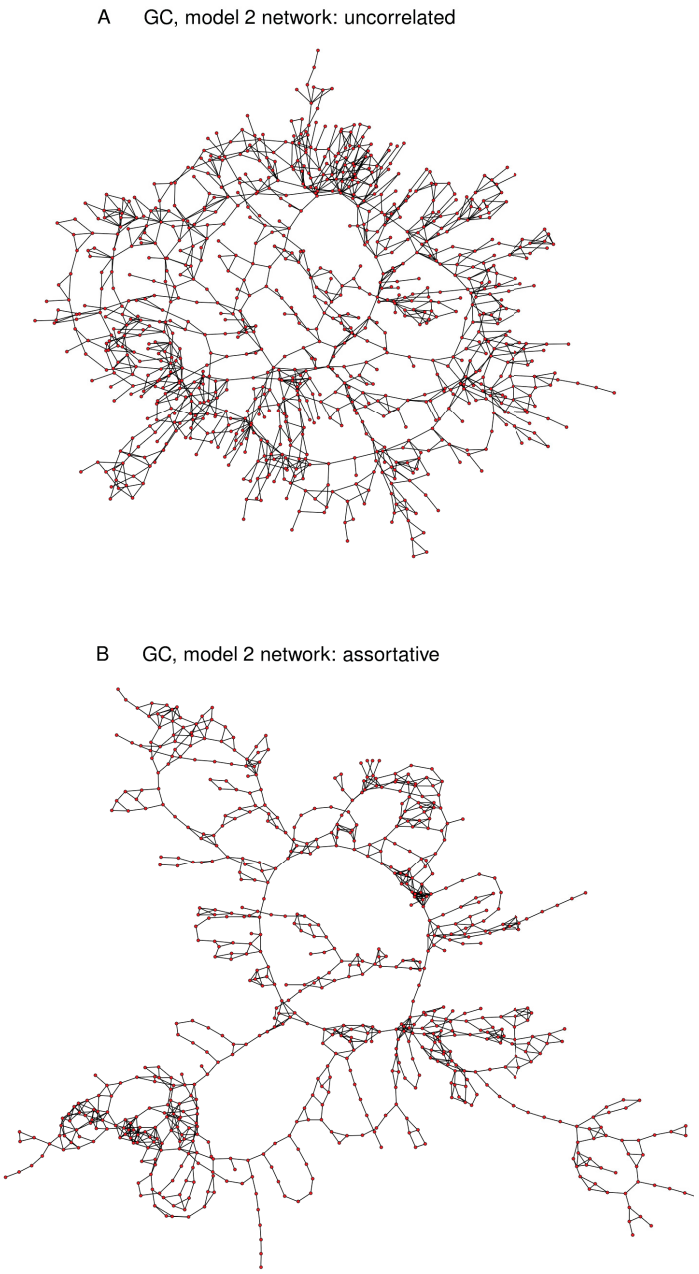

Figure 3.16. Topology of the giant component (GC) of the uncorrelated and assortative model 2 network in the percolating phase for $\alpha = -10$. Nodes are *not* placed according to their position in two-dimensional space in order to better visualize the connectivity structure. Networks are of size $N = 10^4$ and connectivity $q = 1.5$.

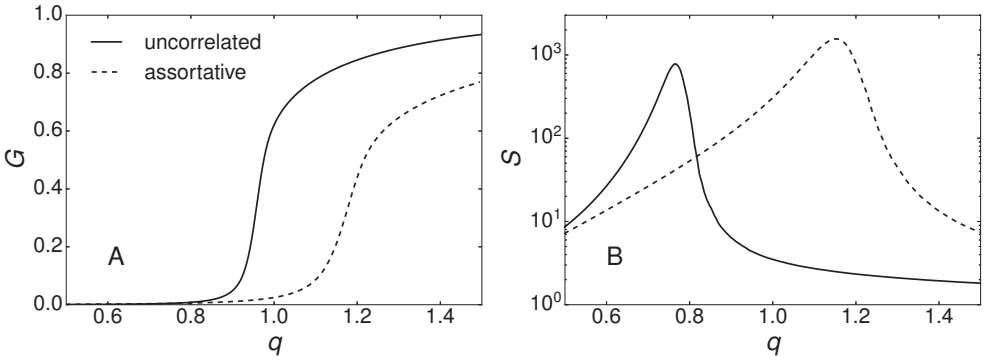

Figure 3.17. Influence of degree correlations on the percolation behavior of model 2 networks for $\alpha = -10$ and $N = 10^5$. (**A**) Largest cluster density and (**B**) mean cluster size. The corresponding Pearson coefficients are $p = 0.00$ (uncorrelated) and $p = 0.88$ (assortative). This figure has been modified from [229].

work with no node segregation.

Figure 3.16 shows snapshots of the giant component structure for the assortative and uncorrelated network for $\alpha = -10$. The giant component of the uncorrelated network (Figure 3.16A) is a highly branched and highly clustered structure with no shortcuts across the network. In contrast, the giant component of the assortative network (Figure 3.16B) is made of densely connected subgraphs that are joined by few extended chains of poorly connected nodes.

Exemplary plots of the largest component density and mean cluster size are shown in Figure 3.17 for networks of size $N = 10^5$ for $\alpha = -10$. Apparently, the assortative

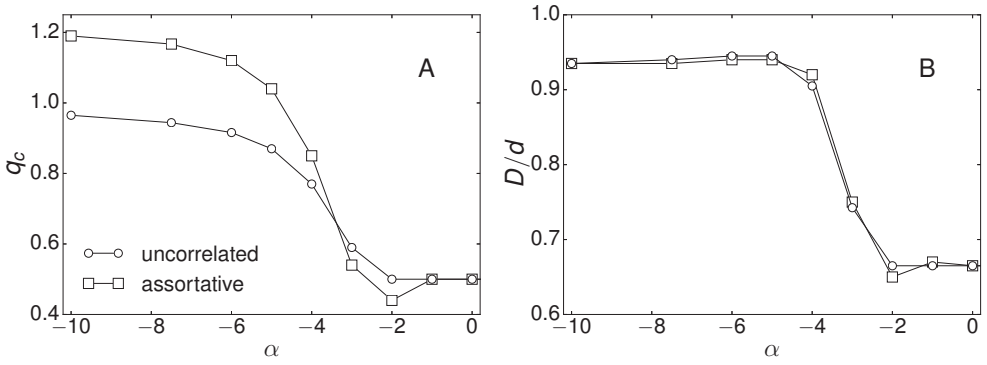

Figure 3.18. Critical behavior of correlated model 2 networks. (**A**) Percolation threshold and (**B**) fractal dimension at criticality as a function of α. Uncorrelated networks with $W = 0$ and assortative networks with $W = 10^3 N$. This figure has been modified from [229].

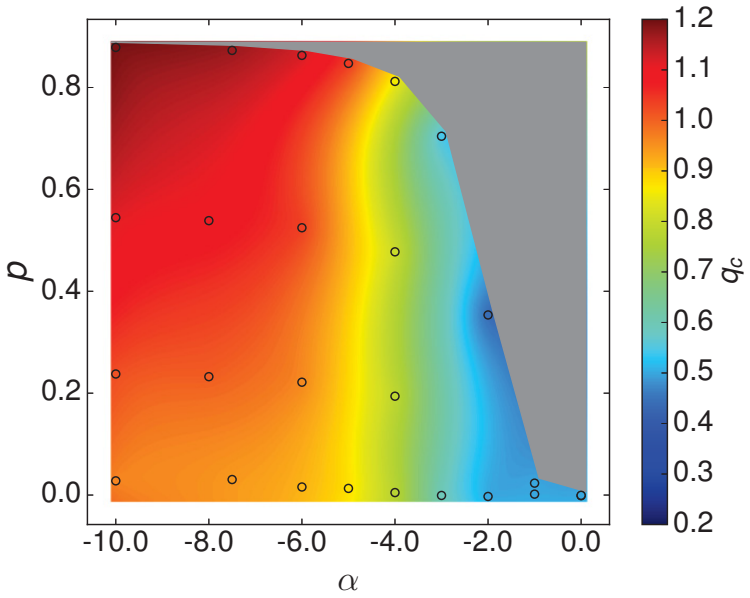

Figure 3.19. Dependence of the percolation threshold q_c for model 2 networks on the Pearson coefficient p and the distance exponent α. Open symbols show the actual data points used for linear interpolation. This figure has been modified from [229].

network is less robust than the uncorrelated network, which we explore more quantitatively in the following.

The behavior of the percolation threshold and fractal dimension is shown in Figure 3.18 for different α. In the regime of moderate spatial constraints, $-3 \leq \alpha \leq -2$, assortativity slightly decreases the percolation threshold, similar to the effect for model 1 networks. A possible explanation is that this regime favors the interconnection of spatially close high-degree nodes, while maintaining a sufficient number of long-range links, or short-cuts. Hence, the high-degree nodes form local assemblies that are highly interconnected, constituting a subnetwork that spans the whole spatial domain. This 'core' is resilient to random failure of links, similar to the strongly connected core in assortative model 1 networks.

For strong spatial constraints, $\alpha \leq -4$, an interesting effect occurs: The percolation threshold significantly increases, reaching values that are substantially larger than for the uncorrelated network ($q_c \simeq 1.2$ vs. $q_c \simeq 0.94$). This can be understood as follows. For increasing metric constraints the graph contains less long-range links that connect the localized assemblies of high-degree nodes. Hence, these groups become separated by sparsely connected areas that appear in Figure 3.16B as extended chains of low-degree nodes. Consequently, random removal of links easily disintegrates the graph into dis-

connected subnetworks, which causes a higher percolation threshold. This behavior is contrary to the behavior of model 1 networks, where assortativity persistently increases the resilience of the embedded graphs. Another interesting result is that assortativity in model 2 networks has no significant effect on the fractal dimension D/d (Figure 3.18B).

The mutual effect of assortativity and spatial embedding on the network resilience is illustrated in Figure 3.19, where we show the dependence of the percolation threshold on p and α. The plot confirms that the threshold-increasing effect of increasing spatial constraints (decreasing α) is intensified by assortative degree correlations (increasing p): Strongly local and assortative networks have a significantly higher percolation threshold than uncorrelated networks (top left corner of Figure 3.19). Note that assortativity emerges only for networks with sufficiently large negative α so that we cannot access the top right corner of the plot (gray area).

3.3.4 Comparison of model 1 and model 2

The two network models serve well to illustrate the interplay of assortative degree correlations and spatial embedding. Both architectures conform to the same metric constraints of two-dimensional embedding with power-law dependency of the link length distribution, but they differ in the way how degree correlations are imposed on the network. In model 1, assortative degree correlations are introduced directly by connecting nodes in preference of the desired correlations and in model 2, assortativity emerges from metric constraints due to the prior segregation of the nodes. Both models are equivalent in the uncorrelated case. For uncorrelated networks we find that increasing spatial constraints generally increase the percolation threshold and shift the percolation transition from the universality class of random networks to the universality class of two-dimensional lattices.

The influence of assortativity on the percolation transition differs for both architectures. In model 1 assortativity decreases the percolation threshold, whereas in model 2 it generally increases the threshold with the exception of the regime $-3 \leq \alpha \leq 0$. Assortative model 1 networks percolate more easily, because high-degree nodes connect to a subnetwork, or 'core', that is very robust against random removal of links. This effect has been found in numerous studies of assortative non-local random networks, where the percolation threshold decreases or even vanishes, depending on the degree distribution [197, 201, 289, 287, 40, 276, 203, 123]. Moreover, strongly assortative model 1 networks exhibit a qualitatively different percolation transition that is characterized by a non-diverging mean cluster size and substantially decreased values of D/d.

In model 2 the prior segregation of the nodes affects the percolation behavior differently. For weak metric constraints, $-4 < \alpha < -1$, the percolation threshold is slightly reduced. In this regime a domain-spanning, robust core emerges that consists of local assemblies of high-degree nodes that are interconnected by a sufficient number of

long-range links. For $\alpha \leq -4$, less long-range links exist so that this core can be easily disintegrated into isolated local assemblies, which is reflected in a higher percolation threshold. Although in this regime the percolation threshold is strongly increased due to the strong assortativity, the fractal dimension is similar to the one of the uncorrelated network. Note that we here only compare positively correlated networks, because negative correlations could only be generated with model 1. However, we found that disassortativity has only a small impact on the percolation transition, similar to findings by Noh [203].

In order to better understand the different percolation behavior of the models we compare their topology in the assortative case. Recall that the strongest correlations appear in model 1 for $\alpha = 0$ and in model 2 for $\alpha = -10$. In highly assortative model 1 networks ($\alpha = 0$), a strongly connected core appears that is resilient to random removal of links. This core can be revealed by decomposing the network into subnetworks of increasing connectivity using k-core decomposition [232] (see Section 1.1.1). In short, a k-core is obtained by successively pruning all nodes with degree less than k. Do we find a similar core in highly assortative model 2 networks for $\alpha = -10$?

Figure 3.20 shows the k-cores for a strongly assortative model 1 and model 2 network. In the first model a domain-spanning highly connected core forms, whereas in the second model several local subnetworks exist that form disconnected communities in the higher k-cores. This modular structure is responsible for the increased percolation threshold of assortative model 2 networks. We conclude that the different structural properties of model 1 and model 2 networks are not sensed by the Pearson coefficient and hence, additional measures (such as modularity) would be needed to predict the percolation behavior of the networks.

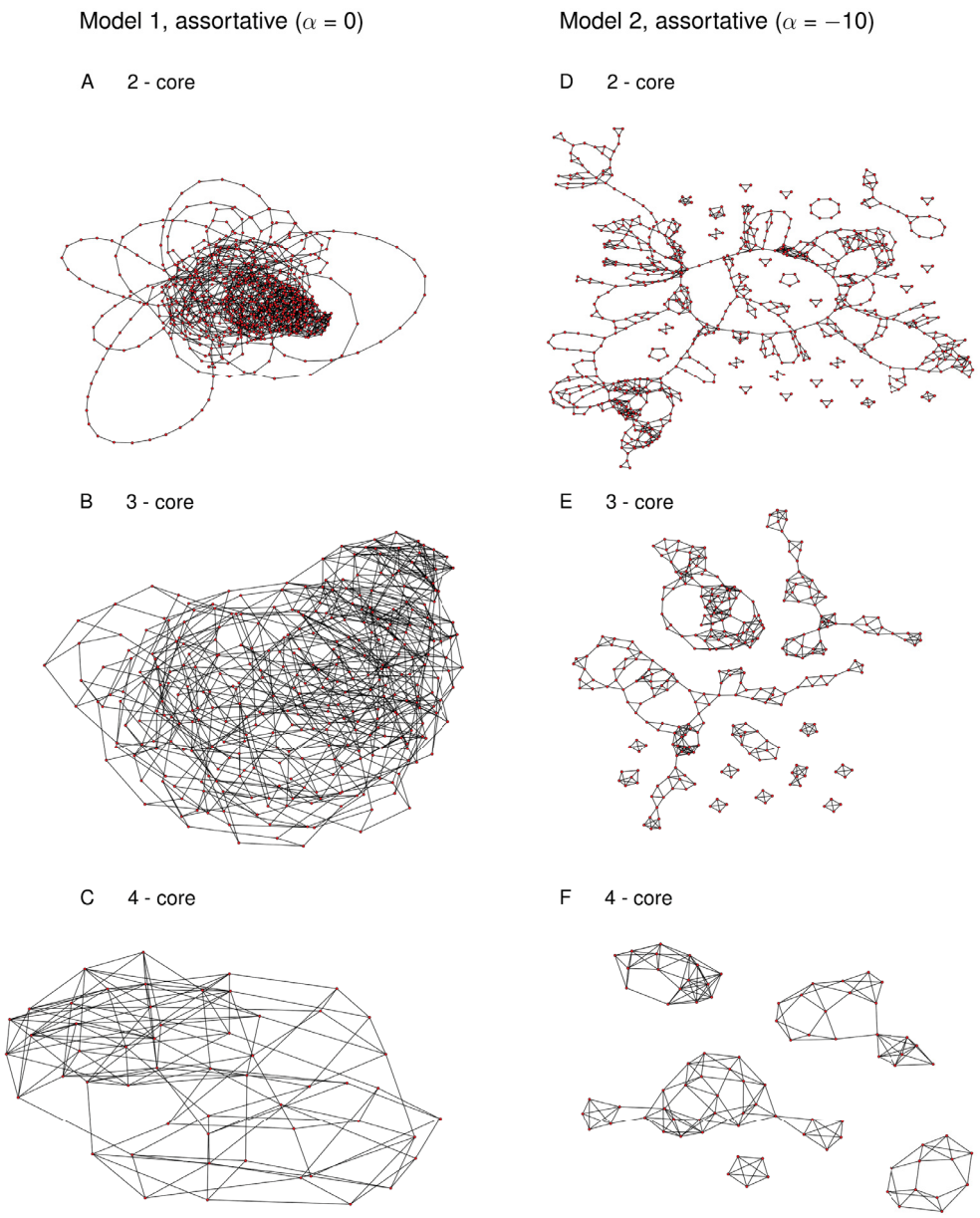

Figure 3.20. k-core decomposition of a highly assortative model 1 network (left column) and model 2 network (right column). A k-core is obtained by successively pruning all nodes with degree less than k. Nodes are *not* placed according to their position in two-dimensional space in order to better visualize the connectivity structure. In the model 1 network a global spanning highly connected core forms and in the model 2 network the k-cores disassemble into several communities that are disconnected from each other. Following parameters were used for the networks: $N = 1000$ and $q = 1.5$. The corresponding Pearson coefficients are $p = 0.92$ (model 1) and $p = 0.88$ (model 2).

3.4 Discussion

Many real world networks are embedded in space and evolve under geographical constraints. Prominent examples are power-grids, transportation networks, the internet, and neuronal networks [25, 247]. Spatial constraints have been found to strongly influence various structural properties of a network and the processes taking place on it [24, 179, 288, 280, 131, 25]. Nevertheless, this property has been often ignored in the analysis of the structure and function of many systems, especially neuronal networks [247].

Modern neuro-biological techniques allow for growing neuronal cultures that certainly show features of metric networks [286, 114, 95, 261, 263]. Additionally, these networks can be modified to follow specific patterns and designs which are associated with specific graph-theoretical properties such as degree correlations and small-world features [237, 261, 87]. The percolation framework is a powerful tool to investigate the structural properties of these networks without the needs to infer the full connectivity matrix [45, 246, 81]. With this method, Soriano et al. [246, 45] examined a developing neuronal network in the context of non-spatial Erdős-Rényi (ER) graphs. However, the length distribution of axons in neuronal cultures has been shown to change substantially with age and location of the neurons [286, 114, 261, 263].

In this chapter we developed a percolation model based on the ER graph that takes into account more complex topological features of such a network in order to describe its connectivity structure more accurately. In addition to spatial embedding we also allow for the possibility that the connectivity structure features degree correlations, which have been found for several neuronal networks [282, 36, 260, 87]. Our results are twofold. First, increasing locality of links generally raises the percolation threshold of the graphs and shifts the percolation transition to the universality class of two-dimensional lattices. This observation complements previous findings by Li et al. [169], who found a similar behavior for uncorrelated spatial ER networks on a two-dimensional grid. Second, the effect of assortativity on the percolation transition depends on the spatial structure of the networks: Assortativity decreases the percolation threshold when the nodes are distributed randomly in space, whereas it increases the threshold when nodes with similar degree are placed spatially close to each other. Unfortunately, this difference is not captured by the Pearson degree correlation coefficient. Therefore, in the context of percolation, degree correlations and metric constraints are no independent topological features a network, but they must be taken into account mutually for an accurate description of its structural properties.

Our model could be further refined by considering bootstrap percolation, where nodes are activated, if sufficient number of preceding nodes are active at the same time. The bootstrap percolation behavior of a network is strongly sensitive to the statistical properties of its connectivity structure [27] as well as to metric constraints and network

size [266, 11]. However, the effect of degree correlations on the bootstrap percolation properties of a spatially embedded network has not been investigated so far.

Finally, we propose that our findings are relevant for various other fields dealing with the resilience of networks to random failure of links, e.g. power-grids, transportation networks, or social networks in the context of disease spreading. Social networks in particular exhibit both strong metric constraints [25] and assortative degree correlations [197, 201]. In a related study on correlated random graphs [201], Newman concluded as follows:

> *First, we find that networks that are assortatively mixed by degree percolate more easily that [sic] their disassortative counterparts. That is, a giant component of connected vertices forms in the network at lower edge density than in another network with the same degree distribution but zero or negative assortativity. This result may imply, for instance, that assortatively mixed social networks would support epidemic disease outbreaks more easily than disassortatively mixed ones, which would be a disheartening conclusion, given our finding that most social networks appear to be assortative.* [201, page 4])

Our findings suggest that, at least in in some situations, assortative degree correlations may have the opposite effect due to the network's geometric properties, which may paint a more positive picture.

4 Conclusion

In this thesis we have examined how the dynamics of a large neuronal network is related to the properties of its connectivity structure. The main focus has been laid on two particular structural features, namely a heterogeneous degree distribution, and degree correlations. In neuroscience, much emphasis has been put on correlations in the neuronal activity, but the relevance of structural correlations for the system's dynamics has been much less studied so far.

As a central result of the thesis, we have introduced a **mean-field model** that expresses the dynamics of heterogeneous, degree-correlated neuronal networks in terms of reduced rate equations, which make it possible to efficiently explore the dynamical behavior of the system. Our approach is based on grouping neurons with equal number of inputs (equal in-degree) together into populations and describing the mean activity of these populations rather than the spiking of individual neurons. The distinction of the neurons by in-degree is motivated by the fact that the firing rate of a neuron is closely related to the number of its inputs: Strongly connected neurons receive larger input currents and fire at higher rates than poorly connected neurons.

An important assumption within the mean-field approach is that the spiking input to the neurons can be approximated by a Gaussian process. This assumption allows for a probabilistic description of the neuronal dynamics, which we have used to derive a set of coupled population rate equations in Section 2.3. This set of equations can be solved self-consistently for the stationary firing rate of each population. We have found that the network structure is sufficiently captured by a reduced matrix that contains the coupling strength between the populations, which can be easily computed from the adjacency matrix of the network. The reduced matrix is of size $M \times M$, where M is the number of different in-degrees in the system. For several generic random networks it can be calculated analytically in the limit of large network size, which considerably simplifies the analysis of these systems.

Using the population rate equations and numerical simulations we have examined in Section 2.5 how in-degree correlations affect the dynamics of an excitatory heterogeneous neuronal network that is stimulated by external input. Main attention has been paid to the regime of weak stimuli, where neuronal spiking is largely driven by recurrent activity and thus, the influence of the network structure on the global dynamics becomes most pronounced. Results from numerical simulations of 10^5 neurons agree very well with the mean-field calculations. Moreover, we have shown in Sec-

tion 2.5.2 that it is possible to approximate the distribution of neuronal firing rates from the mean population activity. Expectedly, a highly heterogeneous distribution of in-degrees leads to a large variability of neuronal firing rates. Assortative in-degree correlations further broaden the distribution of neuronal firing rates by increasing the activity of strongly connected neurons and decreasing the activity of weakly connected neurons. Disassortative in-degree correlations have the opposite effect. Driven by the raised activity of the strongly connected neurons, the assortative network sustains its activity for very small inputs, where its uncorrelated and disassortative counterparts fail to fire. Therefore, we conclude that assortative in-degree correlations enhance the network's sensitivity to weak stimuli. This effect is reminiscent of percolation, where assortativity has been shown to increase the structural robustness of a network.

The enhanced sensitivity of the network to weak stimuli can be interpreted as an improved capability to amplify and transmit small input signals, which is an important function of recurrent excitation in neuronal circuits. To examine this property more quantitatively, we have calculated the mutual information of the stimulus/response relationship in Section 2.6. The analysis has revealed that the network's information transfer capability is optimized for intermediate levels of assortativity. While small amounts of assortative in-degree correlations improve the network's sensitivity to small inputs, an excess of assortativity promotes extremely inhomogeneous activity that is detrimental for signal transmission: A large proportion of neurons is inactive, whereas a small number of strongly connected neurons receives sufficient recurrent input to fire almost at the highest possible rate, regardless of the stimulus. Thus, the neuronal activity does not contain much information about the input that evoked it. Moreover, extreme levels of assortativity (or disassortativity) lead to a segregation of the system into disconnected subnetworks, which prevents cross-communication between the populations. Intuitively, this effect is detrimental for information processing, hence it is hardly surprising that such high levels of correlations are rarely observed in real biological systems.

In chapter 3 we have examined the effect of degree correlations on the structural robustness of a neuronal network in terms of a simplified **percolation model**, which reveals how easily the network can be disintegrated into several isolated components by successively removing links from it. The model is based on the undirected Erdős-Rényi (ER) graph, whose structural properties are very well understood. Additionally, we have included an important metric property of neuronal systems: Spatially close nodes are more likely to be connected to each other than distant nodes. Although the property of disadvantaged long-range connections is relevant for many real-world networks, it is often neglected in the theoretical analysis of such systems. We use finize-size scaling to extrapolate the critical behavior of the system from numerical simulations of networks with different size. With this approach we have demonstrated in Section 3.3 that increasing metric constraints (increasing locality of links) generally

decrease the robustness of the network: A higher density of links is needed to form a giant component that connects a significant proportion of the graph. Moreover, increasing metric constraints shift the percolation transition from the universality class of random networks to the universality class of two-dimensional lattices, which features distinct characteristic percolation exponents.

Concerning the role of degree correlations in this context, we have seen in Section 3.3.2 that assortativity increases the resilience of a metric graph, if the strongly connected nodes form a domain-spanning subgraph. This subnetwork resembles a characteristic robust 'core' that promotes an unusual percolation behavior with a non-diverging mean cluster size in strongly assortative networks. However, we have also found in Section 3.3.3 that for networks with strong metric constraints the existence of assortative degree correlations may imply the opposite. They are associated with a *decreased* robustness of the graph, if nodes with similar degree are placed spatially close to each other. In this case the high-degree nodes form localized assemblies that cannot form a single domain-spanning core due to the lack of long-range connections. This finding contradicts the prevailing opinion that assortative degree correlations generally make a graph more robust. Hence, degree correlations and metric properties of a network are interrelated and have to be taken into account mutually in the structural analysis of the system. We point out that this observation is also relevant for many other real-world systems that exhibit both features. Social networks in particular feature assortative correlations and thus, they have been labeled as robust in the context of epidemiology. Considering that these networks are often subject to strong metric constraints, this conclusion is challenged by our findings.

Main results and research questions. In the introduction we have identified the central questions that have driven our research. We shall now answer them by summarizing our main results.

Can we devise a stochastic model of the global network dynamics that integrates structural heterogeneity and connectivity correlations?

- Yes, we have developed a mean-field model to calculate the average spiking activity of large, heterogeneous excitatory networks of leaky integrate-and-fire (LIF) neurons that exhibit connectivity correlations in form of in-degree correlations.

- The model is based on sorting neurons with equal in-degree into populations and describing the average activity of these populations in terms of reduced rate equations. These equations can be derived with a probabilistic approach by assuming that the spiking input to the neurons can be approximated by a Gaussian process.

- Numerical simulations of large LIF networks and mean-field calculations agree very well.

How do heterogeneity and connectivity correlations influence the dynamical behavior of the system?

- A heterogeneous distribution of in-degrees promotes a broad distribution of neuronal firing rates.
- Assortative in-degree correlations further broaden the distribution of firing rates, while disassortative in-degree correlations narrow it.
- Moreover, assortative in-degree correlations enhance the ability of the network to sustain its activity for very small external excitation.

Can we interpret the network's dynamics in terms of neuronal processing?

- Yes, we have examined the network's firing response to an external input. This mapping of input to an output is a basic form of signal transmission and processing in neuronal circuits.
- In particular, the network can sense and amplify small inputs through recurrent excitation.
- We have analyzed the signal transmission capability of the network by calculating the input/output mutual information, which has revealed that the network's sensitivity to weak stimuli is optimized by intermediate levels of assortativity.

How do connectivity correlations influence the structural behavior of the system?

- We have examined this problem in terms of a simplified percolation network model that is based on the Erdős-Rényi (ER) graph, taking into account degree correlations and disadvantaged long-range connections.
- Disassortativity slightly decreases the network's robustness.
- Assortativity increases the network's robustness if the strongly connected nodes assemble to a domain-spanning core. This is only possible if a large number of long-range links are present in the network.
- For strong locality of links, assortativity can decrease the network's robustness: Strongly connected nodes form localized assemblies that are only weakly interconnected and thus, they can be easily isolated by removing links from the network.
- We conclude that metric constraints and degree correlations must be taken into account mutually to correctly interpret the structural behavior of the network.

Outlook. Our results show that it is possible to approach the dynamics of certain complex neuronal networks in terms of a reduced mean-field model. While we have focused on basic topological features such as a heterogeneous degree distribution and degree correlations, it is also possible to apply the mean-field model to networks with other properties, e.g. hierarchical or modular systems. The most important prerequisite is that the neurons can be assumed to share only few common inputs, which is reasonable for many sparse random networks. We have distinguished the neurons by their in-degree to account for the heterogeneous network structure. However, one could also consider neuron-specific properties, e.g. by including excitatory and inhibitory neurons, or neurons with different intrinsic parameters. This requires a 'finer' coarse-graining of the activity (and network structure), since additional neuronal populations have to be taken into account.

As a first step in the analysis of the system's dynamics we have mainly focused on the stable stationary activity of the system. Future studies could explore its transient behavior and the stability of the stationary solutions with respect to the role of fluctuations in both the neuronal activity and connectivity structure. A related problem is that neuronal activity appears to fluctuate at two different levels: First, the spiking of individual neurons is highly irregular and second, their mean firing rate varies over time, which has been characterized as a 'doubly stochastic' activity [79]. Numerical simulations suggest that these irregularities may result from non-random features of the network structure [176]. Our mean-field model may be well-suited for further investigation of this phenomenon with respect to the possible role of degree correlations in this regard. An interesting question is whether irregularities in the neuronal firing rates can be linked to multistability of the system, which could possibly be examined by using the stability analysis presented in the Appendix, A.1.

Our mean-field model could be simplified by using rate models for the activity of individual neurons, which would allow for an easier mathematical analysis of the global dynamics at the expense of realism. A further simplification may involve the concept of a bootstrap percolation model, where neurons are activated, if a certain proportion of their afferent neurons is active. Whether or not such a reduced model still captures the effect of assortativity on the network's sensitivity to small inputs is a non-trivial question, and this investigation would deepen our understanding of how to analyze and interpret the structural and dynamical properties of neuronal systems.

Concerning percolation, our finding that degree correlations and spatial constraints are strongly related to each other leads to the question of how these features relate to other complex network properties, e.g. the shortest average path length, clustering coefficient, or modularity. A thorough study of these measures in the context of network resilience could help to identify the most important attributes that capture the structural properties of metric graphs.

A Appendix

A.1 Stability conditions for the stationary solutions

In this section we derive stability conditions for the stationary solutions of the self-consistent rate equations (2.28). Unstable solutions can be associated with cell-to-cell synchronizations, which have been examined recently within a mean-field framework for LIF networks with heterogeneous neurons and strong excitatory coupling [187].

We begin with Equation (2.28), which governs the time-evolution of the population rates,

$$\tau_x \frac{d}{dt}\hat{\mathbf{r}}(t) = -\hat{\mathbf{r}}(t) + \mathbf{\Theta}(\hat{\mathbf{r}}(t), s), \tag{A.1}$$

where $\hat{\mathbf{r}}(t) = [\hat{r}_{k_{\min}}(t), \ldots, \hat{r}_{k_{\max}}(t)]$ is the vector of k-population firing rates at time t, $\mathbf{\Theta}(\hat{\mathbf{r}}(t), s)$ is the vector of transfer functions $\phi_k(\hat{\mathbf{r}}(t), s)$, and τ_x is a time-constant of appropriate choice [118, 89]. Steady-states of the network dynamics correspond to a fixed-point solutions of the above equation. The stability of a fixed point can be investigated by linearizing Equation (A.1) around the fixed point (here denoted as $\hat{\mathbf{r}}_0$) and performing a standard stability analysis. First, we rewrite the transfer functions in abbreviated form as

$$\phi_k = \left[\tau_{\text{ref}} + \tau \int_{a_k}^{b_k} f(z)dz\right]^{-1}, \tag{A.2}$$

where $f(z) = \sqrt{\pi}\exp(z^2)(1 + \text{erf}(z))$. The integration intervals are now

$$a_k = = \frac{V_{\text{r}} - \mu_k(t)}{\sigma_k(t)}, \tag{A.3}$$

$$b_k = = \frac{\Theta - \mu_k(t)}{\sigma_k(t)}, \tag{A.4}$$

with the input mean and variance

$$\mu_k(t) = J\tau\left(\nu_{\text{thr}}s + \sum_{k'} N_{kk'}\hat{r}_{k'}(t)\right), \tag{A.5}$$

$$\sigma_k^2(t) = J\mu_k(t). \tag{A.6}$$

We now expand Equation (A.1) around the fixed point $\hat{\mathbf{r}}_\mathbf{0}$

$$\tau_x \frac{d}{dt}(\hat{\mathbf{r}} - \hat{\mathbf{r}}_0) = (-\mathbf{1} + \mathbf{J}(\hat{\mathbf{r}}_0))(\hat{\mathbf{r}} - \hat{\mathbf{r}}_0), \tag{A.7}$$

where $\mathbf{J}(\hat{\mathbf{r}}_\mathbf{0})$ is the Jacobian of the transfer function vector $\mathbf{\Theta}(\hat{\mathbf{r}}, s)$ at $\hat{\mathbf{r}}_0$. Solutions $\mathbf{v}$ of the linearized system evolve exponentially in time as

$$\mathbf{v}(t) = \sum_i C_i \mathbf{v}_i e^{\frac{\lambda_i - 1}{\tau_x}t}, \tag{A.8}$$

where $\mathbf{v}_i$ are the eigenvectors of $\mathbf{J}(\hat{\mathbf{r}})$ with eigenvalues λ_i. The solutions are stable, if $\lambda_i < 1$ for all i. Using the definition for the transfer function (A.2) we can evaluate the entries of the Jacobian to

$$J_{kl} = \frac{\partial \phi_k}{\partial \hat{r}_l} = \frac{-\tau \frac{\partial}{\partial \hat{r}_l} \int_{a_k}^{b_k} f(z)dz}{\left[\tau_{ref} + \tau \int_{a_k}^{b_k} f(z)dz\right]^2}. \tag{A.9}$$

To evaluate the integral in the numerator of Equation (A.9), we use following equality

$$\frac{\partial}{\partial \hat{r}_l} \int_{a_k}^{b_k} f(z)dz = f(b_k)\frac{\partial b_k}{\partial \hat{r}_l} - f(a_k)\frac{\partial a_k}{\partial \hat{r}_l}. \tag{A.10}$$

Using the definitions of a_k and b_k in Equations (A.3) and (A.4), we obtain

$$\frac{\partial a_k}{\partial \hat{r}_l} = \frac{-\partial \mu_k}{\partial \hat{r}_l}\frac{1}{\sigma_k} + \frac{\partial \sigma_k}{\partial \hat{r}_l}\frac{\mu_k}{\sigma_k^2} - \frac{\partial \sigma_k}{\partial \hat{r}_l}\frac{V_\text{r}}{\sigma_k^2}, \tag{A.11}$$

$$\frac{\partial b_k}{\partial \hat{r}_l} = \frac{-\partial \mu_k}{\partial \hat{r}_l}\frac{1}{\sigma_k} + \frac{\partial \sigma_k}{\partial \hat{r}_l}\frac{\mu_k}{\sigma_k^2} - \frac{\partial \sigma_k}{\partial \hat{r}_l}\frac{\Theta}{\sigma_k^2}. \tag{A.12}$$

We use $\sigma_k^2 = J\mu_k$, which gives for the partial derivation of the noise intensity

$$\frac{\partial \sigma_k}{\partial \hat{r}_l} = \frac{\partial \sqrt{J\mu_k}}{\partial \hat{r}_l} = \frac{\sqrt{J}}{2\sqrt{\mu_k}} \frac{\partial \mu_k}{\partial \hat{r}_l} = \frac{J}{2\sigma_k} \frac{\partial \mu_k}{\partial \hat{r}_l}. \tag{A.13}$$

Inserting (A.13) into Equations (A.11) and (A.12) we obtain

$$\frac{\partial a_k}{\partial \hat{r}_l} = -\frac{\partial \mu_k}{\partial \hat{r}_l} \left(\frac{1}{2\sigma_k} - \frac{JV_\mathrm{r}}{2\sigma_k^3} \right) = -\frac{\partial \mu_k}{\partial \hat{r}_l} A_k, \tag{A.14}$$

$$\frac{\partial b_k}{\partial \hat{r}_l} = -\frac{\partial \mu_k}{\partial \hat{r}_l} \left(\frac{1}{2\sigma_k} - \frac{J\Theta}{2\sigma_k^3} \right) = -\frac{\partial \mu_k}{\partial \hat{r}_l} B_k, \tag{A.15}$$

where $A_k \equiv \left(\frac{1}{2\sigma_k} - \frac{JV_\mathrm{r}}{2\sigma_k^3} \right)$ and $B_k \equiv \left(\frac{1}{2\sigma_k} - \frac{J\Theta}{2\sigma_k^3} \right)$. Now we insert μ_k from Equation (A.5), which gives

$$\frac{\partial a_k}{\partial \hat{r}_l} = -J\tau A_k \frac{\partial}{\partial \hat{r}_l} \sum_{k'} N_{kk'} \hat{r}_{k'} = -J\tau A_k N_{kl}, \tag{A.16}$$

$$\frac{\partial b_k}{\partial \hat{r}_l} = -J\tau B_k N_{kl}. \tag{A.17}$$

The above expression can be inserted into Equation (A.10), giving

$$\frac{\partial}{\partial \hat{r}_l} \int_{a_k}^{b_k} f(z)dz = -J\tau N_{kl}(B_k f(b_k) - A_k f(a_k)), \tag{A.18}$$

which we use for Equation (A.9), so that we finally arrive at following terms for the Jacobian

$$J_{kl} = N_{kl} \frac{J\tau^2 \left[B_k f(b_k) - A_k f(a_k) \right]}{\left[\tau_\mathrm{ref} + \tau \int_{a_k}^{b_k} f(z)dz \right]^2}. \tag{A.19}$$

The linear appearance of the joint-in-degree distribution in the Jacobian is to be expected, because it is a linear measure of the coupling strength between the populations. If the network is extremely assortative, then $N_{kk'} = \delta(k, k')$, and the Jacobian is of di-

agonal form with elements

$$J_{kk} = \frac{J\tau^2 \left[B_k f(b_k) - A_k f(a_k)\right]}{\left[\tau_{ref} + \tau \int_{a_k}^{b_k} f(z)dz\right]^2}. \tag{A.20}$$

In this case the stability conditions for each k-population are decoupled,

$$\frac{J\tau^2 \left[B_k f(b_k) - A_k f(a_k)\right]}{\left[\tau_{ref} + \tau \int_{a_k}^{b_k} f(z)dz\right]^2} < 1. \tag{A.21}$$

The above equation is similar[1] to the stability condition for a single neuronal population, which has been previously described in [187].

A.2 Diffusion approximation

In this section we stochastically describe the neuronal population activity, following the approach of Gerstner and Kistler [118] (see also [121, 71, 218]). The goal is to derive the set of Langevin equations (2.10) for the time-evolution of the neuron membrane voltage using the so-called diffusion approximation.

Consider a neuron i with in-degree k that receives stochastic input from the stimulus and afferent spiking neurons. Since we do not know the exact input spike train the neuron receives, we cannot calculate its membrane potential $V_i^{(k)}(t)$ directly. Therefore, we instead consider the probability $p_k(v_k, t)$ that its membrane potential lies in the interval $[v_k, v_k + dv_k]$

$$p_k(v_k, t)dv_k = \text{Prob}\left\{V_i^{(k)} \in [v_k, v_k + dv_k]\right\}. \tag{A.22}$$

Since we assume all k-neurons to be statistically indistinguishable, the probability density of a single k-neuron is representative for the probability density of all neurons in a k-population. Thus, we discard the neuron index i in the following derivation and interpret $p_k(v_k, t)$ as the density of membrane potentials in a k-population.

Recall that a k-neuron receives synaptic input from the stimulus with rate $s\nu_{\text{thr}}$ and, on average, recurrent input from $N_{kk'}$ afferent k'-neurons in the network with rates $\hat{r}_{k'}(t)$. We assume that the superposition of all these input spike trains can be regarded as a Poisson process with rate that is the sum of rates of the individual spike trains.

[1] In [187] the noise intensity σ is assumed to be constant so that the second and third term on the right-hand side of Equations (A.11) and (A.12) become zero and $A_k = B_k = 1/\sigma_k$.

Hence, the rate of the summed input to a k-neuron is

$$\lambda_k(t) \equiv s\nu_{\text{thr}} + \sum_{k'} N_{kk'}\hat{r}_{k'}(t). \tag{A.23}$$

Considering that the input is Poissonian with rate $\lambda_k(t)$, we can calculate the probability that a spike arrives at the neuron's dendrites in a small time window Δt, which is

$$\text{Prob}\left\{\text{spike in } [t, t+\Delta t]\right\} = \lambda_k(t)\Delta t. \tag{A.24}$$

Consequently, the probability that no spike arrives in this time window is $1-\lambda_k(t)\Delta t$. If no spike arrives, the membrane potential $v_k(t) \equiv v'_k$ of the k-neuron decays to $v_k(t+\Delta t) = v'e^{-\Delta t/\tau}$ due to the leakage term in the membrane voltage equation (2.3). On the other hand, if a spike arrives at time $t+s \in [t, t+\Delta t]$, the membrane potential changes to $v_k(t+\Delta t) = v'_k e^{-\Delta t/\tau} + Je^{-(\Delta t-s)/\tau}$ due to the voltage jump J induced by the spike[2]. Given that the membrane potential of the neuron at time t is v'_k, we can calculate the probability density to find the membrane potential v_k of the neuron at $t+\Delta t$, which is

$$\begin{aligned} p_k^{\text{trans}}(v_k, t+\Delta t|v'_k, t) = &\left[1-\Delta t\lambda_k(t)\right]\delta(v_k - v'_k e^{-\Delta t/\tau}) \\ &+ \Delta t\lambda_k(t)\delta(v_k - v'_k e^{-\Delta t/\tau} - Je^{-(\Delta t-s)/\tau}). \end{aligned} \tag{A.25}$$

We rewrite the above equation to

$$\begin{aligned} p_k^{\text{trans}}(v_k, t+\Delta t|v'_k, t) = &[1-\Delta t\lambda_k(t)]\delta\left(-e^{-\Delta t/\tau}(v'_k - v_k e^{\Delta t/\tau})\right) \\ &+ \Delta t\lambda_k(t)\delta\left(-e^{-\Delta t/\tau}(v'_k - v_k e^{\Delta t/\tau} + Je^{s/\tau})\right). \end{aligned} \tag{A.26}$$

Equation (A.26) describes the transition probability of the membrane potential for a small time-step Δt. Since we assume the input to be Poissonian, the evolution of the membrane potential is memoryless and thus resembles a Markov Process that is described by [273]

$$p_k(v_k, t+\Delta t) = \int p_k^{\text{trans}}(v_k, t+\Delta t|v'_k, t)p_k(v'_k, t)dv'_k. \tag{A.27}$$

[2]The membrane potential immediately after the spike is $v_k(t+s) = v'_k e^{-s/\tau} + J$. It then decays to $v_k(t+\Delta t) = (v'_k e^{-s/\tau} + J)e^{-(\Delta t-s)/\tau} = v'_k e^{-\Delta t/\tau} + Je^{-(\Delta t-s)/\tau}$.

We insert Equation (A.26) in Equation (A.27) and perform the integration, using the rule for delta-functions, $\delta\left(a(x-x_0)\right) = |a|^{-1}\delta(x-x_0)$. The integration results in

$$\begin{aligned} p_k(v_k, t+\Delta t) = &\left[1-\Delta t\lambda_k(t)\right] e^{\Delta t/\tau} p_k(v_k e^{\Delta t/\tau}, t) \\ &+ \Delta t\lambda_k(t) e^{\Delta t/\tau} p_k(v_k e^{\Delta t/\tau} - J e^{s/\tau}, t). \end{aligned} \tag{A.28}$$

We rearrange the terms in the above equation and write

$$\begin{aligned} p_k(v_k, t+\Delta t) = &e^{\Delta t/\tau} p_k(v_k e^{\Delta t/\tau}, t) \\ &+ \Delta t\lambda_k(t) e^{\Delta t/\tau} [p_k(v_k e^{\Delta t/\tau} - J e^{s/\tau}, t) - p_k(v_k e^{\Delta t/\tau}, t)]. \end{aligned} \tag{A.29}$$

Since the time-window Δt is assumed to be very small, we can expand Equation (A.29) about $\Delta t = 0$. We use the fact that $\Delta t = 0$ implies $s = 0$, since $0 \leq s \leq \Delta t$. Keeping only terms up to the first order in Δt the expansion yields

$$\begin{aligned} p_k(v_k, t+\Delta t) = p_k(v_k, t) &+ \Delta t \frac{1}{\tau}\left[p_k(v_k, t) + v_k \frac{\partial}{\partial v_k} p_k(v_k, t)\right] \\ &+ \Delta t\lambda_k(t)\left[p_k(v_k - J, t) - p_k(v_k, t)\right]. \end{aligned} \tag{A.30}$$

Again we rearrange the terms in the the above equation and write

$$\begin{aligned} \frac{p_k(v_k, t+\Delta t) - p_k(v_k, t)}{\Delta t} = &\frac{1}{\tau}\left[p_k(v_k, t) + v_k \frac{\partial}{\partial v_k} p_k(v_k, t)\right] \\ &+ \lambda_k(t)\left[p_k(v_k - J, t) - p_k(v_k, t)\right]. \end{aligned} \tag{A.31}$$

Let us consider the limit $\Delta t \to 0$ so that the left-hand side of Equation (A.31) turns to a partial derivative. Moreover, we assume that the voltage jumps J are small and expand the second term on the right-hand side of Equation (A.31) about $J = 0$ as follows

$$\lambda_k(t)\left[p_k(v_k - J, t) - p_k(v_k, t)\right] = \lambda_k(t) \sum_{l=1}^{\infty} \frac{(-1)^l}{l!} J^l \frac{\partial^l}{\partial v_k^l} p_k(v_k, t). \tag{A.32}$$

This expansion is called the *Kramers-Moyal expansion*. The first and second order give

$$-J\lambda_k(t) \frac{\partial}{\partial v_k} p_k(v_k, t) \tag{A.33}$$

and

$$J^2 \lambda_k(t) \frac{\partial^2}{\partial v_k^2} p_k(v_k, t), \tag{A.34}$$

respectively. Keeping only the first and second order in the expansion and considering $\Delta t \to 0$, we turn Equation (A.31) to a Fokker-Planck equation

$$\frac{\partial}{\partial t}p(v_k,t) = \frac{\partial}{\partial v_k}\left[\frac{v_k}{\tau} - J\lambda_k(t)\right]p_k(v_k,t) + \frac{1}{2}\left[J^2\lambda_k(t)\right]\frac{\partial^2}{\partial v_k^2}p_k(v_k,t). \tag{A.35}$$

This approximation - neglecting all terms of higher order than two in the Kramers-Moyal expansion - is called the diffusion approximation. Terms of the l-th order in this expansion are proportional to $J^l\lambda_k(t)$. Therefore, the diffusion approximation is reasonable for small voltage jumps J and becomes exact if $J^{l>2}\lambda_k = 0$. The latter can be achieved, for example, in models where the number of inputs per neuron increases with network size and J scales appropriately so that in the thermodynamic limit $J^2\lambda_k \to$ const., but $J^{l>2}\lambda_k \to 0$. In our model the number of inputs per neuron and J are fixed so that higher-order terms do not vanish, but they become very small. The accuracy of our model could be increased by increasing the in-degrees of the neurons and at the same time reducing the synaptic strength J, which would however require more computational resources for full LIF simulations, since larger networks would have to be simulated.

The first term in rectangular brackets in Equation (A.35) is called *drift coefficient*, because it describes the deterministic drift of the membrane potential due to the leakage and mean input current. The second term in rectangular brackets is the *diffusion coefficient* that describes the fluctuations of the membrane potential due to fluctuations of the input current. If we identify the mean and variance of the input current as

$$\mu_k(t) = J\tau\lambda_k(t) = J\tau\left(\nu_{\text{thr}}s + \sum_{k'}N_{kk'}r_{k'}(t)\right) \tag{A.36}$$

and

$$\sigma_k^2(t) = J^2\tau\lambda_k(t) = J^2\tau\left(\nu_{\text{thr}}s + \sum_{k'}N_{kk'}r_{k'}(t)\right), \tag{A.37}$$

respectively, we obtain the Fokker-Planck equations (2.12)

$$\frac{\partial p_k(v_k,t)}{\partial t} = \frac{\partial}{\partial v_k}\left[\left(\frac{v_k-\mu_k(t)}{\tau}\right)p_k(v_k,t)\right] + \frac{\partial^2}{\partial v_k^2}\left[\frac{\sigma_k^2(t)}{2\tau}p_k(v_k,t)\right]. \tag{A.38}$$

In fact, (A.38) represents a set of Fokker-Planck equations that are coupled through the mean and variance of the input current for each k-population. The set of Fokker-

Planck equations is equivalent to the set of Langevin equations

$$\tau \frac{dV^{(k)}(t)}{dt} = -V^{(k)}(t) + \mu_k(t) + \sigma_k(t)\sqrt{\tau}\xi^{(k)}(t), \tag{A.39}$$

where $V^{(k)}$ is the membrane potential of an arbitrary k-neuron and $\xi^{(k)}(t)$ is white noise. Since each neuron i in a k-population is assumed to be statistically equivalent, we can argue that the time-evolution of the membrane potential $V_i^{(k)}$ of the i-th k-neuron is governed by a separate Langevin equation as desribed by (2.10).

On a final note, the above derivation of the Fokker-Planck equation (FPE) is based on the assumption that we can describe each population of neurons by a separate probability density. In general, a coupled dynamical system is described by a multivariate probability density $p(v_{k_1}, v_{k_2}, \dots)$ and the corresponding multivariate FPE. We rely on the fact that populations only interact through uncorrelated spike trains and that there is no direct coupling between the neuron voltages. In the above derivation we assumed for each k-population that the input currents from all populations (including the k-population itself) are independent stochastic processes that are described by 'given' rates. Later, we calculate these rates *self-consistently* for all populations so that the coupling between the populations is properly taken into account.

A.3 Small noise approximation for the mutual information

In this section we apply the small noise approximation introduced by Tkačik et al. [265, 264] to express the mutual information I in terms of the distribution of mean responses $p(\hat{r})$, Equation (2.61). We begin with the expression (2.60) for the mutual information

$$I = -\int dr\ p(r)\log_2 p(r) + \int ds\ p(s)\int dr\ p(r|s)\log_2 p(r|s), \tag{A.40}$$

where $p(s)$ is the distribution of stimuli presented to the network, $p(r|s)$ is the distribution of responses if the same stimulus s is applied repeatedly, and $p(r)$ is the distribution of responses the network generates if it is subjected to the distribution $p(s)$ of stimuli. The response distribution $p(r)$ can be expressed as

$$p(r) = \int ds\ p(r|s)p(s). \tag{A.41}$$

With Equation (A.41) we can rewrite the mutual information (A.40) as

$$I = -\int ds\ p(s)\int dr\ p(r|s)\log_2 p(r) + \int ds\ p(s)\int dr\ p(r|s)\log_2 p(r|s). \tag{A.42}$$

Now we use the Gaussian approximation (2.57) of the conditional probability

$$p(r|s) = \mathcal{G}(r, \hat{r}(s), \sigma(s)) = \frac{1}{\sqrt{2\pi\sigma^2/n}} \exp\left(\frac{[r-\hat{r}(s)]^2}{2\sigma^2(s)/n}\right). \tag{A.43}$$

For the sake of a compact notation, we use in the following $\mathcal{G}(r)$ instead of $\mathcal{G}(r, \hat{r}(s), \sigma(s))$, keeping the other dependencies in mind. The second term on the right-hand side of Equation (A.42) corresponding to the (negative of) the noise entropy can be evaluated exactly for the Gaussian distribution,

$$\int ds\ p(s) \int dr\ \mathcal{G}(r) \log_2 \mathcal{G}(r) = -\frac{1}{2} \int ds\ p(s) \log_2[2\pi e\sigma^2(s)/n]. \tag{A.44}$$

In the first term on the right-hand side of Equation (A.42) we expand the integral over r around the mean value $\hat{r}$. With $f(r) \equiv \log_2 p(r)$ the expansion reads

$$\begin{aligned}\int dr\ \mathcal{G}(r)f(r) = &\int dr\ \mathcal{G}(r)f(\hat{r}) + \int dr\ \mathcal{G}(r)f(\hat{r})\frac{\partial f(r)}{\partial r}\bigg|_{\hat{r}}(r-\hat{r}) \\ &+ \frac{1}{2}\int dr\ \mathcal{G}(r)f(\hat{r})\frac{\partial f(r)^2}{\partial r^2}\bigg|_{\hat{r}}(r-\hat{r})^2 + \dots\ .\end{aligned} \tag{A.45}$$

The second term of the expansion is zero because of the symmetry of $\mathcal{G}(r)$ around $\hat{r}$ and the third term can be evaluated to $\frac{1}{2}f''(\hat{r})\sigma^2(r)/n$. Assuming that $\sigma(r)$ is small, we neglect the third term and all terms of higher order, thus keeping only the zero-th order of the expansion

$$\int dr\ \mathcal{G}(r)f(r) \simeq \int dr\ \mathcal{G}(r)f(\hat{r}) = f(\hat{r}) = \log_2 p(\hat{r}). \tag{A.46}$$

Inserting the approximation (A.46) and the result for the noise entropy (A.44) into the equation for the mutual information (A.42), we obtain

$$I \simeq -\int ds\ p(s) \log_2 p(\hat{r}) - \frac{1}{2}\int ds\ p(s) \log_2[2\pi e\sigma^2(s)/n]. \tag{A.47}$$

Finally, we rewrite the probability distributions in terms of $\hat{r}$ using $p(s)ds = p(\hat{r})d\hat{r}$ so that

$$I \simeq -\int d\hat{r}\ p(\hat{r}) \log_2 p(\hat{r}) - \frac{1}{2}\int d\hat{r}\ p(\hat{r}) \log_2[2\pi e\sigma^2(\hat{r})/n], \tag{A.48}$$

which is Equation (2.61).

A.4 Finite-size scaling method

In order to characterize the phase transition of the model networks we have to examine the behavior of $S(q)$ and $G(q)$ in the region around q_c. Unfortunately, this is the region where finite-size effects are most pronounced, hence it is crucial to know how these quantities behave in finite systems. We have already briefly touched on this problem in the introduction by showing that the probability $P_{\text{conn}}(q)$ to find a pecolating cluster in a finite lattice approaches a step function for increasing lattice size (Figure 3.3). The largest cluster density $G(q)$ of the network shows a similar behavior.

Recall that in infinite networks the largest cluster density and the average size of finite clusters $S(q)$ are expected to scale as [59, 255]

$$G(q) \sim (q - q_c)^{\beta}, \quad q > q_c, \tag{A.49}$$

$$S(q) \sim |q - q_c|^{-\gamma}, \tag{A.50}$$

when q approaches the percolation threshold. Since we cannot model infinite networks, we have to extrapolate the behavior of $G(q)$ and $S(q)$ from finite networks using the *finite-size scaling* formalism which has been introduced by Stauffer and Aharony [255]. We already know that right at the percolation threshold q_c the system behaves as a fractal and the largest cluster mass scales with system size N as [59, 255]

$$N \cdot G(q_c, N) \sim N^{\frac{D}{d}}, \tag{A.51}$$

where D is the fractal dimension and d is the spatial dimension of the system. This relation can be used to find the parameters q_c and D/d as follows. For large N, the power-law scaling is expected to be valid only for $q = q_c$ [59, 255]. Hence, we can plot the giant component mass $N \cdot G(N)$ against N for increasing concentrations q, until we see a power-law dependency emerging which shows as a line in a double-logarithmic plot.

However, a more precise method is to use the behavior of the mean cluster size $S(q)$ close to q_c to quantify the percolation transition [255, 59, 203]. Equation (A.50) implies that $S(q)$ diverges at q_c in the limit of large network size. It certainly cannot diverge in a finite system, but it exhibits a peak at a value of $q = q'$ that is very close to the critical point. The behavior of $S(q)$ for different network sizes N is shown in Figure A.1 for the first model network with $\alpha = 0$ and $\rho = 0$. For these parameters, the network behaves equal to the original ER network and thus it is characterized by the same percolation threshold and exponents, which we have proven in Section 3.3. From Figure A.1 we see that the peak of $S(q)$ becomes sharper with a higher maximum as N increases. Moreover, there is also a shift of the peak position q' towards the exact value of the transition point $q_c = 0.5$.

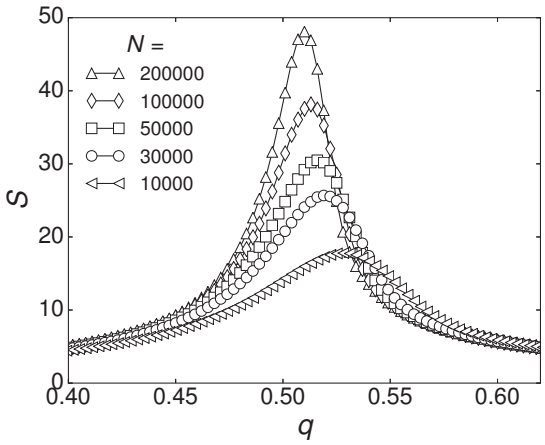

Figure A.1. Average size of finite clusters S for the model 1 network with parameters $\alpha = 0,\ \rho = 0$ for different network sizes N. The scaling behavior is equal to the behavior of the original ER graph. The value of q for which S peaks shifts to the left with increasing network size towards the threshold $q_c = 0.5$ in the limit of infinite size N.

Stauffer and Aharony [255] found that q' approaches the exact percolation threshold as $|q' - q_c| \sim N^{-\frac{1}{\nu d}}$, where ν is another critical exponent. In fact, the relation is valid for any concentration $q = q'$ that is chosen close to the percolation threshold [255] so that we can write

$$|q - q_c| \sim N^{-\frac{1}{\nu d}}. \tag{A.52}$$

This relation can be used to rescale Equations (A.49) and (A.50) for finite systems by substituting $(q - q_c) \to (q - q_c)N^{\frac{1}{\nu d}}$ to account for this finite-size effect. Another consequence of the relation (A.52) is that right at the real critical threshold q_c the largest component density and mean cluster size scale with system size as

$$G(q_c, N) \sim N^{-\frac{\beta}{\nu d}}, \quad \text{and} \quad S(q_c, N) \sim N^{\frac{\gamma}{\nu d}}, \tag{A.53}$$

respectively. If we want to rescale Equations (A.49) and (A.50) such that they hold in finite systems, the resulting equation must lead to the above equations in the limit $q \to q_c$. The required equations read in condensed form [255, 59] for the largest cluster density

$$G(q, N) = N^{-\frac{\beta}{\nu d}} F_1[(q - q_c)N^{\frac{1}{\nu d}}] \tag{A.54}$$

and for the mean cluster size

$$S(q, N) = N^{\frac{\gamma}{\nu d}} F_2[(q - q_c)N^{\frac{1}{\nu d}}]. \tag{A.55}$$

The scaling functions $F_1(x)$ and $F_2(x)$ define the crossover behavior of $G(q, N)$ and $S(q, N)$ as q approaches the critical point [255, 59]. The first scaling function $F_1(x)$

has the limiting behavior

$$F_1(x \to 0) \to \text{const.}, \qquad F_1(x \gg 1) \to x^{\beta}, \tag{A.56}$$

so that for $q \to q_c$ the finite-size Equation (A.54) gives the correct scaling behavior $G(q_c, N) \sim N^{-\frac{\beta}{\nu d}}$ and for $q > q_c$ it gives the behavior of (A.49). The second scaling function $F_2(x)$ has the limiting behavior

$$F_2(|x| \to 0) \to \text{const.}, \qquad F_2(|x| \gg 1) \to x^{-\gamma}, \tag{A.57}$$

so that for $q \to q_c$ the finite-size Equation (A.55) gives the scaling $S(q_c, N) \sim N^{\frac{\gamma}{\nu d}}$ and for $q \neq q_c$ it corresponds to (A.50). We can now use the finite-size relations of Equation (A.54) and Equation (A.55) close to the percolation threshold ($q \to q_c$) to rescale the curves of the largest cluster density and mean cluster size as

$$G(q, N)N^{\frac{\beta}{\nu d}} \sim N^{\frac{1}{\nu d}}(q - q_c), \tag{A.58}$$

$$S(q, N)N^{-\frac{\gamma}{\nu d}} \sim N^{\frac{1}{\nu d}}(q - q_c). \tag{A.59}$$

The rescaled values for $G(q, N)$ and $S(q, N)$ should now follow the same curve for each network size N in a region closely around the percolation threshold q_c, if the correct values for the threshold q_c and exponents $\gamma,\ \nu d$ are used. We use this rescaling method in reverse to obtain these parameters: First, we plot the rescaled curve for $S(q, N)$ using guessed values for $(q_c,\ \gamma,\ \nu d)$. Then, we fit the values of the threshold and exponents such that the data points collapse into a single curve. In principle, this method works also for the largest cluster density $G(q, N)$. Figure A.2 shows exemplary plots of the rescaled mean cluster size for model 1 networks with different parameters $(\alpha,\ \rho)$ using the relation (A.59). Data points collapse into a single curve, indicating that the scaling exponents and percolation threshold are reliable. A similar scaling behavior is valid for model 2 networks, which we show in Figure A.3 for two values of α and maximum segregation of nodes by $S = 10^3$ iterations of the previously described shuffling algorithm. Finally, we can use the hyperscaling relation[3] [59, 255]

$$\frac{D}{d} = \frac{1}{2}\left(1 + \frac{\gamma}{\nu d}\right) \tag{A.60}$$

to calculate the fractal dimension D/d from the exponents γ and νd.

For strongly assortative networks the relation (A.59) breaks down, which has been shown by Noh [203] and hence, we are obliged to use a different method to calculate the relevant parameters. Fortunately, the largest cluster mass $N \cdot G(q, N)$ still shows power-

[3] When the dimensionality d enters into a relation between the critical exponents, it is called a hyperscaling relation.

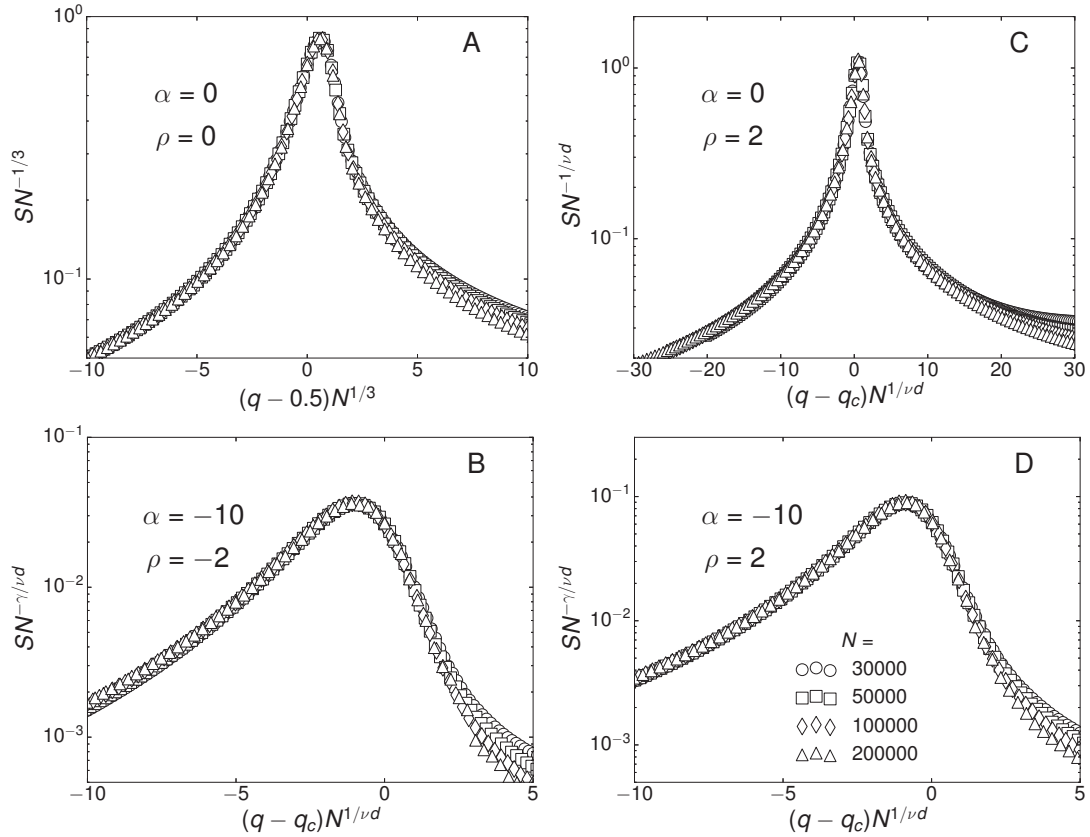

Figure A.2. Finite-size scaling of the mean cluster size of model 1 networks for different values of α and ρ. Data points collapse into a single curve. The numerical results for the percolation threshold and exponents are the following for each plot: (**A**) $q_c = 0.5$, $\frac{1}{\nu d} = 0.33$, $\frac{\gamma}{\nu d} = 0.33$; (**B**) $q_c = 0.82$, $\frac{1}{\nu d} = 0.35$, $\frac{\gamma}{\nu d} = 0.87$; (**C**) $q_c = 0.55$, $\frac{1}{\nu d} = 0.33$, $\frac{\gamma}{\nu d} = 0.33$; and (D) $q_c = 0.96$, $\frac{1}{\nu d} = 0.35$, $\frac{\gamma}{\nu d} = 0.85$. This figure has been modified from [229].

law scaling for $q \leq q_c$ [203]. We use this property to estimate the critical transition point q_c as follows: The largest cluster mass $N \cdot G(q, N)$ is plotted as a function of N for successively smaller values of q. Then, q_c is chosen to be the largest q-value for which a power-law dependency emerges. Power-law scaling is indicated by a linear behavior in the log-log plot, which is shown in Figure A.4 for two exemplary assortative model 1 networks with $\alpha = 0$ and $\alpha = -3$.

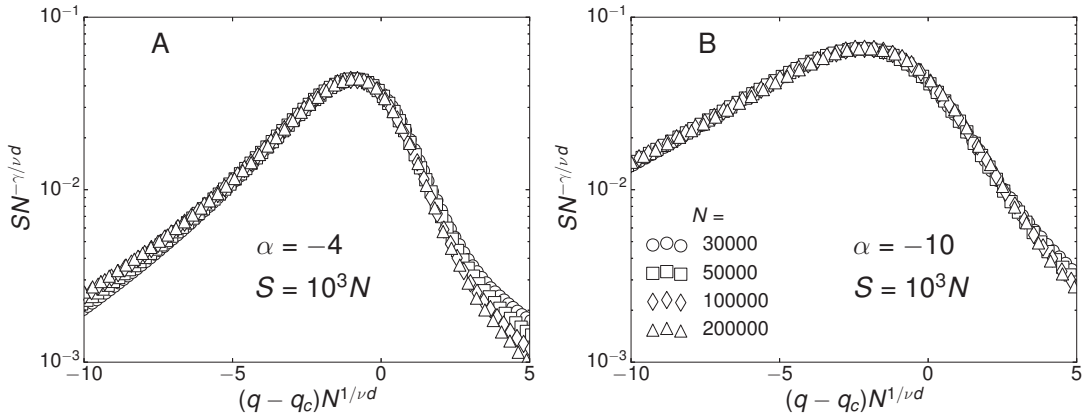

Figure A.3. Finite-size scaling of the mean cluster size of model 2 networks for different values of α and maximum spatial segregation of nodes by $S = 10^3 N$ iterations of the shuffling algorithm. Data points collapse into a single curve. The numerical results for the percolation threshold and exponents are the following for each plot: (**A**) $q_c = 0.85$, $\frac{1}{\nu d} = 0.33$, $\frac{\gamma}{\nu d} = 0.83$; (**B**) $q_c = 1.19$, $\frac{1}{\nu d} = 0.35$, $\frac{\gamma}{\nu d} = 0.88$. This figure has been modified from [229].

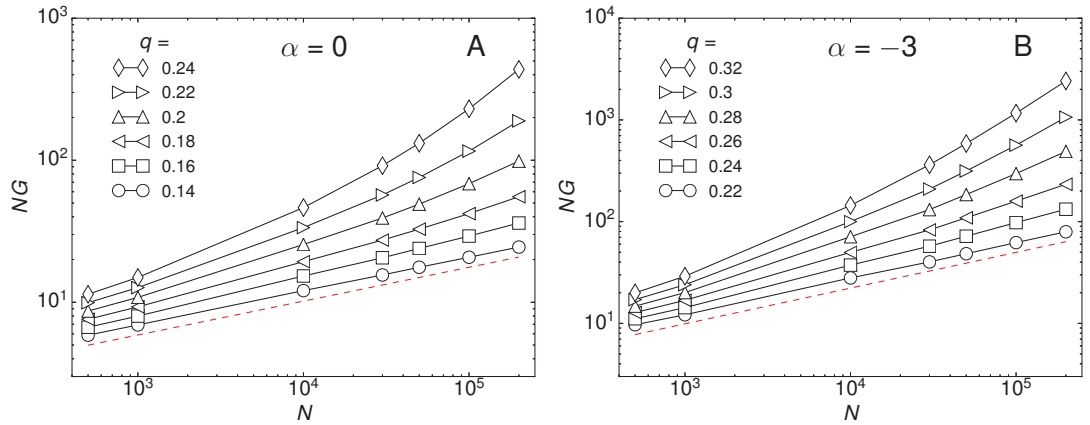

Figure A.4. Scaling of the largest cluster mass $N \cdot G$ at different q for two assortative model 1 networks with $\rho = -2$ and different α. The red dashed lines are guides for the eyes. The numerical results for the percolation threshold and fractal dimension are the following for each plot: (**A**) $q_c = 0.14$, $\frac{D}{d} = 0.95$; (**B**) $q_c = 0.24$, $\frac{D}{d} = 0.88$. This figure has been modified from [229].

Acknowledgement

Foremost, I want to thank my supervisor Sten Rüdiger for his guidance, encouragement and immense support. His ideas have laid the foundation of this thesis, and he has been always open-minded to my own concepts and approaches that we developed together in frequent and intimate discussions.

Within my study, I had the opportunity to spend six months in the experimental neuroscience lab of my co-supervisor Alexandre Kihara in Santo André. I am grateful for his caring attitude that helped me to quickly establish a fruitful collaboration and also for his great many ideas and new concepts of how to interleave theoretical and experimental approaches. It was a pleasure to work with several of the lab members, and I want to give special thanks to Erika Reime-Kinjo, Guilherme Higa, Pedro Royero, Lais Walter, and Cristina Moreira for their support.

For the most part I conducted my study at the Humboldt-University of Berlin within a great working environment. I thank Igor Sokolov for fruitful discussions on network-theoretical aspects and for reviewing our common manuscripts. I owe a great debt of gratitude to David Hansmann for being the point of call for any problems and for doing a great job in organizing the research program. Furthermore, I want to thank my colleque Martin Rückl for sharing his expertise in programming and his thoughts on how to solve the multitude of small issues that typically arise within a study. Also, a thank you to Malte Kähne, Justus Kromer, Till Rohrmann, and Jakob Mainert for offering excellent feedback on parts of this thesis. And to you, Katja Schäfer, much love and deep appreciation for keeping me level-headed during the stressful periods - and for the beautiful drawings you made for my thesis.

Finally, my parents, Beate and Claus Schmeltzer, deserve to receive my deepest gratitude and love for everything. You made me into who I am.

Bibliography

[1] L. Abbott and W. G. Regehr. Synaptic computation. *Nature*, 431(7010):796–803, 2004.

[2] L. Abbott and C. van Vreeswijk. Asynchronous states in networks of pulse-coupled oscillators. *Physical Review E*, 48(2):1483, 1993.

[3] S. Achard, R. Salvador, B. Whitcher, J. Suckling, and E. Bullmore. A resilient, low-frequency, small-world human brain functional network with highly connected association cortical hubs. *The Journal of Neuroscience*, 26(1):63–72, 2006.

[4] E. D. Adrian. The impulses produced by sensory nerve endings. *The Journal of Physiology*, 61(1):49–72, 1926.

[5] E. D. Adrian. *The basis of sensation.* WW Norton & Co, 1928.

[6] E. Agliari, A. Annibale, A. Barra, A. C. C. Coolen, and D. Tantari. Immune networks: multi-tasking capabilities at medium load. *Journal of Physics A: Mathematical and Theoretical*, 46(33):335101, 2013.

[7] R. Albert and A.-L. Barabási. Statistical mechanics of complex networks. *Reviews of Modern Physics*, 74(1):47, 2002.

[8] G. Alexanderson. About the cover: Euler and Königsberg's bridges: A historical view. *Bulletin of the American Mathematical Society*, 43(4):567–573, 2006.

[9] J. I. Alvarez-Hamelin, L. Dall'Asta, A. Barrat, and A. Vespignani. Large scale networks fingerprinting and visualization using the k-core decomposition. In *Advances in Neural Information Processing Systems*, pages 41–50, 2005.

[10] S.-i. Amari. A method of statistical neurodynamics. *Kybernetik*, 14(4):201–215, 1974.

[11] H. Amini. Bootstrap percolation in living neural networks. *Journal of Statistical Physics*, 141:459–475, 2010.

[12] D. J. Amit and N. Brunel. Model of global spontaneous activity and local structured activity during delay periods in the cerebral cortex. *Cerebral Cortex*, 7(3):237–252, 1997.

[13] A. Arenas, A. Díaz-Guilera, J. Kurths, Y. Moreno, and C. Zhou. Synchronization in complex networks. *Physics Reports*, 469(3):93–153, 2008.

[14] B. B. Averbeck, P. E. Latham, and A. Pouget. Neural correlations, population coding and computation. *Nature Reviews Neuroscience*, 7(5):358–366, 2006.

[15] S. B. Babu, C. Schmeltzer, and H. Stark. Swimming at low reynolds number: From sheets to the african trypanosome. In *Nature-Inspired Fluid Mechanics*, pages 25–41. Springer, 2012.

[16] J. Badham and R. Stocker. A Spatial Approach to Network Generation for Three Properties: Degree Distribution, Clustering Coefficient and Degree Assortativity. *Journal of Artificial Societies and Social Simulation*, 13(1):11, 2010.

[17] J. Baladron, D. Fasoli, O. Faugeras, J. Touboul, et al. Mean-field description and propagation of chaos in networks of hodgkin-huxley and fitzhugh-nagumo neurons. *The Journal of Mathematical Neuroscience*, 2(1):10, 2012.

[18] A.-L. Barabási and R. Albert. Emergence of scaling in random networks. *Science*, 286(5439):509–512, 1999.

[19] A.-L. Barabási, R. Albert, and H. Jeong. Scale-free characteristics of random networks: the topology of the world-wide web. *Physica A: Statistical Mechanics and its Applications*, 281(1):69–77, 2000.

[20] A.-L. Barabási et al. Scale-free networks: a decade and beyond. *Science*, 325(5939):412, 2009.

[21] A.-L. Barabâsi, H. Jeong, Z. Néda, E. Ravasz, A. Schubert, and T. Vicsek. Evolution of the social network of scientific collaborations. *Physica A: Statistical Mechanics and its Applications*, 311(3):590–614, 2002.

[22] H. Barlow. Single units and sensation: A neuron doctrine for perceptual psychology? *Perception*, 1:371–394, 1972.

[23] A. Barrat, M. Barthélemy, and A. Vespignani. The effects of spatial constraints on the evolution of weighted complex networks. *Journal of Statistical Mechanics: Theory and Experiment*, 2005:P05003, 2005.

[24] M. Barthélemy. Crossover from scale-free to spatial networks. *Europhysics Letters*, 63(6):915, 2003.

[25] M. Barthélemy. Spatial networks. *Physics Reports*, 499(1):1–101, 2011.

[26] D. S. Bassett and E. Bullmore. Small-world brain networks. *The Neuroscientist*, 12(6):512–523, 2006.

[27] G. Baxter, S. Dorogovtsev, A. Goltsev, and J. Mendes. Bootstrap percolation on complex networks. *Physical Review E*, 82(1):011103, 2010.

[28] J. M. Beggs. The criticality hypothesis: how local cortical networks might optimize information processing. *Philosophical Transactions of the Royal Society A: Mathematical, Physical and Engineering Sciences*, 366(1864):329–343, 2008.

[29] J. M. Beggs and D. Plenz. Neuronal avalanches in neocortical circuits. *The Journal of Neuroscience*, 23(35):11167–11177, 2003.

[30] J. M. Beggs and N. Timme. Being critical of criticality in the brain. *Frontiers in Physiology*, 3, 2012.

[31] M. G. Bell and Y. Iida. *Transportation network analysis*. Wiley, 1997.

[32] D. Ben-Avraham and S. Havlin. Diffusion on percolation clusters at criticality. *Journal of Physics A: Mathematical and General*, 15(12):L691, 1982.

[33] R. Ben-Yishai, R. L. Bar-Or, and H. Sompolinsky. Theory of orientation tuning in visual cortex. *Proceedings of the National Academy of Sciences*, 92(9):3844–3848, 1995.

[34] M. Benayoun, J. D. Cowan, W. van Drongelen, and E. Wallace. Avalanches in a stochastic model of spiking neurons. *PLoS Computational Biology*, 6(7):e1000846, 2010.

[35] M. Bennett, L. Barrio, T. Bargiello, D. Spray, E. Hertzberg, and J. Saez. Gap junctions: new tools, new answers, new questions. *Neuron*, 6(3):305–320, 1991.

[36] L. Bettencourt, G. Stephens, M. Ham, and G. Gross. Functional structure of cortical neuronal networks grown in vitro. *Physical Review E*, 75(2):021915, 2007.

[37] R. L. Beurle. Properties of a mass of cells capable of regenerating pulses. *Philosophical Transactions of the Royal Society B: Biological Sciences*, 240(669):55–94, 1956.

[38] G. Bianconi, P. Pin, and M. Marsili. Assessing the relevance of node features for network structure. *Proceedings of the National Academy of Sciences*, 106(28):11433–11438, 2009.

[39] S. Boccaletti, V. Latora, Y. Moreno, M. Chavez, and D.-U. Hwang. Complex networks: Structure and dynamics. *Physics Reports*, 424(4):175–308, 2006.

[40] M. Boguñá, R. Pastor-Satorras, and A. Vespignani. Absence of Epidemic Threshold in Scale-Free Networks with Degree Correlations. *Physical Review Letters*, 90:028701, Jan 2003.

[41] B. Bollobás. *Random graphs*. Springer, 1998.

[42] V. Braitenberg and A. Schüz. *Anatomy of the cortex: Statistics and geometry*. Springer, 1991.

[43] M. Brecht, A. Roth, and B. Sakmann. Dynamic receptive fields of reconstructed pyramidal cells in layers 3 and 2 of rat somatosensory barrel cortex. *The Journal of Physiology*, 553(1):243–265, 2003.

[44] M. Brede and S. Sinha. Assortative mixing by degree makes a network more unstable. *ArXiv Preprint Cond-Mat/0507710*, 2005.

[45] I. Breskin, J. Soriano, E. Moses, and T. Tlusty. Percolation in living neural networks. *Physical Review Letters*, 97:188102, Oct 2006.

[46] S. L. Bressler. Understanding cognition through large-scale cortical networks. *Current Directions in Psychological Science*, 11(2):58–61, 2002.

[47] P. Bressloff. Mean-field theory of globally coupled integrate-and-fire neural oscillators with dynamic synapses. *Physical Review E*, 60(2):2160, 1999.

[48] P. C. Bressloff. Stochastic neural field theory and the system-size expansion. *SIAM Journal on Applied Mathematics*, 70(5):1488–1521, 2009.

[49] R. Brette, M. Rudolph, T. Carnevale, M. Hines, D. Beeman, J. M. Bower, M. Diesmann, A. Morrison, P. H. Goodman, F. C. Harris Jr, et al. Simulation of networks of spiking neurons: a review of tools and strategies. *Journal of Computational Neuroscience*, 23(3):349–398, 2007.

[50] S. R. Broadbent and J. M. Hammersley. Percolation processes. In *Mathematical Proceedings of the Cambridge Philosophical Society*, volume 53, pages 629–641. Cambridge University Press, 1957.

[51] D. Brockmann, L. Hufnagel, and T. Geisel. The scaling laws of human travel. *Nature*, 439(7075):462–465, 2006.

[52] K. Brodmann. *Vergleichende Lokalisationslehre der Großhirnrinde in ihren Prinzipien dargestellt auf Grund des Zellenbaues*. Barth, 1909.

[53] N. Brunel. Dynamics of sparsely connected networks of excitatory and inhibitory spiking neurons. *Journal of Computational Neuroscience*, 8(3):183–208, 2000.

[54] N. Brunel and M. C. Van Rossum. Lapicque,Äôs 1907 paper: from frogs to integrate-and-fire. *Biological Cybernetics*, 97(5-6):337–339, 2007.

[55] M. A. Buice and J. D. Cowan. Field-theoretic approach to fluctuation effects in neural networks. *Physical Review E*, 75(5):051919, 2007.

[56] E. Bullmore and O. Sporns. Complex brain networks: graph theoretical analysis of structural and functional systems. *Nature Reviews Neuroscience*, 10(3):186–198, 2009.

[57] E. Bullmore and O. Sporns. The economy of brain network organization. *Nature Reviews Neuroscience*, 13(5):336–349, 2012.

[58] A. Bunde and W. Dieterich. Percolation in composites. *Journal of Electroceramics*, 5(2):81–92, 2000.

[59] A. Bunde and S. Havlin. *Fractals and disordered systems*. Springer, 1991.

[60] A. N. Burkitt. A review of the integrate-and-fire neuron model: Ii. inhomogeneous synaptic input and network properties. *Biological Cybernetics*, 95(2):97–112, 2006.

[61] D. A. Butts, C. Weng, J. Jin, C.-I. Yeh, N. A. Lesica, J.-M. Alonso, and G. B. Stanley. Temporal precision in the neural code and the timescales of natural vision. *Nature*, 449(7158):92–95, 2007.

[62] G. Buzsáki. Large-scale recording of neuronal ensembles. *Nature Neuroscience*, 7(5):446–451, 2004.

[63] G. Buzsáki and A. Draguhn. Neuronal oscillations in cortical networks. *Science*, 304(5679):1926–1929, 2004.

[64] G. Buzsáki and K. Mizuseki. The log-dynamic brain: how skewed distributions affect network operations. *Nature Reviews Neuroscience*, 15(4):264–278, 2014.

[65] D. Cai, L. Tao, M. Shelley, and D. W. McLaughlin. An effective kinetic representation of fluctuation-driven neuronal networks with application to simple and complex cells in visual cortex. *Proceedings of the National Academy of Sciences of the United States of America*, 101(20):7757–7762, 2004.

[66] D. Cai, L. Tao, M. S. Shkarayev, A. V. Rangan, D. W. McLaughlin, and G. Kovacic. The role of fluctuations in coarse-grained descriptions of neuronal networks. *Communications in Mathematical Sciences*, 10:307–354, 2012.

[67] S. R. Cajal. Instituto Cajal, Madrid, 1899.

[68] D. S. Callaway, M. E. Newman, S. H. Strogatz, and D. J. Watts. Network robustness and fragility: Percolation on random graphs. *Physical Review Letters*, 85(25):5468, 2000.

[69] X. Campi, H. Krivine, and N. Sator. Percolation line of self-bound clusters in supercritical fluids. *Physica A: Statistical Mechanics and its Applications*, 296(1):24–30, 2001.

[70] X. Campi, H. Krivine, N. Sator, and E. Plagnol. Analyzing fragmentation of simple fluids with percolation theory. *The European Physical Journal D-Atomic, Molecular, Optical and Plasma Physics*, 11(2):233–238, 2000.

[71] R. Capocelli and L. Ricciardi. Diffusion approximation and first passage time problem for a model neuron. *Kybernetik*, 8(6):214–223, 1971.

[72] H. Câteau and A. D. Reyes. Relation between single neuron and population spiking statistics and effects on network activity. *Physical Review Letters*, 96(5):058101, 2006.

[73] M. J. Chacron, B. Lindner, and A. Longtin. Noise shaping by interval correlations increases information transfer. *Physical Review Letters*, 92(8):080601, 2004.

[74] M. J. Chacron, A. Longtin, and L. Maler. Negative interspike interval correlations increase the neuronal capacity for encoding time-dependent stimuli. *The Journal of Neuroscience*, 21(14):5328–5343, 2001.

[75] D. Chialvo. Critical brain networks. *Physica A: Statistical Mechanics and its Applications*, 340(4):756–765, 2004.

[76] D. B. Chklovskii, T. Schikorski, and C. F. Stevens. Wiring optimization in cortical circuits. *Neuron*, 34(3):341–347, 2002.

[77] R. Christopher deCharms and M. M. Merzenich. Primary cortical representation of sounds by the coordination of action-potential timing. *Nature*, 381:13, 1996.

[78] F. R. Chung. *Spectral graph theory*, volume 92. American Mathematical Society, 1997.

[79] M. M. Churchland and L. Abbott. Two layers of neural variability. *Nature Neuroscience*, 15(11):1472–1474, 2012.

[80] A. Clauset, C. R. Shalizi, and M. E. Newman. Power-law distributions in empirical data. *SIAM Review*, 51(4):661–703, 2009.

[81] O. Cohen, A. Keselman, E. Moses, M. R. Martínez, J. Soriano, and T. Tlusty. Quorum percolation in living neural networks. *Europhysics Letters*, 89(1):18008, 2010.

[82] R. Cohen, D. Ben-Avraham, and S. Havlin. Percolation critical exponents in scale-free networks. *Physical Review E*, 66(3):036113, 2002.

[83] R. Cohen, K. Erez, D. Ben-Avraham, and S. Havlin. Resilience of the internet to random breakdowns. *Physical Review Letters*, 85(21):4626, 2000.

[84] L. Daqing, K. Kosmidis, A. Bunde, and S. Havlin. Dimension of spatially embedded networks. *Nature Physics*, 7(6):481–484, 2011.

[85] P. Dayan and L. F. Abbott. *Theoretical Neuroscience: Computational and Mathematical Modeling of Neural Systems*. The MIT Press, 2005.

[86] S. de Franciscis, S. Johnson, and J. J. Torres. Enhancing neural-network performance via assortativity. *Physical Review E*, 83(3):036114, 2011.

[87] D. de Santos-Sierra, I. Sendiña-Nadal, I. Leyva, J. A. Almendral, S. Anava, A. Ayali, D. Papo, and S. Boccaletti. Emergence of small-world anatomical networks in self-organizing clustered neuronal cultures. *PloS One*, 9(1):e85828, 2014.

[88] I. Dean, N. S. Harper, and D. McAlpine. Neural population coding of sound level adapts to stimulus statistics. *Nature Neuroscience*, 8(12):1684–1689, 2005.

[89] G. Deco, V. K. Jirsa, P. A. Robinson, M. Breakspear, and K. Friston. The dynamic brain: from spiking neurons to neural masses and cortical fields. *PLoS Computational Biology*, 4(8):e1000092, 2008.

[90] R. Dermietzel and D. C. Spray. Gap junctions in the brain: where, what type, how many and why? *Trends in Neurosciences*, 16(5):186–192, 1993.

[91] S. N. Dorogovtsev, A. V. Goltsev, and J. F. F. Mendes. K-core organization of complex networks. *Physical Review Letters*, 96(4):040601, 2006.

[92] S. N. Dorogovtsev and J. F. Mendes. Evolution of networks. *Advances in Physics*, 51(4):1079–1187, 2002.

[93] R. J. Douglas and K. A. Martin. Recurrent neuronal circuits in the neocortex. *Current Biology*, 17(13):R496–R500, 2007.

[94] J. Downes, M. Hammond, D. Xydas, M. Spencer, V. Becerra, K. Warwick, B. Whalley, and S. Nasuto. Emergence of a Small-World Functional Network in Cultured Neurons. *PLoS Computational Biology*, 8(5):e1002522, 2012.

[95] J.-P. Eckmann, O. Feinerman, L. Gruendlinger, E. Moses, J. Soriano, and T. Tlusty. The physics of living neural networks. *Physics Reports*, 449(1):54–76, 2007.

[96] G. M. Edelman and G. Tononi. *A universe of consciousness: How matter becomes imagination*. Basic Books, 2000.

[97] V. M. Eguiluz, D. R. Chialvo, G. A. Cecchi, M. Baliki, and A. V. Apkarian. Scale-free brain functional networks. *Physical Review Letters*, 94(1):018102, 2005.

[98] P. Erdős and A. Rényi. On random graphs. *Publicationes Mathematicae Debrecen*, 6:290–297, 1959.

[99] P. Erdős and A. Rényi. On the evolution of random graphs. *Publ. Math. Inst. Hungar. Acad. Sci*, 5:17–61, 1960.

[100] J. W. Essam. Percolation theory. *Reports on Progress in Physics*, 43(7):833, 1980.

[101] M. Faloutsos, P. Faloutsos, and C. Faloutsos. On power-law relationships of the internet topology. In *ACM SIGCOMM Computer Communication Review*, volume 29, pages 251–262. ACM, 1999.

[102] D. J. Felleman and D. C. Van Essen. Distributed hierarchical processing in the primate cerebral cortex. *Cerebral Cortex*, 1(1):1–47, 1991.

[103] S. Finger. *Origins of neuroscience: a history of explorations into brain function*. Oxford University Press, 2001.

[104] E. Fino and R. Yuste. Dense inhibitory connectivity in neocortex. *Neuron*, 69(6):1188–1203, 2011.

[105] R. FitzHugh. Impulses and physiological states in theoretical models of nerve membrane. *Biophysical Journal*, 1(6):445, 1961.

[106] P. J. Flory. Molecular size distribution in three dimensional polymers. i. gelation. *Journal of the American Chemical Society*, 63(11):3083–3090, 1941.

[107] L. Franco, E. T. Rolls, N. C. Aggelopoulos, and J. M. Jerez. Neuronal selectivity, population sparseness, and ergodicity in the inferior temporal visual cortex. *Biological Cybernetics*, 96(6):547–560, 2007.

[108] L. C. Freeman. Centrality in social networks conceptual clarification. *Social Networks*, 1(3):215–239, 1979.

[109] P. Fries. A mechanism for cognitive dynamics: neuronal communication through neuronal coherence. *Trends in Cognitive Sciences*, 9(10):474–480, 2005.

[110] P. Fries. Neuronal gamma-band synchronization as a fundamental process in cortical computation. *Annual Review of Neuroscience*, 32:209–224, 2009.

[111] P. Fries, J. H. Reynolds, A. E. Rorie, and R. Desimone. Modulation of oscillatory neuronal synchronization by selective visual attention. *Science*, 291(5508):1560–1563, 2001.

[112] K. J. Friston. Functional and effective connectivity in neuroimaging: a synthesis. *Human Brain Mapping*, 2(1-2):56–78, 1994.

[113] K. J. Friston. Modalities, modes, and models in functional neuroimaging. *Science*, 326(5951):399–403, 2009.

[114] T. Gabay, E. Jakobs, E. Ben-Jacob, and Y. Hanein. Engineered self-organization of neural networks using carbon nanotube clusters. *Physica A: Statistical Mechanics and its Applications*, 350(2):611–621, 2005.

[115] F. J. Gall. *On the functions of the brain and of each of its parts: with observations on the possibility of determining the instincts, propensities, and talents, or the moral and intellectual dispositions of men and animals, by the configuration of the brain and head*, volume 1. Marsh, Capen & Lyon, 1835.

[116] S. Gasparini and J. C. Magee. State-dependent dendritic computation in hippocampal ca1 pyramidal neurons. *The Journal of Neuroscience*, 26(7):2088–2100, 2006.

[117] A. P. Georgopoulos, A. B. Schwartz, and R. E. Kettner. Neuronal population coding of movement direction. *Science*, 233(4771):1416–1419, 1986.

[118] W. Gerstner and W. M. Kistler. *Spiking neuron models: Single neurons, populations, plasticity*. Cambridge University Press, 2002.

[119] W. Gerstner and J. L. van Hemmen. Associative memory in a network of'spiking'neurons. *Network: Computation in Neural Systems*, 3(2):139–164, 1992.

[120] J. P. Gleeson and S. Melnik. Analytical results for bond percolation and k-core sizes on clustered networks. *Physical Review E*, 80(4):046121, 2009.

[121] B. Gluss. A model for neuron firing with exponential decay of potential resulting in diffusion equations for probability density. *The Bulletin of Mathematical Biophysics*, 29(2):233–243, 1967.

[122] J. R. Goldman. Stochastic point processes: Limit theorems. *The Annals of Mathematical Statistics*, 38(3):771–779, 1967.

[123] A. Goltsev, S. Dorogovtsev, and J. Mendes. Percolation on correlated networks. *Physical Review E*, 78(5):051105, 2008.

[124] M. B. Goodman, D. H. Hall, L. Avery, and S. R. Lockery. Active currents regulate sensitivity and dynamic range in c. elegans neurons. *Neuron*, 20(4):763–772, 1998.

[125] C. M. Gray and W. Singer. Stimulus-specific neuronal oscillations in orientation columns of cat visual cortex. *Proceedings of the National Academy of Sciences*, 86(5):1698–1702, 1989.

[126] P. Hagmann, L. Cammoun, X. Gigandet, R. Meuli, C. J. Honey, V. J. Wedeen, and O. Sporns. Mapping the structural core of human cerebral cortex. *PLoS Biology*, 6(7):e159, 2008.

[127] C. Haldeman and J. M. Beggs. Critical branching captures activity in living neural networks and maximizes the number of metastable states. *Physical Review Letters*, 94(5):58101, 2005.

[128] J. Hammersley. Comparison of atom and bond percolation processes. *Journal of Mathematical Physics*, 2(5):728–733, 1961.

[129] J. Hammersley and D. Welsh. Percolation theory and its ramifications. *Contemporary Physics*, 21(6):593–605, 1980.

[130] T. E. Harris. *The theory of branching processes*. Courier Dover Publications, 2002.

[131] Y. Hayashi. A Review of Recent Studies of Geographical Scale-Free Networks. *IPSJ Digital Courier*, 2:155–164, 2006.

[132] Y. He, Z. J. Chen, and A. C. Evans. Small-world anatomical networks in the human brain revealed by cortical thickness from mri. *Cerebral Cortex*, 17(10):2407–2419, 2007.

[133] B. Hellwig. A quantitative analysis of the local connectivity between pyramidal neurons in layers 2/3 of the rat visual cortex. *Biological Cybernetics*, 82(2):111–121, 2000.

[134] M. H. Hennig, C. Adams, D. Willshaw, and E. Sernagor. Early-stage waves in the retinal network emerge close to a critical state transition between local and global functional connectivity. *The Journal of Neuroscience*, 29(4):1077–1086, 2009.

[135] S. Hill and G. Tononi. Modeling sleep and wakefulness in the thalamocortical system. *Journal of Neurophysiology*, 93(3):1671–1698, 2005.

[136] A. L. Hodgkin and A. F. Huxley. A quantitative description of membrane current and its application to conduction and excitation in nerve. *The Journal of Physiology*, 117(4):500–544, 1952.

[137] C. J. Honey, R. Kötter, M. Breakspear, and O. Sporns. Network structure of cerebral cortex shapes functional connectivity on multiple time scales. *Proceedings of the National Academy of Sciences*, 104(24):10240–10245, 2007.

[138] H. Hong, M. Ha, and H. Park. Finite-size scaling in complex networks. *Physical Review Letters*, 98(25):258701, 2007.

[139] J. J. Hopfield. Neural networks and physical systems with emergent collective computational abilities. *Proceedings of the National Academy of Sciences*, 79(8):2554–2558, 1982.

[140] J. J. Hopfield and D. W. Tank. "neural" computation of decisions in optimization problems. *Biological Cybernetics*, 52(3):141–152, 1985.

[141] B. Horwitz. The elusive concept of brain connectivity. *Neuroimage*, 19(2):466–470, 2003.

[142] A. R. Houweling, G. Doron, B. C. Voigt, L. J. Herfst, and M. Brecht. Nanostimulation: manipulation of single neuron activity by juxtacellular current injection. *Journal of Neurophysiology*, 103(3):1696–1704, 2010.

[143] T. Hromádka, M. R. DeWeese, and A. M. Zador. Sparse representation of sounds in the unanesthetized auditory cortex. *PLoS Biology*, 6(1):e16, 2008.

[144] J. Huxter, N. Burgess, and J. O'Keefe. Independent rate and temporal coding in hippocampal pyramidal cells. *Nature*, 425(6960):828–832, 2003.

[145] F. Iglói and L. Turban. First-and second-order phase transitions in scale-free networks. *Physical Review E*, 66(3):036140, 2002.

[146] E. M. Izhikevich. Which model to use for cortical spiking neurons? *IEEE Transactions on Neural Networks*, 15(5):1063–1070, 2004.

[147] E. M. Izhikevich and G. M. Edelman. Large-scale model of mammalian thalamocortical systems. *Proceedings of the National Academy of Sciences*, 105(9):3593–3598, 2008.

[148] E. M. Izhikevich et al. Simple model of spiking neurons. *IEEE Transactions on Neural Networks*, 14(6):1569–1572, 2003.

[149] A. L. Jacobs, G. Fridman, R. M. Douglas, N. M. Alam, P. E. Latham, G. T. Prusky, and S. Nirenberg. Ruling out and ruling in neural codes. *Proceedings of the National Academy of Sciences*, 106(14):5936–5941, 2009.

[150] V. K. Jirsa. Connectivity and dynamics of neural information processing. *Neuroinformatics*, 2(2):183–204, 2004.

[151] E. R. Kandel, J. H. Schwartz, T. M. Jessell, et al. *Principles of neural science*, volume 4. McGraw-Hill Medical, 2000.

[152] H. Kesten. *Percolation theory for mathematicians*. Springer, 1982.

[153] A. H. Kihara, L. Mantovani de Castro, M. A. Belmonte, C. Y. I. Yan, A. S. Moriscot, and D. E. Hamassaki. Expression of connexins 36, 43, and 45 during postnatal development of the mouse retina. *Journal of Neurobiology*, 66(13):1397–1410, 2006.

[154] O. Kinouchi and M. Copelli. Optimal dynamical range of excitable networks at criticality. *Nature Physics*, 2(5):348–351, 2006.

[155] B. W. Knight. Dynamics of encoding in a population of neurons. *The Journal of General Physiology*, 59(6):734–766, 1972.

[156] B. W. Knight. Dynamics of encoding in neuron populations: some general mathematical features. *Neural Computation*, 12(3):473–518, 2000.

[157] R. Kosinski and M. Zaremba. Dynamics of the model of the caenorhabditis elegans neural network. *Acta Physica Polonica Series B*, 38(6):2201, 2007.

[158] R. Kotter and F. T. Sommer. Global relationship between anatomical connectivity and activity propagation in the cerebral cortex. *Philosophical Transactions of the Royal Society B: Biological Sciences*, 355(1393):127–134, 2000.

[159] G. Kovačič, L. Tao, A. V. Rangan, and D. Cai. Fokker-planck description of conductance-based integrate-and-fire neuronal networks. *Physical Review E*, 80:021904, 2009.

[160] R. Lambiotte, V. Blondel, C. De Kerchove, E. Huens, C. Prieur, Z. Smoreda, and P. Van Dooren. Geographical dispersal of mobile communication networks. *Physica A: Statistical Mechanics and its Applications*, 387(21):5317–5325, 2008.

[161] L. Lapicque. Recherches quantitatives sur l,Äôexcitation électrique des nerfs traitée comme une polarisation. *J. Physiol. Pathol. Gen*, 9(1):620–635, 1907.

[162] V. Latora and M. Marchiori. Efficient behavior of small-world networks. *Physical Review Letters*, 87(19):198701, 2001.

[163] V. Latora and M. Marchiori. Is the boston subway a small-world network? *Physica A: Statistical Mechanics and its Applications*, 314(1):109–113, 2002.

[164] S. B. Laughlin. Energy as a constraint on the coding and processing of sensory information. *Current Opinion in Neurobiology*, 11(4):475–480, 2001.

[165] M. Lavzin, S. Rapoport, A. Polsky, L. Garion, and J. Schiller. Nonlinear dendritic processing determines angular tuning of barrel cortex neurons in vivo. *Nature*, 490(7420):397–401, 2012.

[166] C. Lee, W. H. Rohrer, D. L. Sparks, et al. Population coding of saccadic eye movements by neurons in the superior colliculus. *Nature*, 332(6162):357–360, 1988.

[167] L. Lee, L. M. Harrison, and A. Mechelli. A report of the functional connectivity workshop, dusseldorf 2002. *Neuroimage*, 19(2):457–465, 2003.

[168] M. Leone, A. Vázquez, A. Vespignani, and R. Zecchina. Ferromagnetic ordering in graphs with arbitrary degree distribution. *The European Physical Journal B-Condensed Matter and Complex Systems*, 28(2):191–197, 2002.

[169] D. Li, G. Li, K. Kosmidis, H. Stanley, A. Bunde, and S. Havlin. Percolation of spatially constraint networks. *Europhysics Letters*, 93:68004, 2011.

[170] Y. Li, Y. Liu, J. Li, W. Qin, K. Li, C. Yu, and T. Jiang. Brain anatomical network and intelligence. *PLoS Computational Biology*, 5(5):e1000395, 2009.

[171] D. Liben-Nowell, J. Novak, R. Kumar, P. Raghavan, and A. Tomkins. Geographic routing in social networks. *Proceedings of the National Academy of Sciences of the United States of America*, 102(33):11623, 2005.

[172] B. Lindner. Superposition of many independent spike trains is generally not a poisson process. *Physical Review E*, 73(2):022901, 2006.

[173] B. Lindner, M. J. Chacron, and A. Longtin. Integrate-and-fire neurons with threshold noise: A tractable model of how interspike interval correlations affect neuronal signal transmission. *Physical Review E*, 72(2):021911, 2005.

[174] B. Lindner, J. Garcıa-Ojalvo, A. Neiman, and L. Schimansky-Geier. Effects of noise in excitable systems. *Physics Reports*, 392(6):321–424, 2004.

[175] R. P. Lippmann. An introduction to computing with neural nets. *ASSP Magazine, IEEE*, 4(2):4–22, 1987.

[176] A. Litwin-Kumar and B. Doiron. Slow dynamics and high variability in balanced cortical networks with clustered connections. *Nature Neuroscience*, 15(11):1498–1505, 2012.

[177] Z. F. Mainen and T. J. Sejnowski. Reliability of spike timing in neocortical neurons. *Science*, 268(5216):1503–1506, 1995.

[178] B. B. Mandelbrot. *Fractals: form, chance and dimension*. Freeman, San Francisco, 1977.

[179] S. S. Manna and P. Sen. Modulated scale-free network in euclidean space. *Physical Review E*, 66(6):066114, 2002.

[180] E. Marder and J.-M. Goaillard. Variability, compensation and homeostasis in neuron and network function. *Nature Reviews Neuroscience*, 7(7):563–574, 2006.

[181] T. W. Margrie, M. Brecht, and B. Sakmann. In vivo, low-resistance, whole-cell recordings from neurons in the anaesthetized and awake mammalian brain. *Pflügers Archiv*, 444(4):491–498, 2002.

[182] S. Maslov, M. Paczuski, and P. Bak. Avalanches and 1 f noise in evolution and growth models. *Physical Review Letters*, 73(16):2162, 1994.

[183] O. Mason and M. Verwoerd. Graph theory and networks in biology. *Systems Biology, IET*, 1(2):89–119, 2007.

[184] J. H. Maunsell and D. C. Van Essen. Functional properties of neurons in middle temporal visual area of the macaque monkey. ii. binocular interactions and sensitivity to binocular disparity. *Journal of Neurophysiology*, 49(5):1148–1167, 1983.

[185] A. R. McIntosh. Towards a network theory of cognition. *Neural Networks*, 13(8):861–870, 2000.

[186] D. McLaughlin, R. Shapley, M. Shelley, and D. Wielaard. A neuronal network model of macaque primary visual cortex (v1): Orientation selectivity and dynamics in the input layer 4cα. *Proceedings of the National Academy of Sciences*, 97(14):8087–8092, 2000.

[187] J. Mejias and A. Longtin. Optimal heterogeneity for coding in spiking neural networks. *Physical Review Letters*, 108(22):228102, 2012.

[188] R. K. Merton. *Social theory and social structure*. Simon and Schuster, 1968.

[189] S. Milgram. The small world problem. *Psychology Today*, 2(1):60–67, 1967.

[190] R. Milo, N. Kashtan, S. Itzkovitz, M. Newman, and U. Alon. On the uniform generation of random graphs with prescribed degree sequences. *ArXiv Preprint Cond-Mat/0312028*, 2003.

[191] G. Mitchison. Neuronal branching patterns and the economy of cortical wiring. *Proceedings of the Royal Society of London. Series B: Biological Sciences*, 245(1313):151–158, 1991.

[192] M. Molloy and B. Reed. A critical point for random graphs with a given degree sequence. *Random Structures & Algorithms*, 6(2-3):161–180, 1995.

[193] M. Molloy and B. Reed. The size of the giant component of a random graph with a given degree sequence. *Combinatorics, Probability and Computing*, 7(03):295–305, 1998.

[194] C. Morris and H. Lecar. Voltage oscillations in the barnacle giant muscle fiber. *Biophysical Journal*, 35(1):193, 1981.

[195] K. A. Newhall, G. Kovačič, P. R. Kramer, and D. Cai. Cascade-induced synchrony in stochastically driven neuronal networks. *Physical Review E*, 82(4):041903, 2010.

[196] M. Newman. *Networks: an introduction*. Oxford University Press, 2010.

[197] M. E. Newman. Assortative mixing in networks. *Physical Review Letters*, 89(20):208701, 2002.

[198] M. E. Newman. Mixing patterns in networks. *Physical Review E*, 67(2):026126, 2003.

[199] M. E. Newman. The structure and function of complex networks. *SIAM Review*, 45(2):167–256, 2003.

[200] M. E. Newman, S. H. Strogatz, and D. J. Watts. Random graphs with arbitrary degree distributions and their applications. *Physical Review E*, 64(2):026118, 2001.

[201] M. E. J. Newman. Mixing patterns in networks. *Physical Review E*, 67:026126, Feb 2003.

[202] W. Nicola and S. A. Campbell. Bifurcations of large networks of two-dimensional integrate and fire neurons. *Journal of Computational Neuroscience*, 35(1):87–108, 2013.

[203] J. D. Noh. Percolation transition in networks with degree-degree correlation. *Physical Review E*, 76:026116, Aug 2007.

[204] D. Q. Nykamp and D. Tranchina. A population density approach that facilitates large-scale modeling of neural networks: Analysis and an application to orientation tuning. *Journal of Computational Neuroscience*, 8(1):19–50, 2000.

[205] A. Omurtag, B. W. Knight, and L. Sirovich. On the simulation of large populations of neurons. *Journal of Computational Neuroscience*, 8(1):51–63, 2000.

[206] J. G. Orlandi, J. Soriano, E. Alvarez-Lacalle, S. Teller, and J. Casademunt. Noise focusing and the emergence of coherent activity in neuronal cultures. *Nature Physics*, 9(9):582–590, 2013.

[207] S. Pajevic and D. Plenz. Efficient network reconstruction from dynamical cascades identifies small-world topology of neuronal avalanches. *PloS Computational Biology*, 5(1):e1000271, 2009.

[208] R. Pandey, D. Stauffer, A. Margolina, and J. Zabolitzky. Diffusion on random systems above, below, and at their percolation threshold in two and three dimensions. *Journal of Statistical Physics*, 34(3-4):427–450, 1984.

[209] V. Pernice, M. Deger, S. Cardanobile, and S. Rotter. The relevance of network micro-structure for neural dynamics. *Frontiers in Computational Neuroscience*, 7, 2013.

[210] A. G. Phillips. Brain reward circuitry: a case for separate systems. *Brain Research Bulletin*, 12(2):195–201, 1984.

[211] M. Piraveenan, M. Prokopenko, and A. Zomaya. Assortative mixing in directed biological networks. *IEEE/ACM Transactions on Computational Biology and Bioinformatics (TCBB)*, 9(1):66–78, 2012.

[212] G. Pola, A. Thiele, K. Hoffmann, and S. Panzeri. An exact method to quantify the information transmitted by different mechanisms of correlational coding. *Network-Computation in Neural Systems*, 14(1):35–60, 2003.

[213] A. Polsky, B. Mel, and J. Schiller. Encoding and decoding bursts by nmda spikes in basal dendrites of layer 5 pyramidal neurons. *The Journal of Neuroscience*, 29(38):11891–11903, 2009.

[214] A. Pouget, P. Dayan, and R. Zemel. Information processing with population codes. *Nature Reviews Neuroscience*, 1(2):125–132, 2000.

[215] A. A. Prinz, D. Bucher, and E. Marder. Similar network activity from disparate circuit parameters. *Nature Neuroscience*, 7(12):1345–1352, 2004.

[216] M. I. Rabinovich, P. Varona, A. I. Selverston, and H. D. Abarbanel. Dynamical principles in neuroscience. *Reviews of Modern Physics*, 78(4):1213, 2006.

[217] T. Ray and N. Jan. Anomalous approach to the self-organized critical state in a model for life at the edge of chaos. *Physical Review Letters*, 72(25):4045, 1994.

[218] L. Ricciardi. Diffusion approximation for a multi-input model neuron. *Biological Cybernetics*, 24(4):237–240, 1976.

[219] L. M. Ricciardi and L. Sacerdote. The ornstein-uhlenbeck process as a model for neuronal activity. *Biological Cybernetics*, 35(1):1–9, 1979.

[220] F. Rieke, D. Warland, R. Deruytervansteveninck, and W. Bialek. *Spikes: Exploring the Neural Code (Computational Neuroscience)*. The MIT Press, London, 1999.

[221] H. Risken. *The Fokker-Planck Equation*. Springer, 1984.

[222] E. M. Rogers and D. L. Kincaid. *Communication networks: Toward a new paradigm for research.* New York Free Press, New York, 1981.

[223] E. T. Rolls and G. Deco. *The noisy brain: stochastic dynamics as a principle of brain function*, volume 34. Oxford University Press, 2010.

[224] A. Roxin. The role of degree distribution in shaping the dynamics in networks of sparsely connected spiking neurons. *Frontiers in Computational Neuroscience*, 5, 2011.

[225] M. Sahini and M. Sahimi. *Applications of percolation theory*. CRC Press, 1994.

[226] B. Sapoval, M. Rosso, and J.-F. Gouyet. The fractal nature of a diffusion front and the relation to percolation. *Journal de Physique Lettres*, 46(4):149–156, 1985.

[227] C. Schmeltzer, A. Kihara, I. Sokolov, and S. Rüdiger. A k-population model to calculate the firing rate of neuronal networks with degree correlations. *BMC Neuroscience*, 15(Suppl 1):O14, 2014.

[228] C. Schmeltzer, A. Kihara, I. Sokolov, and S. Rüdiger. Degree correlations optimize neuronal network sensitivity to sub-threshold stimuli. *PloS One*, 10(6):e0121794, 2015.

[229] C. Schmeltzer, J. Soriano, I. Sokolov, and S. Rüdiger. Percolation of spatially constrained Erdős-Rényi networks with degree correlations. 89, 2014.

[230] J. Schmidhuber. Deep learning in neural networks: An overview. *Neural Networks*, 61:85–117, 2015.

[231] J. Scott. *Social network analysis*. Sage, 2012.

[232] S. B. Seidman. Network structure and minimum degree. *Social networks*, 5(3):269–287, 1983.

[233] P. Sen, S. Dasgupta, A. Chatterjee, P. Sreeram, G. Mukherjee, and S. Manna. Small-world properties of the indian railway network. *Physical Review E*, 67(3):036106, 2003.

[234] M. Á. Serrano and M. Boguná. Percolation and epidemic thresholds in clustered networks. *Physical Review Letters*, 97(8):088701, 2006.

[235] M. N. Shadlen and W. T. Newsome. Noise, neural codes and cortical organization. *Current Opinion in Neurobiology*, 4(4):569–579, 1994.

[236] M. N. Shadlen and W. T. Newsome. The variable discharge of cortical neurons: implications for connectivity, computation, and information coding. *The Journal of Neuroscience*, 18(10):3870–3896, 1998.

[237] M. Shein-Idelson, E. Ben-Jacob, and Y. Hanein. Engineered neuronal circuits: a new platform for studying the role of modular topology. *Frontiers in Neuroengineering*, 4, 2011.

[238] M. Shelley and D. McLaughlin. Coarse-grained reduction and analysis of a network model of cortical response: I. drifting grating stimuli. *Journal of Computational Neuroscience*, 12(2):97–122, 2002.

[239] W. L. Shew, H. Yang, T. Petermann, R. Roy, and D. Plenz. Neuronal avalanches imply maximum dynamic range in cortical networks at criticality. *The Journal of Neuroscience*, 29(49):15595–15600, 2009.

[240] W. L. Shew, H. Yang, S. Yu, R. Roy, and D. Plenz. Information capacity and transmission are maximized in balanced cortical networks with neuronal avalanches. *The Journal of Neuroscience*, 31(1):55–63, 2011.

[241] W. Singer. Synchronization of cortical activity and its putative role in information processing and learning. *Annual Review of Physiology*, 55(1):349–374, 1993.

[242] M. A. Smith and A. Kohn. Spatial and temporal scales of neuronal correlation in primary visual cortex. *The Journal of Neuroscience*, 28(48):12591–12603, 2008.

[243] W. R. Softky and C. Koch. The highly irregular firing of cortical cells is inconsistent with temporal integration of random EPSPs. *The Journal of Neuroscience*, 13(1):334–350, 1993.

[244] I. Sokolov. Dimensionalities and other geometric critical exponents in percolation theory. *Physics-Uspekhi*, 29(10):924–945, 1986.

[245] S. Solomon, G. Weisbuch, L. de Arcangelis, N. Jan, and D. Stauffer. Social percolation models. *Physica A: Statistical Mechanics and its Applications*, 277(1):239–247, 2000.

[246] J. Soriano, M. Rodríguez Martínez, T. Tlusty, and E. Moses. Development of input connections in neural cultures. *Proceedings of the National Academy of Sciences*, 105(37):13758–13763, 2008.

[247] O. Sporns. *Networks of the Brain*. MIT Press, 2011.

[248] O. Sporns. *Discovering the human connectome*. MIT Press, 2012.

[249] O. Sporns, D. Chialvo, M. Kaiser, and C. C. Hilgetag. Organization, development and function of complex brain networks. *Trends in Cognitive Sciences*, 8(9):418–425, 2004.

[250] O. Sporns, C. J. Honey, and R. Kötter. Identification and classification of hubs in brain networks. *PloS One*, 2(10):e1049, 2007.

[251] O. Sporns, G. Tononi, and G. M. Edelman. Theoretical neuroanatomy: relating anatomical and functional connectivity in graphs and cortical connection matrices. *Cerebral Cortex*, 10(2):127–141, 2000.

[252] O. Sporns, G. Tononi, and R. Kötter. The human connectome: a structural description of the human brain. *PLoS Computational Biology*, 1(4):e42, 2005.

[253] O. Sporns and J. D. Zwi. The small world of the cerebral cortex. *Neuroinformatics*, 2(2):145–162, 2004.

[254] H. E. Stanley. Cluster shapes at the percolation threshold: and effective cluster dimensionality and its connection with critical-point exponents. *Journal of Physics A: Mathematical and General*, 10(11):L211, 1977.

[255] D. Stauffer and A. Aharony. *Introduction to percolation theory*. Taylor and Francis, 1991.

[256] M. Steriade, F. Amzica, and D. Contreras. Synchronization of fast (30-40 Hz) spontaneous cortical rhythms during brain activation. *The Journal of Neuroscience*, 16(1):392–417, 1996.

[257] M. Steriade, D. A. McCormick, and T. J. Sejnowski. Thalamocortical oscillations in the sleeping and aroused brain. *Science*, 262(5134):679–685, 1993.

[258] W. H. Stockmayer. Theory of molecular size distribution and gel formation in branched-chain polymers. *The Journal of Chemical Physics*, 11(2):45–55, 1943.

[259] D. Strauss. On a general class of models for interaction. *SIAM Review*, 28(4):513–527, 1986.

[260] S. Teller, C. Granell, M. De Domenico, J. Soriano, S. Gómez, and A. Arenas. Emergence of assortative mixing between clusters of cultured neurons. *Entropy*, 15:5464–5474, 2013.

[261] S. Teller and J. Soriano. Experiments on clustered neuronal networks. In *Physics, Computation, and the Mind-Advances and Challenges at Interfaces*, volume 1510, pages 244–246. AIP Publishing, 2013.

[262] S. Thorpe, A. Delorme, and R. Van Rullen. Spike-based strategies for rapid processing. *Neural Networks*, 14(6):715–725, 2001.

[263] E. Tibau, C. Bendiksen, S. Teller, N. Amigo, and J. Soriano. Interplay activity-connectivity: dynamics in patterned neuronal cultures. In *Proceedings of the 12th Granada Seminar on Computational and Statistical Physics*, volume 1510, pages 54–63. AIP Publishing, 2013.

[264] G. Tkačik, C. G. Callan, and W. Bialek. Information flow and optimization in transcriptional regulation. *Proceedings of the National Academy of Sciences*, 105(34):12265–12270, 2008.

[265] G. Tkačik, C. G. Callan Jr, and W. Bialek. Information capacity of genetic regulatory elements. *Physical Review E*, 78(1):011910, 2008.

[266] T. Tlusty and J.-P. Eckmann. Remarks on bootstrap percolation in metric networks. *Journal of Physics A: Mathematical and Theoretical*, 42(20):205004, 2009.

[267] G. Tononi. Consciousness as integrated information: a provisional manifesto. *The Biological Bulletin*, 215(3):216–242, 2008.

[268] G. Tononi, O. Sporns, and G. M. Edelman. A measure for brain complexity: relating functional segregation and integration in the nervous system. *Proceedings of the National Academy of Sciences*, 91(11):5033–5037, 1994.

[269] M. V. Tsodyks, W. E. Skaggs, T. J. Sejnowski, and B. L. McNaughton. Population dynamics and theta rhythm phase precession of hippocampal place cell firing: a spiking neuron model. *Hippocampus*, 6(3):271–280, 1996.

[270] P. A. Valdes-Sosa, A. Roebroeck, J. Daunizeau, and K. Friston. Effective connectivity: influence, causality and biophysical modeling. *Neuroimage*, 58(2):339–361, 2011.

[271] M. P. van den Heuvel and O. Sporns. Rich-club organization of the human connectome. *The Journal of Neuroscience*, 31(44):15775–15786, 2011.

[272] M. P. van den Heuvel, C. J. Stam, M. Boersma, and H. H. Pol. Small-world and scale-free organization of voxel-based resting-state functional connectivity in the human brain. *Neuroimage*, 43(3):528–539, 2008.

[273] N. G. Van Kampen. *Stochastic processes in physics and chemistry*, volume 1. Elsevier, 1992.

[274] L. R. Varshney, B. L. Chen, E. Paniagua, D. H. Hall, and D. B. Chklovskii. Structural properties of the caenorhabditis elegans neuronal network. *PLoS Computational Biology*, 7(2):e1001066, 2011.

[275] J. C. Vasquez, A. R. Houweling, and P. Tiesinga. Simultaneous stability and sensitivity in model cortical networks is achieved through anti-correlations between the in-and out-degree of connectivity. *Frontiers in Computational Neuroscience*, 7, 2013.

[276] A. Vázquez and Y. Moreno. Resilience to damage of graphs with degree correlations. *Physical Review E*, 67:015101, Jan 2003.

[277] J. D. Victor and K. P. Purpura. Nature and precision of temporal coding in visual cortex: a metric-space analysis. *Journal of Neurophysiology*, 76(2):1310–1326, 1996.

[278] N. Voges and L. Perrinet. Complex dynamics in recurrent cortical networks based on spatially realistic connectivities. *Frontiers in Computational Neuroscience*, 6, 2012.

[279] B. Wang, T. Zhou, Z. Xiu, and B. Kim. Optimal synchronizability of networks. *The European Physical Journal B*, 60(1):89–95, 2007.

[280] C. P. Warren, L. M. Sander, and I. M. Sokolov. Geography in a scale-free network model. *Physical Review E*, 66:056105, Nov 2002.

[281] S. Wasserman. *Social network analysis: Methods and applications*, volume 8. Cambridge University Press, 1994.

[282] D. J. Watts and S. H. Strogatz. Collective dynamics of small-world networks. *Nature*, 393(6684):440–442, 1998.

[283] J. White, E. Southgate, J. Thomson, and S. Brenner. The structure of the nervous system of the nematode caenorhabditis elegans: the mind of a worm. *Phil. Trans. R. Soc. Lond*, 314:1–340, 1986.

[284] K. Wu, Y. Taki, K. Sato, Y. Sassa, K. Inoue, R. Goto, K. Okada, R. Kawashima, Y. He, A. C. Evans, et al. The overlapping community structure of structural brain network in young healthy individuals. *PloS One*, 6(5):e19608, 2011.

[285] S. Wuchty and E. Almaas. Peeling the yeast protein network. *Proteomics*, 5(2):444–449, 2005.

[286] C. Wyart, C. Ybert, L. Bourdieu, C. Herr, C. Prinz, and D. Chatenay. Constrained synaptic connectivity in functional mammalian neuronal networks grown on patterned surfaces. *Journal of Neuroscience Methods*, 117(2):123–131, 2002.

[287] R. Xulvi-Brunet. *Structural properties of scale-free networks*. PhD thesis, Humboldt-Universität zu Berlin, Mathematisch-Naturwissenschaftliche Fakultät I, 2007.

[288] R. Xulvi-Brunet and I. M. Sokolov. Evolving networks with disadvantaged long-range connections. *Physical Review E*, 66:026118, Aug 2002.

[289] R. Xulvi-Brunet and I. M. Sokolov. Reshuffling scale-free networks: From random to assortative. *Physical Review E*, 70:066102, Dec 2004.

[290] L. Yassin, B. L. Benedetti, J.-S. Jouhanneau, J. A. Wen, J. F. Poulet, and A. L. Barth. An embedded subnetwork of highly active neurons in the neocortex. *Neuron*, 68(6):1043–1050, 2010.

[291] M. Y. Yim, A. Aertsen, and S. Rotter. Impact of intrinsic biophysical diversity on the activity of spiking neurons. *Physical Review E*, 87(3):032710, 2013.

[292] S. Yook, H. Jeong, and A. Barabási. Modeling the Internet's large-scale topology. *Proceedings of the National Academy of Sciences*, 99(21):13382, 2002.

[293] R. M. Young. *Mind, brain, and adaptation in the nineteenth century: cerebral localization and its biological context from Gall to Ferrier*. Number 3. Oxford University Press, 1970.

[294] W. W. Zachary. An information flow model for conflict and fission in small groups. *Journal of Anthropological Research*, 33(4):452–473, 1977.

[295] L. Zhao, I. Bryce Beverlin, T. Netoff, and D. Q. Nykamp. Synchronization from second order network connectivity statistics. *Frontiers in Computational Neuroscience*, 5, 2011.

[296] C. Zhou, L. Zemanová, G. Zamora, C. C. Hilgetag, and J. Kurths. Hierarchical organization unveiled by functional connectivity in complex brain networks. *Physical Review Letters*, 97(23):238103, 2006.

Selbstständigkeitserklärung

Ich erkläre, dass ich die vorliegende Arbeit selbstständig und nur unter Verwendung der angegebenen Literatur und Hilfsmittel angefertigt habe.

Berlin, den 5. April 2016 Christian Claus Schmeltzer

List of publications

1. **C. Schmeltzer**, A. Kihara, I. Sokolov, and S. Rüdiger. Degree correlations optimize neuronal network sensitivity to sub-threshold stimuli. *PloS One*, 10(6): e0121794, 2015

2. **C. Schmeltzer**, A. Kihara, I. Sokolov, and S. Rüdiger. A k-population model to calculate the firing rate of neuronal networks with degree correlations. *BMC Neuroscience*, 15(Suppl 1):O14, 2014

3. **C. Schmeltzer**, J. Soriano, I. Sokolov, and S. Rüdiger. Percolation of spatially constrained Erdős-Rényi networks with degree correlations. *Physical Review E*, 89(1):012116, 2014

4. L. Walter, G. Higa, **C. Schmeltzer**, E. Sousa, E. Kinjo, S. Rüdiger, D. Hamassaki, G. Cerchiaro, and A. Kihara. Functional regulation of neuronal nitric oxide synthase expression and activity in the rat retina. *Experimental Neurology 261*, 510-517, 2014

5. S. Babu, **C. Schmeltzer**, and H. Stark. Swimming at Low Reynolds Number: From Sheets to the African Trypanosome. In *Nature-Inspired Fluid Mechanics*, pages 25-41. Springer, 2012